This is to certify that the

dissertation entitled

INVESTIGATION OF THE FILM PROPERTIES AND DEPOSITION PROCESS OF a-C:H FILMS DEPOSITED WITH A MICROWAVE ECR PLASMA REACTOR

presented by

Bo Keun Kim

has been accepted towards fulfillment
of the requirements for

Doctor of Philosophy degree in Electrical Engineering

Timothy Gutgot
Major professor

Date May 11, 2000

INVESTIGATION OF THE FILM PROPERTIES AND DEPOSITION PROCESS OF a-C:H FILMS DEPOSITED WITH A MICROWAVE ECR PLASMA REACTOR

By

Bo Keun Kim

A DISSERTATION

Submitted to
Michigan State University
in partial fulfillment of the requirement
for the degree of

DOCTOR OF PHILOSOPHY

Department of Electrical and Computer Engineering

2000

ABSTRACT

INVESTIGATION OF THE FILM PROPERTIES AND DEPOSITION PROCESS OF a-C:H FILMS DEPOSITED WITH A MICROWAVE ECR PLASMA REACTOR

By

Bo Keun Kim

Hydrogenated amorphous carbon (a-C:H) films are deposited from acetylene gas at pressures in the submillitorr range (0.2-0.6 mTorr), and methane-argon and acetylene-argon gas mixtures at pressures in the millitorr range (1-5 mTorr) in a microwave ECR plasma reactor operated with rf biased substrate holder. The films deposited at pressures in the submillitorr range showed a strong influence of ion energy and ion flux to neutral flux ratio on the deposition process and film properties. The films showed a peak value of optical bandgap when deposited at -200 V of rf induced substrate bias revealing the ion energy effect. The effect of ion flux to neutral flux ratio was seen in the depositions done with varied substrate positions from the discharge region and the threshold ratio of ion flux to neutral flux for deposition of films with the peak is found to be in the range of 0.06-0.1. Maintaining a low deposition pressure is found to be critical to obtain films of high optical bandgaps. The deposition rate (~90 nm/min) at 7.0 sccm of acetylene flow rate is much higher than the filtered ion beam and plasma beam deposition systems used for tetrahedral (hydrogenated) amorphous carbon film depositions in the literature.

The films deposited at pressures in the millitorr range showed variation of the film properties dependent on the deposition condition. The films deposited with the two

different gas mixtures including argon-methane and argon-acetylene under similar input variable conditions have substantially different properties including deposition rate, mass density, optical absorption coefficient, refractive index, optical bandgap and hydrogen content. The deposition variables varied included rf induced dc substrate bias voltage (0 to -100 V), argon/hydrocarbon gas flow ratio (0-1.0) and pressure (1-5 mTorr).

The discharge properties including electron temperature, ion saturation current, and residual gas composition of the exit gas flow for the various gas mixtures were measured to help explain the different deposition results from the acetylene-based and methane-based gas mixtures. From the discharge properties, the ion flux to neutral flux ratio is estimated and the carbon flux in the input gas flow is shown to be the rate-limiting process of deposition. The variation of film property is attributed to the hydrogen content in the film composition and the hydrogen content is controlled by the ion bombardment effect in the film deposition process. For the films deposited from acetylene-argon discharges the use of lower pressures to obtain an increased ion flux to neutral flux ratio to the substrate was found to be critical for obtaining dense, low hydrogen content films. For the films deposited from methane-argon discharge the addition of argon to the discharge increased the film's mass density and lowered the hydrogen content. In both methane-based and acetylene-based deposition processes the rf induced bias was also a critical determining factor of film properties.

The variation of film properties in the film deposition at millitorr pressures can be mainly explained with the consideration of the hydrogen content of the films. In contrast, the variation of film properties in the film deposition at submillitorr pressures is mainly attributed to sp^3 to sp^2 carbon bonding ratio changes in the film composition.

ACKNOWLEDGEMENTS

The author is indebted to many individuals for the successful completion of this dissertation and his degree program. The author wishes to thank his advisor, Dr. Timothy A. Grotjohn, for his thoughtful and inspiring guidance and support, and also for his painstaking review of this manuscript. He also wishes to extend his thanks to Dr. Donnie K. Reinhard, Dr. Jes Asmussen, Department of Electrical and Computer Engineering, and Dr. Brage Golding, Department of Physics and Astronomy, for serving on author's guidance committee, and for their great lectures and academic advices. A special thanks is given to the author's wife, Kyungsim Yoon, and to his family for their patience, understanding and sacrifice during the course of this program.

TABLE OF CONTENTS

Chapter 4

Chapter 5

Chapter 6

LIST OF TABLES

LIST OF FIGURES

Chapter 1

1. Introduction

1.1 Motivation

Hydrogenated amorphous carbon (a-C:H) films are amorphous materials containing a mixture of sp^3 and sp^2 hybridized carbon and hydrogen. The films do not have long range order in their spatial structure unlike diamond which is an sp^3 hybridized carbon crystal and graphite which is a sp^2 hybridized carbon crystal. They do have short range order and possibly medium range order. a-C:H films contain lower levels of hydrogen as compared to hydrocarbon polymers.

The properties of a-C:H films are mainly determined by the sp^3/sp^2 ratio and hydrogen content. The content of sp^3 hybridization sites determines the mechanical properties of the films like density, hardness, stress, etc. and the content of sp^2 sites primarily determines optical and electrical properties like optical bandgap and conductivity. Hydrogen in the films passivates the dangling bonds and influences the mechanical, optical and electrical properties of the films. The films having high sp^3 sites, low sp^2 sites, and low hydrogen content show extreme hardness and high density, and they are called diamond-like carbon (DLC) films or tetrahedral hydrogenated amorphous carbon films (ta-C:H). Graphite-like films have relatively high sp^2 hybridization sites and are soft, and polymer-like films contain high levels of hydrogen and are very soft. Thus, a-C:H films can have a wide range of properties including those of diamond, graphite and polymers depending on the deposition method and deposition conditions.

The interesting properties of DLC films are characterized as extreme hardness, extreme smoothness, low friction coefficient, high optical transparency over a wide spectral range of photon energies, high electrical resistivity and high chemical inertness. Some of film properties from the literatures [1-3] include sp^3 fraction (0.2 - 0.8), hydrogen-content (25 - 65 at.%), optical gap (0.8 - 3.0 eV), index of refraction (1.5 - 2.3), density (1.3 -3.0 g/cm^3), and resistivity (10^6- 10^{15} Ωcm). Thus, the films have applications as protective coatings, and as optical coatings for anti-reflection and infrared filters, etc. [4, 5]. Additionally, possible applications for electronic device materials are under investigation [6-11].

Hydrogenated amorphous carbon (a-C:H) and amorphous carbon (a-C:H) films have been deposited by a wide range of techniques[12] including dc plasma deposition[13], rf plasma deposition [14], plasma beam source deposition [3, 15], filtered ion beam deposition [16-19], and microwave electron cyclotron resonance (ECR) plasma deposition [20-30]. The feed gases for the chemical vapor deposition (CVD) method are usually methane or acetylene as the hydrocarbon gas with or without argon gas or hydrogen gas. The properties of the films change with deposition method, type of feed gases, and deposition conditions. The films are deposited at low temperature, which inhibits growth of crystals and gives an amorphous film structure. The C-C sp^3/sp^2 ratio of the films is mainly determined by ion bombardment energy and carbon ion flux to neutral flux ratio to the substrate during the deposition process. The hydrogen content in the films is also strongly dependent on ion bombardment energy.

For the deposition of films with high sp^3 hybridization sites (ta-C:H), the carbon ion flux to neutral flux ratio onto the substrate is high and the ion bombardment energy

must be at a certain appropriate value which is about 100eV per carbon. The systems used for the deposition of ta-C:H films are the plasma beam source system and filtered ion beam systems, which provide high ion flux to neutral flux ratio onto the substrate. The systems usually have low deposition rates of ta-C:H films.

In this investigation, a microwave ECR-CVD reactor with rf biased substrate holder is used as the deposition system. The microwave ECR-CVD system creates a high density of charged and excited species at low deposition pressure ($< 10^{-3}$ Torr) and it has a low deposition temperature. The high density of charged and excited species gives a high deposition rate and the lack of electrodes in the system inhibits contamination of depositing films giving high quality films. This investigation studies and applies the ECR-CVD system to deposit a-C:H films with a range of properties. Specifically, the deposition of a-C:H films with high sp^3 carbon-carbon bonding percentages at rates exceeding previous investigations and methods will be explored.

1.2 Research Objectives

The objective of this project is to investigate the deposition process and the film properties of a-C:H films deposited using a low-pressure, high-density microwave plasma source. The investigation will characterize a-C:H film properties including thickness, density, optical gap, refractive index and hydrogen content. The investigation will also establish the deposition conditions such as rf induced substrate bias, deposition pressure, argon flow ratio to hydrocarbon feed gas, substrate temperature, position of the substrate and microwave input power that produce desired a-C:H film properties. Further, it will establish the effects of deposition conditions on film properties in terms of discharge

properties such as ion energy, ion flux to neutral flux ratio, ion type and deposition temperature and possible film deposition mechanisms. A specific technological goal is to deposit a-C:H films with a high sp^3 carbon bonding percentage at a high deposition rate exceeding 50 nm/min.

1.3 Research Methods

The methodology to be followed divides the deposition process into three sets of variables including input deposition reactor variables, plasma deposition internal variables and output variables / film properties. In the deposition of the a-C:H films using the microwave ECR-CVD system in this investigation, the input variables are rf induced substrate bias voltage, input microwave power, chamber pressure, substrate heating/cooling, feed gas type and flow rate of feed gases. The input variables then determine the internal variables such as ion density and type, ion energy, neutral / radical concentration and type, ion flux to neutral flux ratio of species onto the substrate, and deposition surface temperature with which films are deposited. Lastly, the internal variables determine the outputs that include the film compositions, i.e., percent sp^3, percent sp^2, hydrogen content and the film's deposition rate. The film properties associated with the outputs are density, internal stress, hardness, index of refraction, optical band gap and deposition rate.

The research plan has two major components.

1) Characterize and quantify for the a-C:H deposition process using C_2H_2, CH_4-Ar and C_2H_2-Ar gas feeds the relationships of (a) input variables to internal variables and (b) internal variables to outputs.

2) Compare the deposition results measured in 1) above to the prediction of a model found in the literature.

1.4 Research Outline

Chapter 2 reviews hydrogenated amorphous carbon films in the literature. The composition and electronic structure of amorphous carbon films are reviewed to explain a-C:H films. Deposition mechanism of amorphous carbon films is also reviewed to show how the films are deposited and what determines the film's properties. Next the various deposition systems of amorphous carbon films are introduced and their film properties are shown. In Chapter 3 the deposition system of this investigation and the characterization methods of discharge properties and film' properties are described. Film properties versus variation of discharge conditions or properties are presented and explained in Chapter 4 and 5. In Chapter 4 films are deposited from acetylene feed gas at pressures in the submillitorr range and the film properties are compared to the deposition models in the literature. The objectives in Chapter 4 are to deposit high sp^3 carbon-carbon bonded ta-C:H or diamond-like films using a microwave ECR plasma reactor at high deposition rate and to understand the deposition process of the films by investigating the effects of ion energy, ion flux to neutral flux ratio, deposition temperature and hydrocarbon flow rate. In Chapter 5, films are deposited from acetylene-argon and methane-argon gas feeds at pressures in the millitorr range to produce a range of film properties and to compare the films from each gas feeds. The objectives in Chapter 5 are to establish the variation of film properties possible by depositing the films at different

deposition conditions and to understand the deposition process of the films by investigating the effects of rf induced substrate bias, pressure and argon flow ratio. In Chapter 6, the results of this investigation are summarized and the conclusions are presented.

Chapter 2

2. Hydrogenated Amorphous Carbon Films: A Review

2.1 Composition of a-C:H Films

In a-C:H films, each carbon atom forms sp^3 or sp^2 hybridization bonds with other carbon atoms and hydrogen atoms. sp^3 sites form four tetrahedral C-C or C-H σ bonds and sp^2 sites form three C-C trigonal σ bonds and one C-C or C-H π bonds. The schematic compositional structure is represented in Fig. 2-1[31]. One group labeled A is for sp^3 bonded carbon atoms, and a group labeled B is for sp^2 carbon atoms in a six-membered aromatic ring. Two sp^2 olefinic carbon atoms in a double bond are labeled C, and one sp^2 carbon atom in an isolated free radical site with a dangling bond (represented by an arrow) is labeled D. The isolated free radical sites is believed to form π bonded carbon pairs to lower the energy of the system. The π bonded carbon pairs ultimately form an aromatic ring and nearby aromatic rings are further condensed to graphite clusters of sp^2 aromatic rings. An example of the graphite cluster with 5 aromatic rings is shown in Fig. 2-2 [31]. Thus the sp^2 sites are embedded in a sp^3 bonded matrix as sp^2 clusters and spatially localized in the structure of the a-C:H films. The sp^2 carbon atoms can also form five-membered rings. Some unbonded hydrogen atoms may also reside in the amorphous film structure.

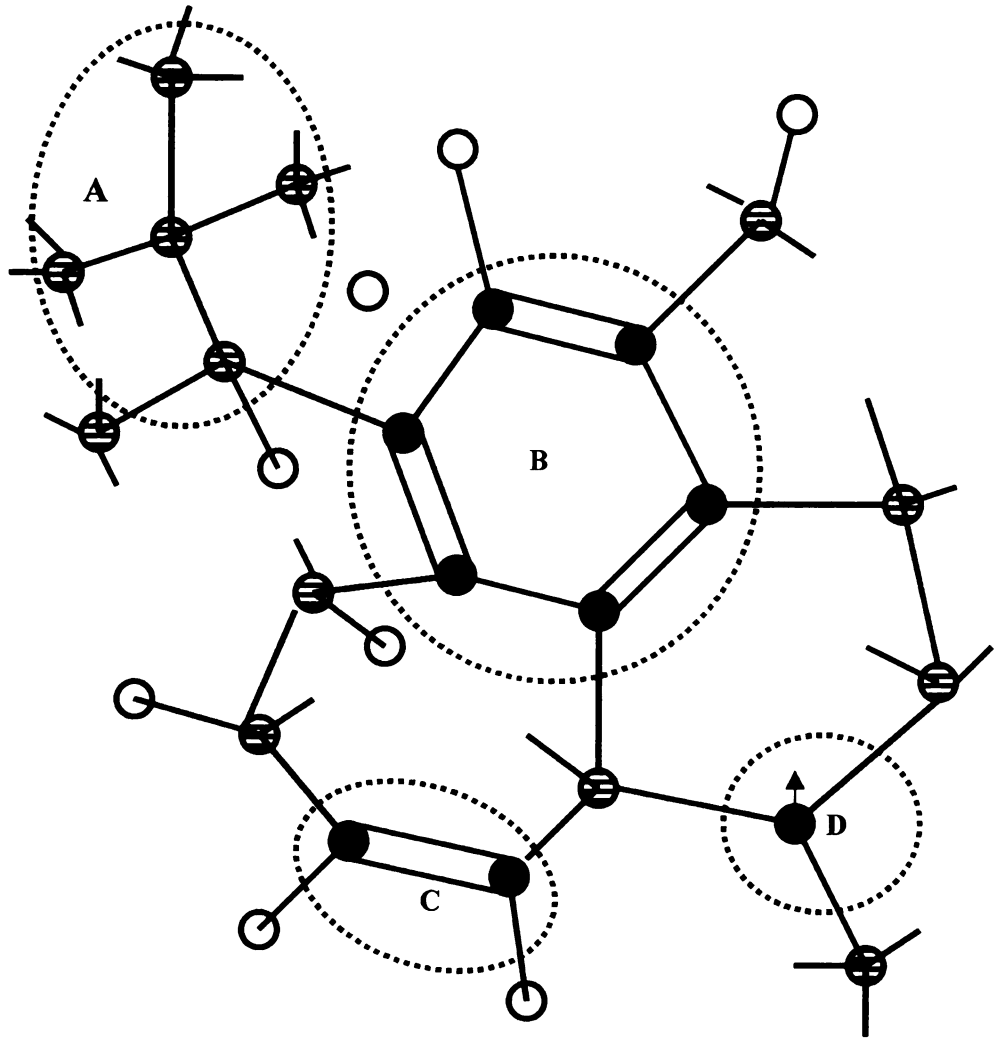

Fig. 2 - 1: Schematic representation of hydrogenated amorphous carbon films (a-C:H). The network is comprised of hydrogen (○), sp^2 carbon atoms (⊖) and sp^3 carbon atoms (●). The lines represent the bonds and the arrows represent the dangling bonds.

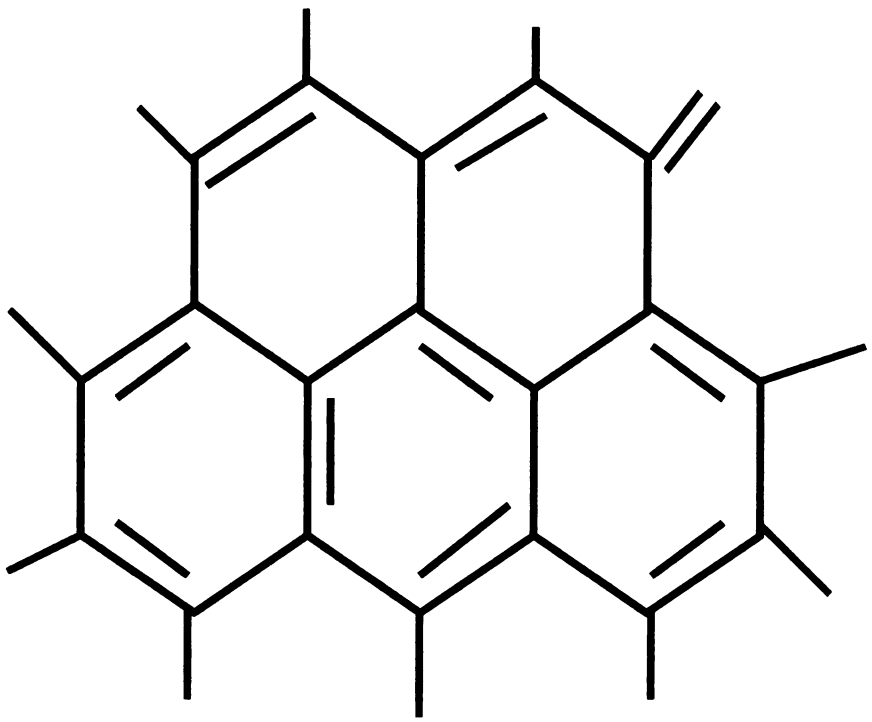

Fig. 2 - 2: sp^2 carbon atoms in a-C:H films in the form of a cluster of six-membered aromatic rings.

Various forms of hydrocarbon films can be distinguished by the content of sp^3 and sp^2 carbon and hydrogen. The ternary phase diagram of the content of sp^3 and sp^2 carbon and hydrogen for hydrocarbon films [32, 33] is shown in Fig. 2-3. The area close to the hydrogen-rich corner marks the region where no stable films can be formed. The top sp^3 corner corresponds to fully diamond-like carbon films, the bottom left corner corresponds to fully graphite-like carbon films, and lastly the bottom right part near the triangle of no film corresponds to polymer-like carbon films. The rigidity boundary indicates the boundary between rigid and floppy, polymer-like networks. The position of this boundary line depends on the number of aromatic rings in the sp^2 graphitic clusters. The diamond-like quality is proportional to the perpendicular distance above this line [3]. The tetrahedral hydrogenated amorphous carbon films (ta-C:H) are a-C:H films, that have a high ratio of sp^3 carbon sites, are shown in the shaded region above the a-C:H region in the figure.

The properties of a-C:H films depends on the composition of the films [31]. The diamond-like properties of films come from a high sp^3 content, which makes the film structure over constrainted. On the other hand, a high hydrogen atom content in the film yields many monovalent C-H bonds. These bonds make the film structure underconstrainted, which makes the film floppy. One sp^2 carbon site forms 3 strong σ bondings in a plane and one weak π bonding perpendicular to the plane, thus it also makes the films soft. Thus density, hardness and Young's modulus are nearly proportional to sp^3 C-C content of the films (Fig. 2-4) assuming a fixed hydrogen content

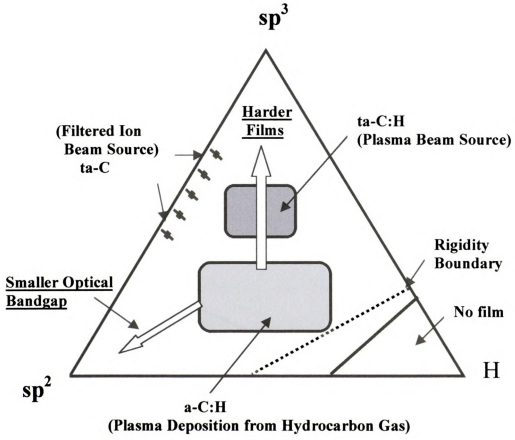

Fig. 2 - 3: Ternary phase diagram of hydrocarbon films.

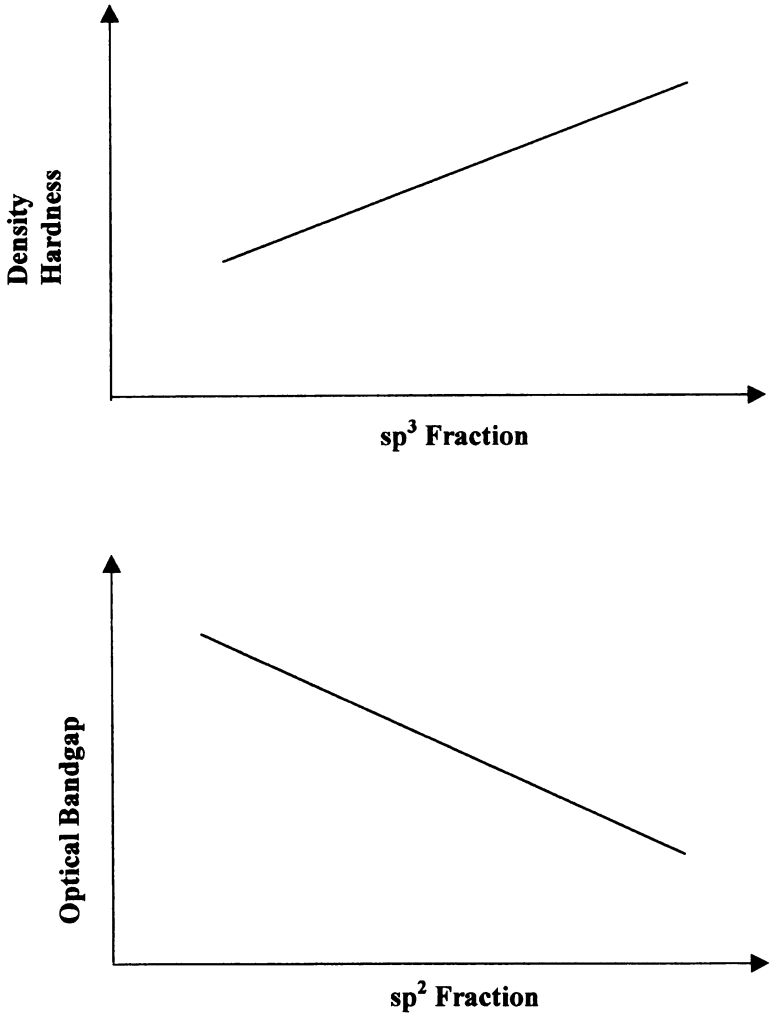

Fig. 2 - 4: These plots show the trends of properties of ta-C:H films with the variation of sp^3 fraction and sp^2 fraction.

Other properties like the optical bandgap are determined primarily by the sp^2 carbo bondings as shown in Fig. 2-4 for ta-C:H films and discussed in more detail in the ne section.

2.2 Electronic Structure of a-C:H Films [34]

The density of states (DOS) is schematically shown in Fig. 2-5.[34]. A sp^3 si forms 4 σ bonds and a sp^2 site forms three σ bonds and one π bond. σ^* and π^* represe antibondings of σ and π bonds. The σ and σ^* states form deep valence and conductio band states and π and π^* states form band edge states. Photoemission spectra shows states are at the top of the valence band and their density can be used to extract an s bonding fraction [35]. The conduction band DOS has been probed by electron energy lo spectroscopy (EELS), which shows a prepeak for the π^* states of sp^2 sites, which can used to measure the sp^2 bonding fraction in DLC films [3, 16, 36].

As seen in the previous section, sp^2 sites form embedded clusters in a sp^3 matr thus the π states are localized. The σ states are not localized except possibility for t states at the edge of the σ and σ^* bands, i.e. the tail states. a-C:H films show hi resistivity because the π states are localized and the gap between σ and σ^* is large. T optical bandgap is determined by the π and π^* states. The optical bandgap is controll by the distortion of sp^2 rings or chains, not by the size of the clusters of sp^2 states [3 38].

There are also defect states deep in the gap. The defect states in a-C:(H) fil come from isolated sp^2 sites and dangling bonds which are not paired up as π bonds [39

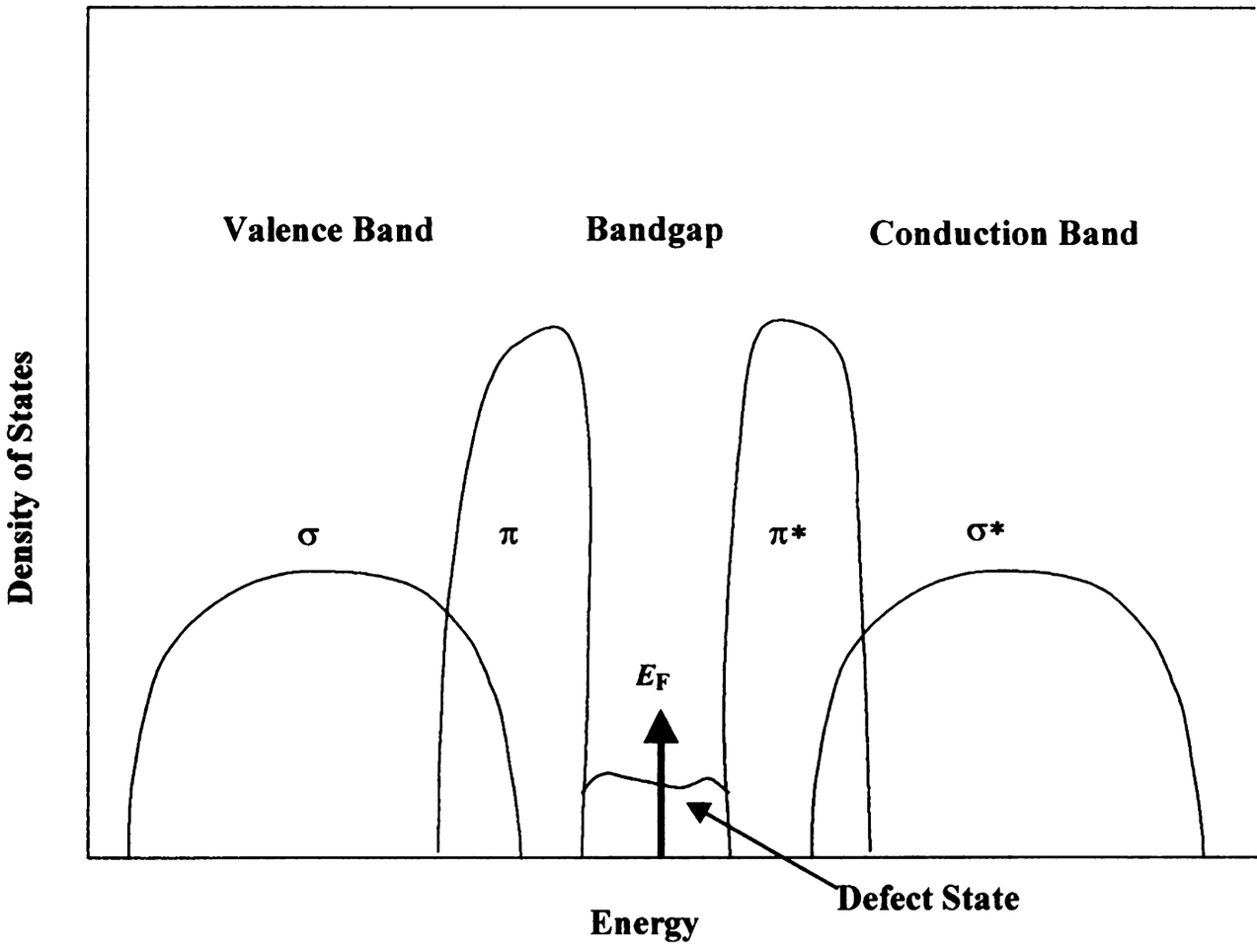

Fig. 2 - 5: A schematic diagram of density of state (DOS) of a-C:H films, which shows σ and π states, and defect states.

and are strongly localized. These defect states generally make the a-C:(H) films show p-type behavior [34].

2.3 Deposition Mechanism of Diamond-like a-C and a-C:H Films

2.3.1 Microscopic Process [2, 40-42]

The local bonding of a-C and a-C:H can be defined principally in terms of two parameters, the hydrogen atom fraction and the sp^3 bonding fraction or the analogous macroscopic parameters hydrogen content and mass density. A model of the deposition processes should be able to account for the variation of these parameters with the deposition conditions.

In the model developed by Robertson [40], the sp^3 bonding occurs due to the ion flux into subsurface positions causing a metastable increase in density. In the highly energetic conditions of ion bombardment, atomic hybridizations are expected to adjust readily to the local density, becoming more sp^2 if the density is low and more sp^3 if the density is high. The density will increase if an incident ion penetrates the first atomic layer of the film and enters an interstitial, subsurface position, where it dissipates energy to the neighboring atoms and acquires bulk bonding of the appropriate hybridization. Lower energy ions do not penetrate but just stick to the surface. Higher energy ions penetrate further and increase the density in deeper layers. However, the ion uses only part of its energy in penetrating the surface. The excess energy dissipates quite rapidly in a thermal spike, during which the excess density can relax. Hence, a maximum density occurs at an optimum ion energy that maximizes the penetrative yield but minimizes the

relaxation of the density increment. Typical energies of various processes in carbon deposition are listed in Table 2 - 1.

Table 2 - 1: Energies of various processes for carbon [43].

Item	Energy (eV)
Sputtering yield by C^+ ions : 0.15	500
Sputtering yield by Ar^+ ions : 0.07	500
Displacement energy of carbon atoms in diamond	80
Displacement energy of carbon atoms in graphite	25
Bond energy of diamond	7.41
Intraplanar bond energy in graphite	7.43
Interplanar bond energy in graphite	0.86
C --H bond energy	3.5

The model by Robertson [40] considers film growth from a beam of flux F containing a fraction ϕ of fast ions of energy E_i. In steady state, the fraction of ions at interstitial sites, n, is given by the difference between the penetration flux and the relaxation flux. The expression is,

$$nF = f\phi F - \beta\phi Fn \qquad (2 - 1)$$

where f is the fraction of ions which penetrate the surface and β is the number of relaxation atoms per each impact ion. Then,

$$n = \frac{f}{1/\phi + \beta} \qquad (2 - 2)$$

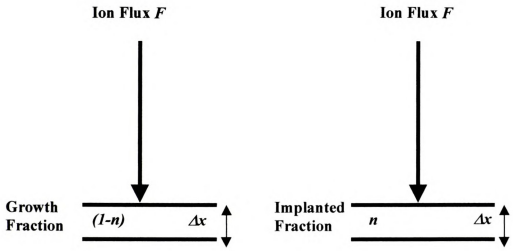

Fig. 2 - 6: How subplanted ions increase local density. A fraction *n* penetrates the surface of the film while the fraction *(1-n)* fails to penetrate and increases film thickness.

n is related to the density increment as follows and as shown in Fig. 2-6. During a time $\Delta\tau$, the deposition of non-penetrating atoms and ions adds a layer of density ρ_0 and thickness Δx on the top of the film,

$$\Delta x = F(1-n)\Delta t / \rho_0 \qquad (2-3)$$

The interstitials formed by penetrating ions produce additional density of $\Delta\rho$,

$$\Delta\rho = Fn\Delta t / \Delta x \qquad (2-4)$$

Thus the density increment, $\Delta\rho$, is

$$\frac{\Delta\rho}{\rho_0} = \frac{n}{1-n} \qquad (2-5)$$

Combining equations of (2-2) and (2-5) gives

$$\frac{\Delta\rho}{\rho} = \frac{f}{1/\phi - f + \beta} \qquad (2-6)$$

The penetration fraction or penetration probability, f, of ions is dependent on the displacement threshold energy, E_d, of target nuclei and the surface binding energy, E_B. The energy increases the kinetic energy of ions by E_B as they enter the solid. Thus, surface binding the net penetration threshold for free ions is $E_{i(th)}=E_d-E_B$. Here, E_d and E_B are 25 eV and 4.5 eV, respectively [44]. The penetration probability, f, can be calculated as a function of ion energy E_i with a simulation code such as TRIM [45]. Fig. 2-7 shows an example of calculated penetration probability. The figure was redrawn after the figure in Ref. [40]

The relaxation of density is described by the thermal spike model [46]. Each incident ion produces a thermal spike. The excess ion energy in the lattice dissipates by

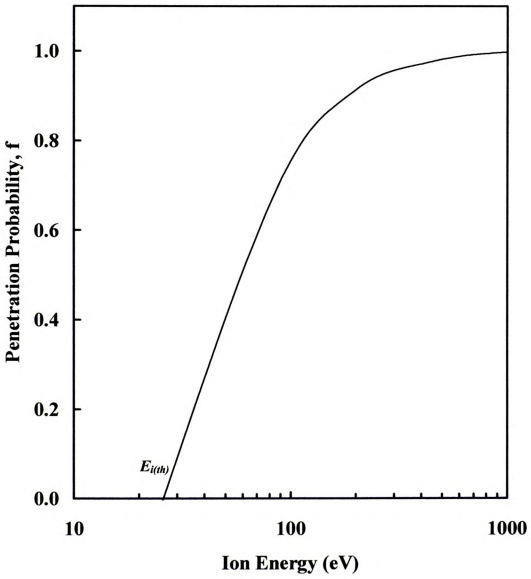

Fig. 2 - 7: An example of penetration probability of C^+ ions into a-C.

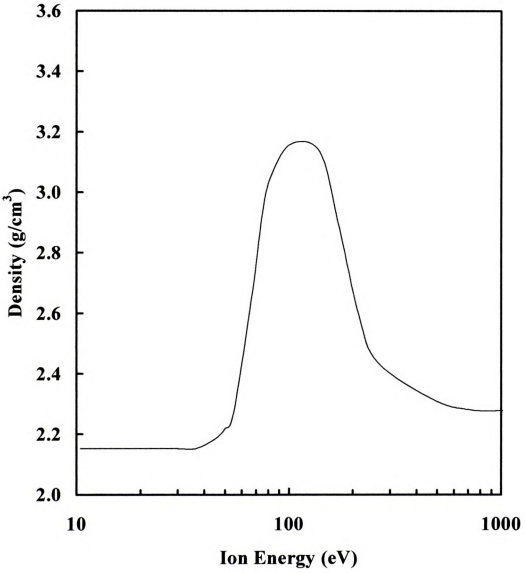

Fig. 2 - 8: An example of calculated dependence of density on ion energy.

thermal diffusivity, which, in turn, anneals the film structure. With the thermal spike model, β is calculated as,

$$\beta = 0.016p\left(\frac{E_i}{E_0}\right) \qquad (2 - 7)$$

where E_i is ion energy, $p=va_o/D$, v is a typical phonon frequency, a_o is the bond length, D is thermal diffusivity and E_o is activation energy of annealing. E_o is estimated from the thermal stability of mass selected ion beam (MSIB) a-C films, whose sp^3 bondings transform at T_t=*750 C* to sp^2 bondings. The value of E_o is estimated to be 3.1 eV as determined in [40]. Combining equations of (2-6) and (2-7) gives

$$\frac{\Delta\rho}{\rho_0} = \frac{f}{1/\phi - f + 0.016p(E_i/E_0)} \qquad (2 - 8)$$

Thus, the density increment depends on two terms f and β, and two parameters, net penetration threshold $E_{t(th)}$ which is embedded in the penetration probability, f, and activation energy of annealing, E_o. In general, $E_{t(th)}$ controls onset of densification at low ion energies and E_o controls the decrease of density at higher ion energy. An example of a typical trend of calculated dependence of density on ion energy from the above equation (2-8) is shown in Fig. 2-8. This figure was redrawn after the figure in Ref. [40]. The relaxation process is also modeled in other literature [47].

In the processes of deposition of a-C:H films, the a-C:H surface layer must be dehydrogenated to form a solid film. Thermal dehydrogenation would leave undesired sp^2 sites because the reaction to form sp^2 bondings is more favored than sp^3 bondings at higher temperatures. Ion bombardment can also dehydrogenate and leave sp^3 sites. The incident ions dehydrogenate a-C:H by the preferential displacement of hydrogen atoms. Hydrogen atoms are preferentially displaced as its displacement threshold is much lower

than C (3.5 eV versus 25 eV in Table 2-1]), basically because a hydrogen atom is monovalent whereas a carbon atom is bonded to four other atoms. The liberated H atoms recombine into hydrogen molecules that then effuse through micropores from the film.

2.3.2 Macroscopic Process

Properties of a-C:H films are mainly determined by the film's sp^3 fraction and hydrogen content, which are strongly dependent on plasma discharge properties and deposition conditions. The main factors that determine the sp^3 fraction and hydrogen content are substrate temperature, energy of ions impacting the substrate and ion flux to neutral flux ratio onto the substrate. Generally to obtain a-C:H films with high mass density and low hydrogen concentration, the desired conditions include a highly ionized plasma (high ion flux to neutral flux ratio), a low substrate temperature and a controlled ion energy (typically about 100 eV per carbon [3]).

Ion bombardment energy onto the substrate can be readily controlled by the magnitude of a negative substrate bias. The kinetic energy of ions impacts or bombards the growing a-C:H films. As described above, ion species containing carbon atoms with sufficient kinetic energy penetrate the growing films to a certain depth, dissociate themselves expelling hydrogen atoms, relax their impact energy to surrounding bonds and are eventually incorporated into the growing films. The magnitude of the impacting ion bombardment energy determines whether the newly incorporating carbon atoms form bondings of sp^3 or sp^2 at low deposition temperatures. In general the ion bombardment energy should not be too low, which forms polymer-like films, and not too high, which forms sp^2 graphite-like films. The bombarding ions may include ions of inert gases. The inert ions only bombard the films giving energy to dissociate the adsorbed or

incorporated hydrocarbon species and to form new bondings of the hydrocarbon species. Most of the inert ions will not be incorporated into the growing films.

From the above brief discussion of effects of ion bombardment energy, it can be inferred that the flux of ions onto the substrate should be high. And the ions in the flux should have the same charge and similar masses so that they give an appropriate uniform ion impacting effect that is needed to form the high sp^3 bonding ratio of diamond-like carbon films. The neutral radicals or molecules are not accelerated by the substrate bias, thus, they cannot give the film impacting energy like the ions. Rather, the neutral radicals and molecules are just adsorbed on the surface of growing films where they may dissociate, but they do not affect the bonds below the surface. The neutral adsorbed species on the surface of growing films can however disturb the ion impacting effect, which results in lower sp^3 C-C ratios. The presence of ions of different energies and masses can also disturb the desired deposition process. Thus it is important to have a high ratio of ion fluxes to neutral flux and a uniform ion energy to deposit hard diamond-like carbon films containing a high sp^3 fraction.

a-C:H films are usually deposited significantly below 350 C for hard diamond-like carbon films. The low temperature (often less than 100 C) inhibits the formation of sp^2 sites in a-C:H films. A high ratio of sp^2 graphite sites, generally resulting from films deposited at high temperature, makes the films soft. The films are then graphite-like carbon films. The substrate temperature is affected by the pressure of the plasma and the power deposited by the bias on the substrate and it can be controlled by heating or cooling the substrate holder.

2.4 Deposition Systems

Hydrogenated amorphous carbon (a-C:H) and amorphous carbon (a-C:H) films have been deposited by a wide range of techniques. RF capacitively-coupled plasma systems are widely used for a-C:H film deposition. The systems require a pressure of 10 mTorr-1 Torr to maintain the plasma [48]. One of the rf power electrodes is used as the substrate holder and the electric field is normal to the substrate holder. The rf induced substrate bias is created by the rf power provided to excite the plasma. Thus the rf induced substrate bias is a function of the rf power. The high pressure induces collisions in the sheath between the plasma and the substrate that reduces the ion energy onto the growing film. And, the higher pressure produces a small ion flux to neutral flux ratio. Because of above reasons, a much higher substrate bias is usually used in rf plasma deposition of a-C:H films than other systems.

Zou et al. [14] used a rf plasma system to deposit a-C:H films. The schematic diagram of the experimental setup is shown in Fig. 2-9. In the rf plasma deposition system the source gas was methane, the pressure range was 1mTorr to 100 mTorr, and the substrate bias range was 0 to 1400V. In general, as the substrate bias voltage was raised above -200 V the deposition rate (0-20 nm/min) increased, and the density (1.5-2.2 g/cm^3), atomic ratio of hydrogen (0.13-0.33), stress (0.42-4 GPa) and hardness (1.5-5x10^3 kp/mm^2) all decreased. The hydrogen content usually decreases with the increasing substrate bias voltage as in other deposition methods. The sp^3/sp^2 ratio (1.5-3) increased first and reached a maximum value and then decreased with the increasing substrate bias.

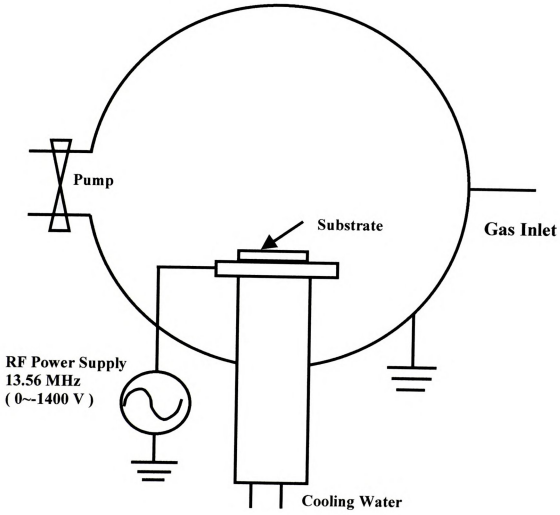

Fig. 2 - 9: Experimental setup of the rf plasma deposition system.

The results in the deposition were that soft polymer-like carbon films were deposited for the range of 0~-100 V of substrate bias voltage, hard diamond-like films for –100~-600 V and soft graphite-like films for 600-1400V.

Weiler et al.[3] used a plasma beam source that provided a highly ionized monoenergetic plasma beam of $C_2H_2^+$ ions to deposit tetrahedral hydrogenated amorphous carbon (ta-C:H) films, which have high sp^3 bonding (up to 80 %) and which are very hard. The schematic diagram of the plasma beam source is shown in Fig. 2-10. This system works at 13.6 MHz rf power and uses acetylene gas at a pressure of 0.38 mTorr. Acetylene gas was selected because it forms mostly $C_2H_2^+$ ions in low pressure plasmas [49]. The gas flow rate was kept constant at 10 sccm. The pressure in the background deposition chamber was 3.8 $x10^{-2}$ mTorr. The ion energy distribution was quite sharp (within 5%). The ion flux to neutral flux ratio on the substrate was estimated to be 0.95. The deposited film density (2.2-2.9 g/cm^3), sp^3 fraction (0.2-0.8), stress (2-9 GPa), Tauc optical gap (1.0-2.3 eV), Young's modulus (170-290 GPa) and hardness (23-60 GPa) increased first, then reached a maximum (90-100 eV) and finally decreased (> 100 eV) with the variation of ion energy. The hydrogen content (22-28 %) showed a decreasing trend with increasing ion energy.

P.J. Fallon et al. [16] deposited a highly tetrahedrally bonded form of nonhydrogenated amorphous carbon films (ta-C) with a filtered beam of C^+ ions produced by a cathodic carbon arc. A schematic figure of the system is shown in Fig. 2-11. The ions produced by cathodic carbon arc are filtered by a magnetic field filter which selects only species of a fixed mass and ion charge. Therefore, the system provides the

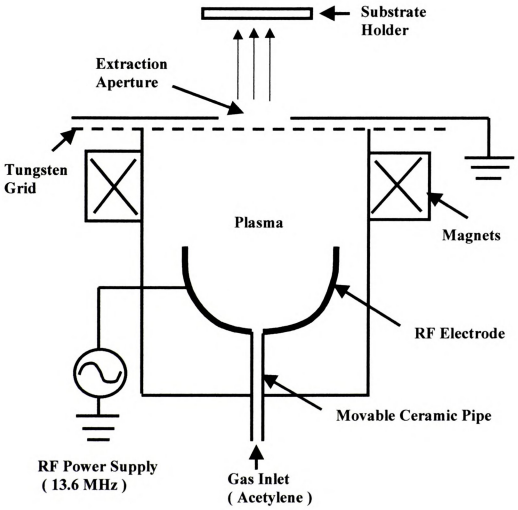

Fig. 2 - 10: Schematic diagram of the plasma beam source.

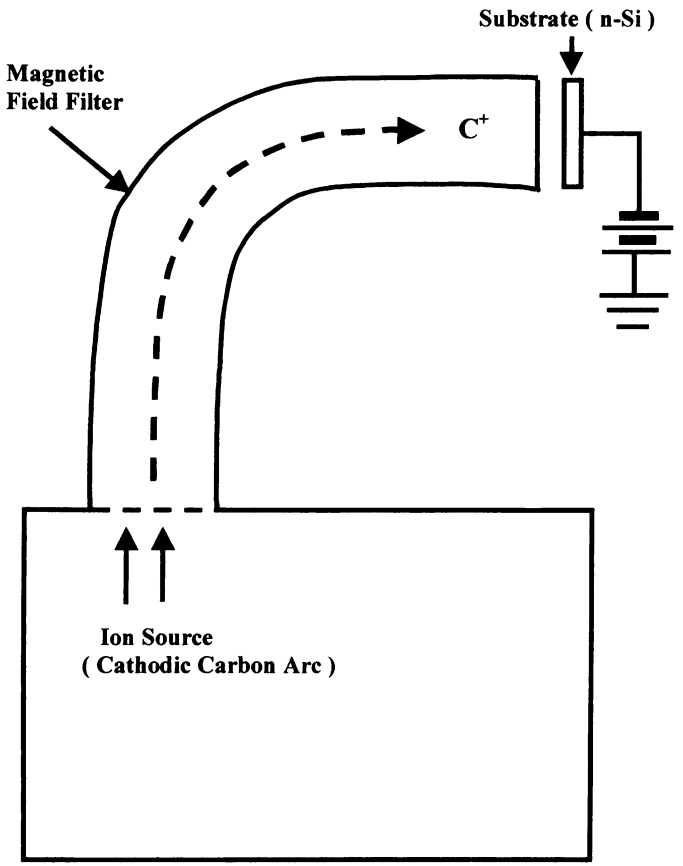

Fig. 2 - 11: Schematic diagram of filtered carbon ion beam system.

substrate with almost 100 % of carbon ions and films grow with mostly carbon ions. The system, however, has a low deposition rate and needs a high vacuum level. The pressure during deposition was 0.01 mTorr. The incident ion energy was varied by applying a negative bias voltage to the substrate. sp^3 fraction, and compressive stress passed through a broad peak at an ion energy of about 120 eV. The density was roughly linear to the percentage of sp^3 bonding.

A mass selected ion beam deposition (MSIBD) method was used to deposit ta-C films by Ronning and his coworkers [19]. The C^+ ions were deposited with energies between 20 eV and 1000 eV in an UHV-deposition chamber in which the pressure was less than 7.5×10^{-6} mTorr. The sp^3 fraction increased rapidly with increasing ion energy at low ion energies and reached a broad maximum with 85 % sp^3 bonded C atoms between 100 and 300 eV. For further increasing ion energies the sp^3 fraction decreased slowly to 55 % for the ta-C films prepared with an ion energy of 1000 eV. They also pointed out that the fraction of sp^3 bonded C atoms of ta-C films deposited with vacuum arc [16] decreased dramatically for ion energies above about 200 eV resulting in sp^2 bonded a-C films. They attributed this sp^3 to sp^2 transition seen for the vacuum arc deposited films to local heating of the films due to a much higher ion flux as compared to MSIBD.

The ECR-CVD (electron cyclotron resonance-chemical vapor deposition) method with a rf powered substrate holder is also used for deposition of a-C:H films. The ECR plasma system excites the plasma through ECR heating which permits operation at relatively low pressure as compared to rf capacitively-coupled discharges. The ECR-CVD method with a rf powered substrate holder has a number of features making it an attractive method [50]. First, microwave ECR plasmas create a high density of ion

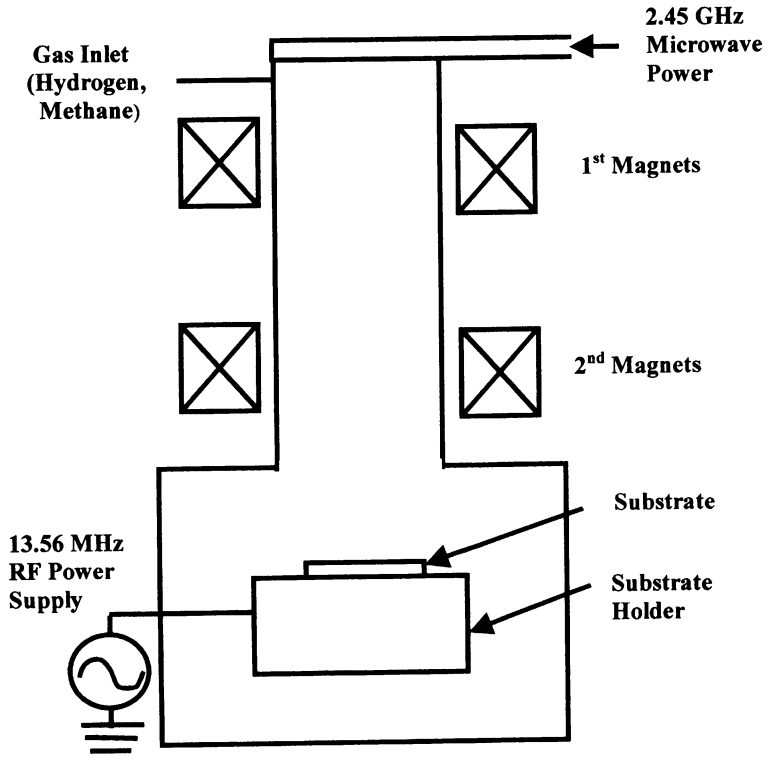

Fig. 2 - 12: Schematic diagram of one type of ECR-CVD system.

species (typically 10^{11}-10^{12} cm^{-3}) at low pressures in the submillitorr to a few millitorr range. This combination of a high ion density with a low pressure (i.e., low neutral density), can produce fluxes of species to the substrate that have a higher ion flux to neutral ratio than capacitively rf coupled systems. The high ion plasma density also yields a faster deposition rate, and the low pressure reduces substrate heating by the neutral gas that assists in maintaining low substrate temperatures during deposition. The substrate bias voltage is readily controlled in ECR-CVD systems by applying a bias to the substrate. Both dc and rf biases have been used [20]. The most versatile approach that permits the use of both conducting and insulating substrates is rf power applied to the substrate holder. Because of the difference in electron current flow and positive ion current flow to the substrate, an induced dc self-bias is produced making the substrate surface negative, which attracts positive ions through the sheath formed between the plasma and the substrate. At the low pressures used in ECR-CVD depositions, the ions cross the sheath and arrive at the film without suffering significant collisions and with a uniform energy produced by the difference in potential between the plasma and the dc induced substrate bias. This use of a microwave ECR plasma source for the plasma generation and a rf power supply for inducing the bias on the substrate allows the ion density and the ion energy to be independently controlled. This control is useful for obtaining desired film properties and for understanding the deposition process.

ECR-CVD systems have used a number of different precursor gases or gas mixtures for the creation of hydrocarbon ions for the deposition of a-C:H films. Pure methane discharges have been used by Zarrabian et. al. [21] at a pressure of 2.6 mTorr, by Kuo, Kunhardt and Srivastsa [22] at pressures of 0.1-0.5 mTorr, by Fujita and

Matsumoto[23] at a pressure of 0.3 mTorr, and by Zeinert et. al.[24] at a pressure of 2.6 mTorr. Mixed methane/hydrogen discharges have been used by Pastel and Varhue [25] at a pressure of 3 mTorr, and by Yoon and coworkers [20, 26, 27] at pressures of 6-15 mTorr. The work by Pool and Shing [28] used a hydrogen gas flow into the plasma generation region and a downstream injection of methane at pressures of 5-55 mTorr. Work by Andry, Pastel and Varhue [29] used both pure benzene and pure methane discharges operating at pressures of 0.3-3.0 mTorr. Another gas mixture utilized was an argon/methane mixture by Kuramoto et. al. [30] in which the argon was injected in the plasma source region and the methane was injected downstream at a pressure of 0.7 mTorr. Yoon and coworkers [20, 26, 27] used a system as shown in Fig. 2-12. They showed that the film hardness increased to a maximum value of ~17 GPa at a substrate bias voltage of -50 V and then decreased thereafter in the range of -50 to -200V substrate bias voltage for the films deposited at 7 mTorr. The optical gaps, E_{04}, of the films decreased rapidly to a minimum (~2.4 eV) at -50 V and then increased slightly thereafter. The IR spectra suggested that the intensity of the C-H absorption peak (bonded hydrogen content) decreased as the induced substrate bias increased. In general, a clear understanding of the ECR-CVD deposition process for a-C:H films is lacking and different researchers using different ECR systems often get different results.

Table 2-2 compares selected deposition parameters of several deposition methods. RF plasma assisted techniques are operated at high pressure and have low ion density, and these give a low ion flux to neutral flux ratio onto the substrate. The advantage of the rf plasma assisted methods is that relatively high deposition rates on a large area are possible. And the disadvantage is that it is hard to control the substrate bias and input

power independently [12]. The ECR plasma methods have higher ion density and are operated at lower pressure, which give a higher ion flux to neutral flux ratio onto the substrate. The advantage of ECR plasma methods is that they have high deposition rates and good control of the substrate bias and the substrate position relative to plasma. Filtered ion beam and plasma beam methods have very high ion flux ratios onto the substrate, but the ion flux to the substrate is low resulting in low deposition rates.

Table 2 - 2: Comparison of deposition methods

Method	Ion Density (cm^{-3})	Pressure (mTorr)	Neutral Density (cm^{-3})	Ion Flux/ Neutral flux	Electron Temp. (eV)	Dep. Rate (nm/min)	Ref.
RF CVD	10^{9}~10^{11}	10~1000	$3x10^{14}$ ~$3x10^{16}$	~10^{-4}	1~5	~20	[14, 48]
ECR Plasma	10^{10}~10^{12}	0.5~15	$1x10^{12}$ ~$5x10^{14}$	~10^{-2}	2~7	~50	[20, 48]
Filtered Ion Beam		0.01		~1		low	[16]
Plasma Beam		0.037		0.95		15	[3]

Chapter 3

3. The Film Deposition System and Film Characterization Methods

3.1 Introduction

The hydrogenated amorphous carbon films of this investigation were deposited with a multipolar electron cyclotron resonance (ECR) microwave-cavity discharge system. In this chapter, the basic principle of electron cyclotron heating is explained and the multipolar electron cyclotron resonance microwave-cavity discharge deposition system is described. This system includes a microwave cavity, a baseplate, a microwave power unit, a deposition chamber, a substrate holder biased with a rf power supply unit, pressure gauges, etc. The methods used to characterize the properties of discharges in the reactor are also described. This chapter then describes pre-deposition preparation of substrates, and the treatment of samples after deposition. Next, characterization methods of the properties of the films are described and explained. The properties of films characterized include thickness of films, mass density, hydrogen content, index of refraction and optical bandgap.

3.2 Electron Cyclotron Resonance

Microwave ECR discharge systems can generate high densities of plasma at low pressure with low neutral gas temperature. This capability of microwave ECR systems yields applications in etching and thin film deposition. In this section, the basic principles of an ECR discharge are explained. The microwave power source provides the deposition system with the energy to maintain the discharge in the microwave ECR system. The

electrons are heated by the microwave energy through the ECR effect in the system. Then the heated electrons ionize, dissociate and excite the species of gases maintaining the discharge inside the discharge chamber. The ECR heating of electrons occurs when the frequency of the microwave energy, ω, is equal to the electron cyclotron frequency ω_{ce} somewhere in discharge region. That is,

$$\omega = \omega_{ce} \tag{3-1}$$

The electron cyclotron frequency is expressed as

$$\omega_{ce} = \frac{qB}{m_e} \tag{3-2}$$

where q is the electron charge, B is an externally applied magnetic field strength, and m_e is electron mass.

The principle of ECR heating of electrons is illustrated in Fig. 3-1 [51]. The electric field vector of the microwave fields can be decomposed into the sum of a right hand polarized (RHP) vector and a left hand polarized (LHP) vector. As shown in Fig. 3-1, a steady state RHP electric field $\boldsymbol{E}$ is directed in the xy plane and an uniform magnetic field $\boldsymbol{B}$ is applied externally along the z direction. Then an electron in the magnetic field gyrates in a right hand direction at the frequency of ω_{ce}. Each figure, (a), (b), (c) and (d) in Fig. 3-1 represents electron motion and direction change of the right hand polarized electric field of the microwave in every one quarter period. With the frequency of the microwave given by, $\omega = \omega_{ce}$, for the right hand polarized wave and an electron, the force, $-q\boldsymbol{E}$ continuously accelerates the electron in the direction of the motion of the electron. Thus, the electron gains energy continuously. For the left hand polarized electric field, the force, $-qE$ is parallel to the motion of electron for the first one quarter period and the

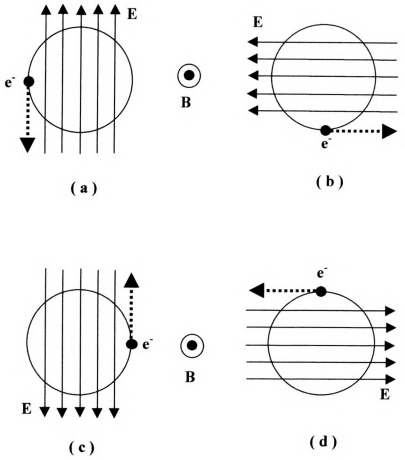

Fig. 3 - 1: Principle of ECR heating. The electron gains microwave energy continuously.

third one quarter period and opposite for the second one quarter period and the fourth one quarter period. Thus, the electron energy oscillates with no time average energy gain for the left hand polarized electric field of the microwave. From the figure, it can be seen that the efficiency of ECR heating is maximized when the electric field of the microwave, ***E***, and the externally applied magnetic field, ***B***, are perpendicular. The microwave frequency is usually 2.45 GHz. Thus, the strength of the magnetic field is obtained to be 875 Gauss for the ECR heating from equations (3-1) and (3-2).

3.3 Deposition System and Conditions

3.3.1 Description of the Deposition System

Hydrogenated amorphous carbon (a-C:H) films in this investigation were deposited using a microwave ECR deposition system as shown in Fig. 3-2 [52-59]. The main parts of the system consist of a cylindrical microwave cavity, a deposition chamber, a baseplate between microwave cavity and deposition chamber, a substrate holder, a pumping system, a microwave power supply unit, an rf power supply unit, and a gas supply unit [60, 61]. The side view of the microwave cavity, baseplate, and deposition chamber parts is shown in detail in Fig. 3-3. The diameter of the cylindrical microwave cavity (L_c) is fixed at 17.6 cm and its height (L_s) is changeable to tune the microwave cavity. The cylindrical quartz dome inside the microwave cavity has dimensions of 9 cm diameter (L_q) and 5 cm height (L_h). The baseplate consists of the upper and the lower parts. The heights of upper part (L_m) and lower part (L_b) are 2.0 cm and 2.8 cm, respectively. s.p. in the figure designates the distance between the bottom of the baseplate and the substrate and is varied to give ion flux variation onto the substrate.

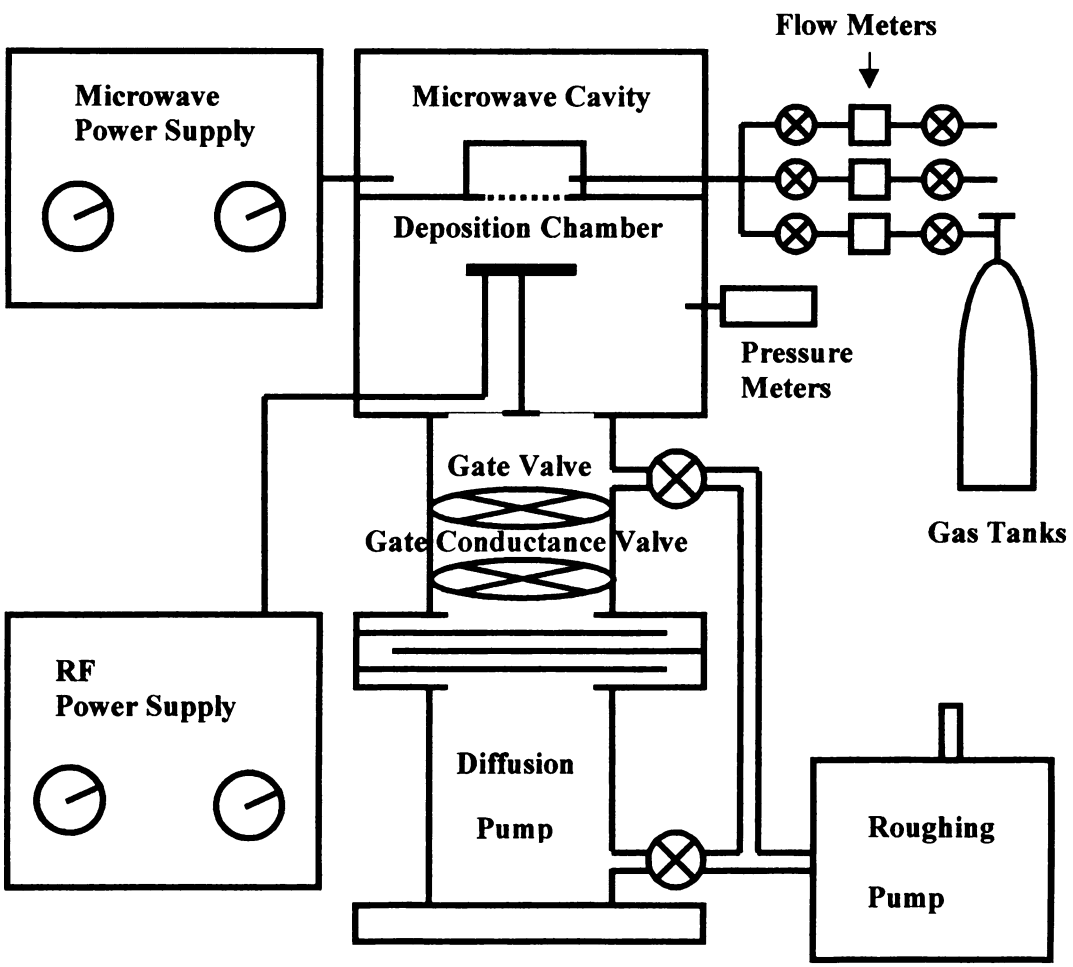

Fig. 3 - 2: The microwave ECR plasma source with the rf biased substrate holder.

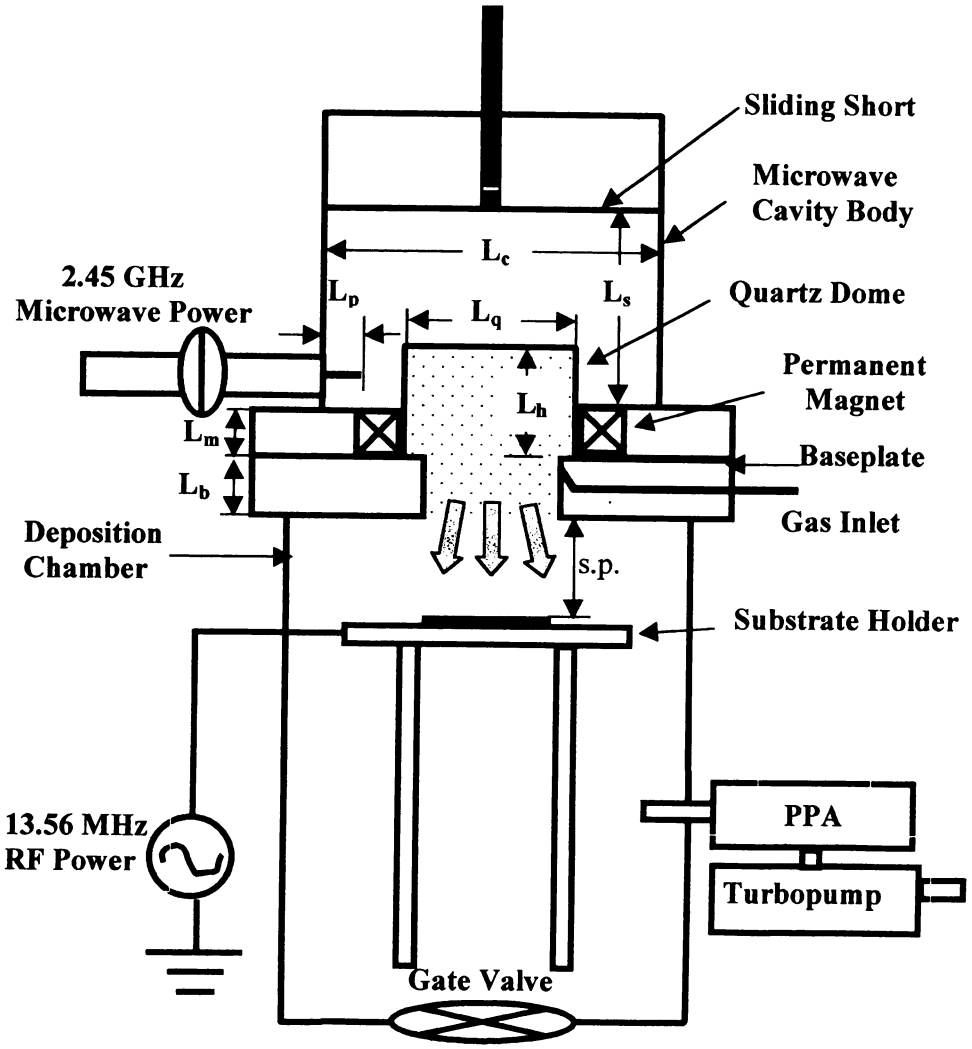

Fig. 3 - 3: The side view of the microwave cavity, the baseplate, and the deposition chamber of the system.

The length of the microwave antenna probe (L_p) is changeable to match the impedance between the microwave source and the microwave cavity. The substrate holder is a rectangular and has dimensions of 10.5 cm x 5.0 cm.

The cylindrical microwave cavity intensifies a specific microwave mode in it and the intensified microwave energy produces the plasma of the feed gases in a cylindrical quartz dome inside the cavity via the ECR heating effect. The microwaves are introduced into the cavity through a microwave antenna that is the core part of the coaxial transmission line and is inserted through the side of the microwave cavity. The impedance of the microwave source unit is matched to that of the microwave cavity by adjusting the height of the microwave cavity (L_s) and the length of the microwave antenna (L_p). The microwave source unit generates microwave energy, controls the power of the microwaves and sends the microwaves to the microwave antenna via waveguides. The microwave source unit consists of a microwave power supply (Model 4074, Thermex INC.), a microwave power source controller (Model 4006, Thermex INC.) and two microwave power meters (Model 432A, Hewlett Packard). The microwave power meters measure the incident microwave power to the microwave cavity and the reflected microwave power from the microwave cavity. The net power that generates the discharge inside the quartz dome is the incident power minus the reflected power.

The gas supply unit sends and controls the flow rate of source gases of a-C:H films from gas tanks into the quartz dome. It consists of three flow meters, three flow controllers (MKS Instruments INC.) and gas tanks so that three kinds of gases can be provided into the deposition system simultaneously. The rf power supply unit is connected to the substrate holder inside the deposition chamber and provides the

substrate with the rf induced substrate negative bias. The rf induced substrate bias provides ion with ion bombardment energy on the surface of growing films and its determination will be discussed later in this section. It has the rf power supply (HFS-500E, Plasma-Therm INC) and a matching network which matches the 13.56 MHz rf power from the rf power supply to the substrate holder. The substrate holder has a heater so that the deposition temperature can be raised. However it has no active cooling, so the temperature of the substrates increase some during the deposition even when the heater is turned off. For example, the temperature increased 80-100 °C for 5 minutes of deposition at 3 mTorr pressure. The height of the substrate holder can be varied so that the distance of the substrate from the region of plasma generation (or, from the bottom of base plate) can be changed. The increasing distance will decrease the ionic flux of species to the substrate. A typical value used is 3.5 cm below the bottom of the baseplate. To measure the pressure in the deposition chamber, a capacitance manometer (Type 627, MKS Instruments INC.) and a hot cathode pressure gauge with yttrium coated iridium filaments (MKS Instruments INC.) are used. The capacitance manometer can determine the pressure from 0.1 mTorr to 100 mTorr and is used to measure the discharge pressure of the deposition chamber. The pressure controller (Type 651, MKS Instruments INC.) reads the capacitance manometer and controls the gate conductance valve to achieve the desired deposition pressure. The hot cathode pressure gauge, which can measure pressure levels of microtorrs, is used to measure base vacuum level and is used to calibrate/zero the capacitance manometer. The hot cathode controller (Type 919, MKS Instruments INC) is used to read the hot cathode pressure gauge.

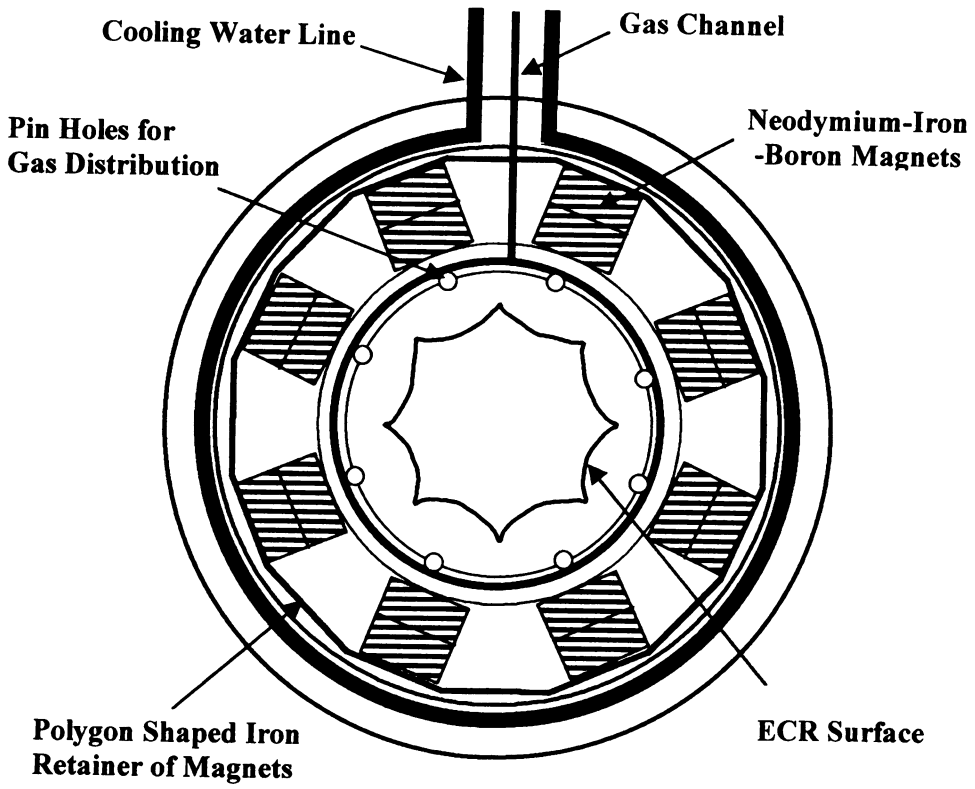

Fig. 3 - 4: The cross section (top view) of the baseplate of the system.

The plasma used to deposit the films is generated in the region of the baseplate via ECR heating. The baseplate is illustrated in Fig. 3-3 and Fig. 3-4. The baseplate consists of upper and lower parts. The upper part has eight neodymium-iron-boron-magnets providing the magnetic field needed for the ECR coupling. The north and south poles of magnets are alternated toward the discharge region and the ECR surface on which ECR coupling occurs is drawn qualitatively in Fig. 3-4. The lower part has eight pin holes for gas distribution. The holes are designed to eject the gas upward so the ejected gas travels through the ECR zones and then diffuses downward to the substrate. The plasma discharge can produce a lot of heat so the baseplate also has a water line to cool the plate.

3.3.2 Deposition Conditions

The microwave ECR system generates a high density of plasma (typically 10^{10}-10^{12} cm^{-3}) through ECR heating at low pressures in the submillitorr to a few millitorr range. This combination of a high ion density with a low pressure (i.e., low neutral density), can produce fluxes of species to the deposition substrate that have high ion flux to neutral flux ratio. The system is operated with 200-400 W input microwave power to create plasma inside the quartz dome. The range of rf induced substrate bias was varied from 0 V to -300 V. The gases injected include primarily acetylene, methane-argon or acetylene-argon mixtures with total flow rates ranging from 7-20 sccm. The argon flow rate is varied from zero to 50% of the total flow rate. The plasma diffuses into the deposition chamber where a rf biased substrate holder is located. The diffusion is designated with the thick arrows in Fig. 3-3. The specific pressure range in this study is

0.2 to 5 mTorr. These pressure values insure that the ions moving through the sheath experience no significant collisions.

3.3.3 Sample Preparation

In this study the substrates used are glass of either 76mm x 25 mm x 1 mm or 12 mm x 12 mm x 0.1 mm in size and pieces of silicon wafers. The glass substrates are cleaned in methyl alcohol using an ultrasonic cleaner for 90 minutes and then rinsed in deionized water for 30 minutes before deposition. For some cases, the glass substrate of 0.1 mm thickness is mounted on the substrate holder using a heat conducting paste on the substrate holder side of the substrate. This helps to get a good thermal contact between the substrate and the substrate holder keeping the temperature of a substrate low. The sample with the heat conducting paste is cleaned again after deposition in methyl alcohol for 90 minutes and then rinsed in deionized water for 30 minutes to remove the heat conducting paste.

3.4 Characterization of Discharge Properties

The discharge properties such as electron temperature, plasma density and saturation ion current of acetylene, methane-argon and acetylene-argon discharges generated in the microwave ECR plasma reactor are characterized by using a double Langmuir probe. The plasma sheath thickness above the substrate and ion energy onto the substrate are estimated with the electron temperature, the plasma density and the rf induced substrate bias using either the matrix sheath potential theory or Child Law sheath potential theory. The gas composition of exit gas from the discharge chamber are analyzed with a partial pressure analyzer (PPA), MKS 600A-PPT.

3.4.1 Double Langmuir Probe Measurement

The double Langmuir was used to measure the electron temperature and ion saturation current for several deposition conditions. The double Langmuir probe has two metal probes 0.5 mm in diameter and 5 mm long. The probes are separated by 3 mm. The Langmuir probe measurements were taken at the substrate position, which was 8.5 cm below the top of the quartz dome that con fines the plasma. The electron temperature of discharge is determined from the I-V curve of double Langmuir probe measurement using the below equation [51].

$$T_e = \frac{I_{ion}}{2}\left(\frac{dI}{dV}\Big|_{V=0}\right)^{-1} \qquad (3\text{-}3)$$

where I_{ion} is the ion saturation current of the I-V curve. The plasma density is obtained from the ion saturation current and electron temperature using the following equation [51].

$$n_0 = \frac{I_{ion}}{0.61eA}\left(\frac{M}{kT_e}\right)^{1/2} \qquad (3\text{–}4)$$

where e is the electron charge, A is surface area of the probe, k is Boltzman constant and M is theion mass of the discharge. The substrate position was also 3.5 cm below the plasma source opening (see Fig. 3-3). At this position the ECR static magnetic field is low and does not interfere with the Langmuir probe measurements.

3.4.2 Determination of Ion Energy and Ion Flux

The ion bombardment energy onto the substrate and the ion flux to neutral flux ratio are important factors for determination of film properties in the deposition process

as discussed in Chapter 2. The ion bombardment energy onto the surface of growing films is determined by the potential difference between the plasma and the substrate. This difference is determined primarily by the rf induced dc bias ϕ_{rf} of the substrate holder. The induced dc bias on the substrate is measured with respect to the chamber wall potential. The actual ion energy is the induced dc bias energy gain plus the potential difference between the plasma and chamber walls. As a measure of this plasma-to-chamber wall difference, the plasma potential with respect to the chamber wall potential id estimated from the plasma sheath potential when the electron and positive ion fluxes to the wall are equal. This condition of equal fluxes occurs when the surface is at the floating potential. This potential between the plasma and an electrically floating wall is

$$\phi_w = C(M_i)\frac{kT_e}{e} + \frac{kT_e}{2e} \qquad (3\text{-}5)$$

where T_e is the electron temperature, e is the electron charge, k is Boltzmann's constant, and $C(M_i)$ is a constant that depends on the ion mass [51]. For example, C=2.8 for the hydrogen ion, 4.2 for the methane ion, 4.5 for the acetylene ion and 4.7 for the argon ion. A potential difference may also exist between the floating potential of a surface in the substrate holder region and the other chamber surfaces. This is due to: (1) ambipolar diffusion effects producing spatial variations in the plasma potential, and (2) variations in the electrical contact of the plasma to the various surfaces resulting from insulating/partially conducting films on the surfaces that can change versus processing history. Hence the energy of the ions is the energy gained due to the induced substrate bias ϕ_{rf} plus the plasma sheath potential between the plasma and the chamber walls ϕ_w plus the potential difference between the floating potential at the substrate location and the chamber walls ϕ_{diff}. The rf induced dc bias is measured by connecting a low pass filter

to the rf power supply output to provide a dc signal to a voltmeter. The sheath potential of equation. (3-5) is determined from the electron temperature, whose measurement is described in the next section. Finally, the potential ϕ_{diff} at the substrate location is measured by inserting a small sputter cleaned probe at the substrate location and measuring the potential between the probe and the chamber walls. Typical values measured for this potential ϕ_{diff} were 2-10 V. Its value depends on both the plasma operating conditions and the history of previous depositions and cleanings of the chamber walls. The rf induced substrate bias was varied from 0 to -300 V in this study.

The actual ion energy on the surface of the substrate will be smaller than the value of $|\phi_{rf}|+\phi_w+\phi_{diff}$ discussed in the above paragraph because the insulating glass substrate has finite thickness in the plasma sheath. The potential on the surface of plasma side of the substrate is the potential of $|\phi_{rf}|+\phi_w+\phi_{diff}$ minus the potential between the surface of the substrate and the substrate holder. The potential on the surface of the substrate can be obtained from the potential of $|\phi_{rf}|+\phi_w+\phi_{diff}$, the thickness of plasma sheath and the thickness of the substrate. The thickness of plasma sheath and the potential at the surface of the substrate are calculated using either the matrix sheath or Child Law sheath given in the below equations [51]. For the matrix sheath,

$$\Phi(x) = -\frac{en_s}{\varepsilon_o}\frac{x^2}{2} \qquad (3\text{-}6)$$

and for Child Law sheath,

$$\Phi(x) = -\left(\frac{3}{2}\left(\frac{en_s u_B}{\varepsilon_o}\right)^{1/2}\left(\frac{2e}{M}\right)^{-1/4} x\right)^{4/3} \qquad (3\text{-}7)$$

where n_s is the plasma density at the sheath edge ($n_s=0.61n_o$), u_B is Bohm velocity ($u_B=(kTe/M)^{1/2}$), and M is the mass of the ion. The plasma density, n_0 and the electron temperature, T_e were measured using a double Langmuir probe. The plasma sheath thickness is calculated, then the potential at the suface of the substrate is calculated using the above equations.

The ion flux to neutral flux ratio onto a substrate is estimated by calculating the neutral flux using the discharge pressure and temperature and the ion flux from the measurement of ion current density of the substrate holder. The neutral flux was calculated with the equation:

$$\Gamma_n = \frac{1}{4} n_g < v > \qquad (3\text{-}8)$$

where n_g is the neutral density calculated from $p=nkT$, and $<v>$ is an average neutral velocity in the discharge given by $<v>=(8kT/\pi M)^{1/2}$. The ion current density of the substrate holder was measured by applying DC bias on the substrate holder in a discharge and measuring the DC current. The ion flux, Γ_i was estimated by dividing the ion current density by the electron charge. Then the ion flux to neutral flux ratio is Γ_i/Γ_n.

3.4.3 Partial Pressure Analysis of Exit Gas and Temperature Measurement

The partial pressure analyzer (PPA) is used to measure the composition of the exit gas. The sampling point is near the bottom of the processing chamber where the residual exit gas is pumped out as shown in Fig. 3-2. The chamber gas composition was sampled by connecting a 6 mm diameter tube from the chamber to a turbomolecular pump/PPA unit. The partial pressures reported in this investigation are the pressures measured at the PPA location; hence they are lower than the chamber pressure. The relative partial

pressures at the PPA location are assumed to be representative of the species concentration in the chamber. The substrate temperature was measured with an F-type thermocouple. The thermocouple was attached to the substrate using a heat conducting paste to keep it a good thermal contact with the substrate and no direct contact with the discharge gas.

3.5 Characterization of a-C:H Films

For the determination of the deposited film's thickness, optical absorption coefficient and refractive index, the transmission and reflection data of light is measured by using a visible-near infrared spectrometer for the wavelengths of 400-1600 nm. The spectrometer is illustrated in (a) of Fig. 3-5. In the figure, the Xe-Hg arc lamp is used for the light source. The arc lamp igniter (model 68705, Oriel Corporation) ignites the lamp and the arc lamp supply (model 68700, Oriel Corporation) is used to give the lamp power. The monochromator (model 77200, ¼ M – 2 nm, Oriel Corporation) selects a specific light of wavelength. The interval of wavelengths was chosen to be 20 nm. The photosensor (model 814-SL silicon detector for light of 400-1000 nm, and model 818-IR germanium detector for the light of 800-1600 nm, Newport Corporation) is used to detect the transmitted and reflected light from the film. The optical power meter (model 835, Newport Corporation) measures the power of the light that is detected with the photosensors. The lens of focal length L_1 (16 cm) focuses the light into the entrance slit S_1 (fixed at 600 μm) of the monochromator, the lens of focal length L_2 (1.5 cm) focuses the light from the slit S_2 (700 μm) on the substrate which has the film to be characterized and the lens of focal length L_3 (1.5 cm) collects the light into the sensor of the photometer. The filter F_1 preselects some spectral band of light to remove the second

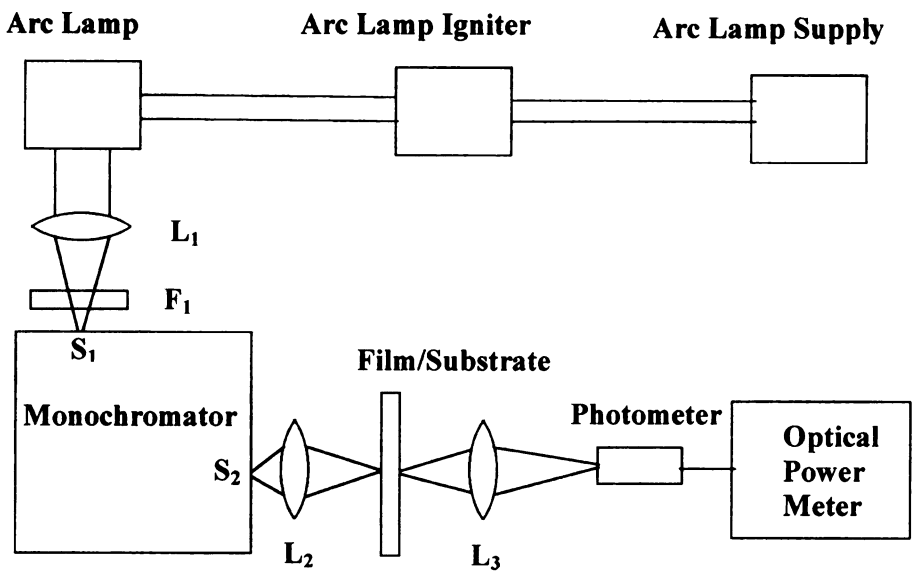

(a)

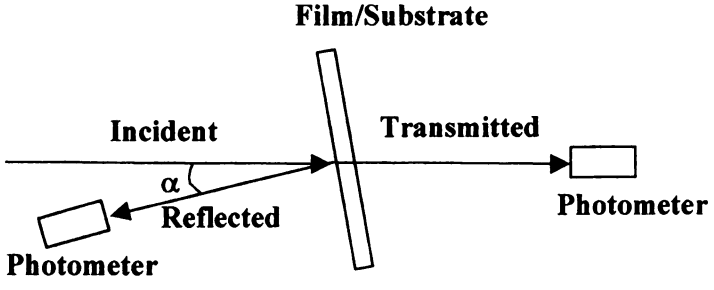

(b)

Fig. 3 - 5: (a) The spectrometer used to measure the transmittance and reflectacnce of the films and (b) the tilted angle needed to measure the reflected beam.

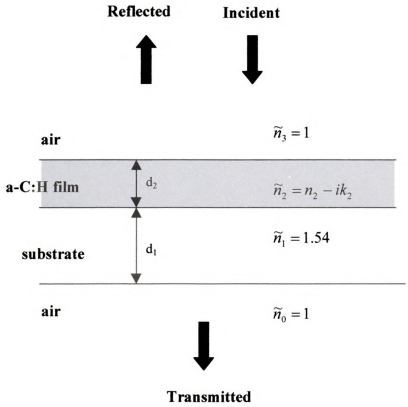

Fig. 3 - 6: The measurement of transmittance and reflectance of light for an a-C:H film on glass substrate.

order wavelength of light from the monochromator. Three different filters are used and their preselecting bands are 400-650 nm, 650-1000 nm and 850-1600 nm. The incident light is not exactly normal to the surface of the film, but slightly tilted to measure the reflected beam. The tilted angle, α between the incident and reflected beams is illustrated in (b) of Fig. 3-5 and is about 15°.

The transmittance and reflectance of an a-C:H film deposited on a glass substrate is shown schematically in Fig. 3-6. The equations [62] describing the transmittance T and the reflectance R in terms of the quantities defined in Fig. 3-6 are

$$T = \frac{n_1}{n_3}\left|t_1\right|^2 \frac{1-r_{10}^{\ 2}}{1-\left|r_1'\right|^2 r_{10}^{\ 2}} \tag{3-9}$$

$$R = \left|r_1\right|^2 + \frac{\left|t_1\right|^4 r_{10}^{\ 2}}{1-\left|r_1'\right|^2 r_{10}^{\ 2}} \tag{3-10}$$

where

$$t_1 = \frac{t_{32}\exp(i\beta_2)t_{21}}{1-r_{23}r_{21}\exp(-2i\beta_2)}$$

$$r_1 = \frac{r_{32}+r_{21}\exp(2i\beta_2)}{1-r_{23}r_{21}\exp(-2i\beta_2)}$$

$$r_1' = \frac{r_{12}+r_{23}\exp(2i\beta_2)}{1-r_{23}r_{21}\exp(-2i\beta_2)}$$

and

$$r_{10} = (\tilde{n}_1-\tilde{n}_0)/(\tilde{n}_1+\tilde{n}_0)$$

$$r_{21} = (\tilde{n}_2-\tilde{n}_1)/(\tilde{n}_2+\tilde{n}_1)$$

$$r_{12} = -r_{21}$$

$$r_{32} = (\tilde{n}_3-\tilde{n}_2)/(\tilde{n}_3+\tilde{n}_2)$$

$$r_{23} = -r_{32}$$

$$t_{10} = 2\tilde{n}_1/(\tilde{n}_1 + \tilde{n}_0)$$

$$t_{21} = 2\tilde{n}_2/(\tilde{n}_2 + \tilde{n}_1)$$

$$t_{32} = 2\tilde{n}_3/(\tilde{n}_3 + \tilde{n}_2)$$

$$\beta_2 = 2\pi\tilde{n}_2 d_2 / \lambda$$

The indices of refraction are

$\tilde{n}_0 = 1$ for air,

$\tilde{n}_1 = 1.54$ for the glass substrate,

$\tilde{n}_2 = n_2 - i\kappa_2$ for the a-C:H film and

$\tilde{n}_3 = 1$ for air

$\tilde{n}_2$ is the complex index of refraction of the deposited film where n_2 is the conventional real index of refraction and κ_2 is the extinction coefficient of the films. For the measured transmittance, T and reflectance, R, n_2 and κ_2 are found from the above equations of T and R. The nonlinear equations of (3-9) and (3-10) are solved by using the command of 'fsolve' in Matlab. Then the absorption coefficient, α, is also found from the extinction coefficient, κ_2, with the following equation,

$$\alpha = \frac{4\pi\kappa_2}{\lambda} \qquad (3\text{-}11)$$

An example of the measured transmittance and reflectance is shown in Fig. 3-7. The thickness and index of refraction are determined by comparing the measured reflectance of light with a modeled reflectance found by choosing appropriate film

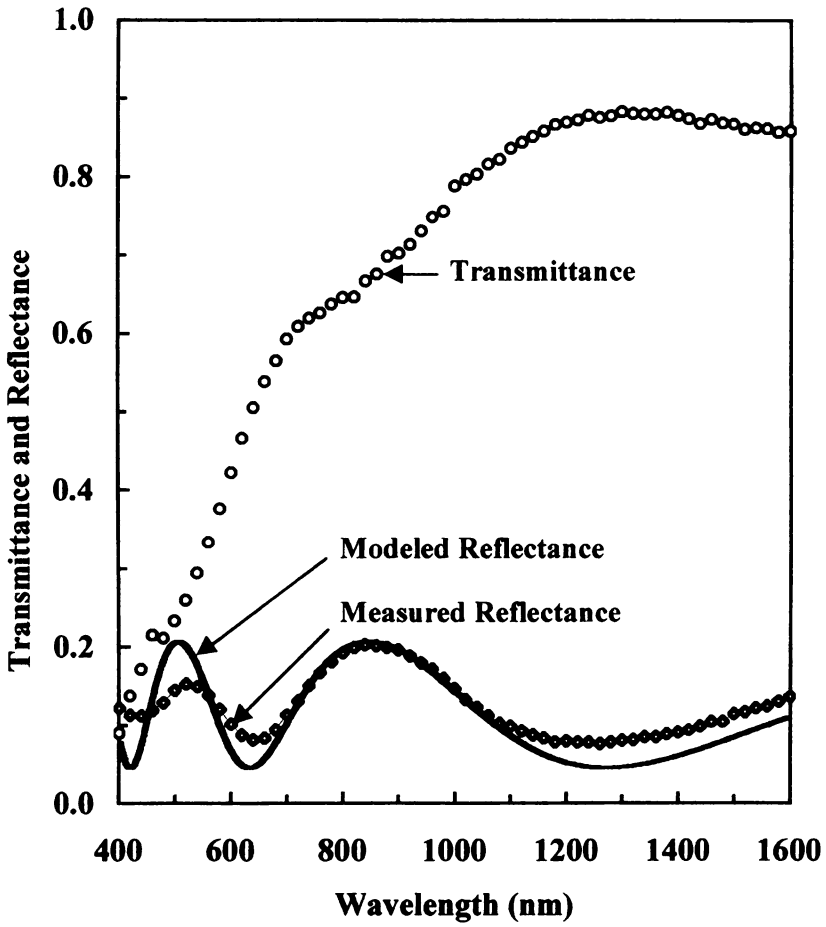

Fig. 3 - 7: The transmittance and reflectance of an a-C:H film versus wavelength. The modeled reflectance data is simulated for the determination of thickness and index of refraction of the film.

thickness and index of refraction values. The thickness of films is mainly determined by the periodicity of the reflectance and the index of refraction by the amplitude of the reflectance At the shorter wavelengths the oscillating amplitude of reflection data is faded due to the absorption of light by the a-C:H film. The modeled reflectance is not faded because the absorption of light is not considered in the model. In the example of Fig. 3-7, the modeled value of thickness and the index of refraction are 310 nm and 2.4, respectively. The thickness can be determined within 10 % error bound of its value. Then, the thickness is returned to equations of (3-9) and (3-10) for the calculation of the extinction coefficient, κ_2 and index of refraction, n_2 with the variation of the light frequency. Thickness was also checked on several films using SEM cross- sections. An example of a SEM cross-section is shown in Fig. 3-8. The thickness from the optical method coincides with that of the SEM picture within 10 %. The absorption coefficient versus wavelength is calculated from equation (3-11) for films whose thickness is less than 300 nm. Fig. 3-9 and Fig. 3-10 show typical plots of the index of refraction and absorption coefficient of the film versus photon energy which are found by using equations (3-9) and (3-10).

However the above procedure to find n_2 and κ_2 does not work for the films whose thickness is more than 300 nm because the command 'fsolve' in Matlab has difficulty to find the convergence point of the solutions. Thus, for thicker films an alternative simplifed equation is used to find the absorption coefficient, α, from the measured transmittance, T, and reflectance, R. The simplified equation is expressed as

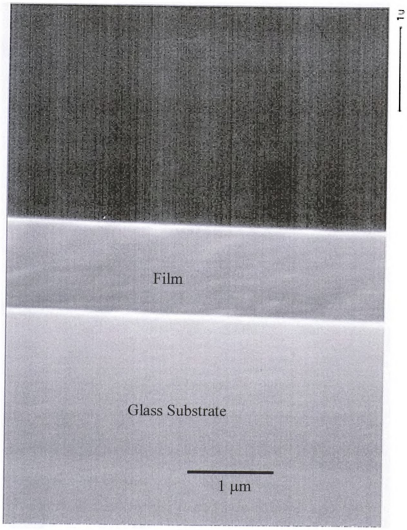

Fig. 3 - 8: An example of a SEM cross-section for determination of thickness of the film.

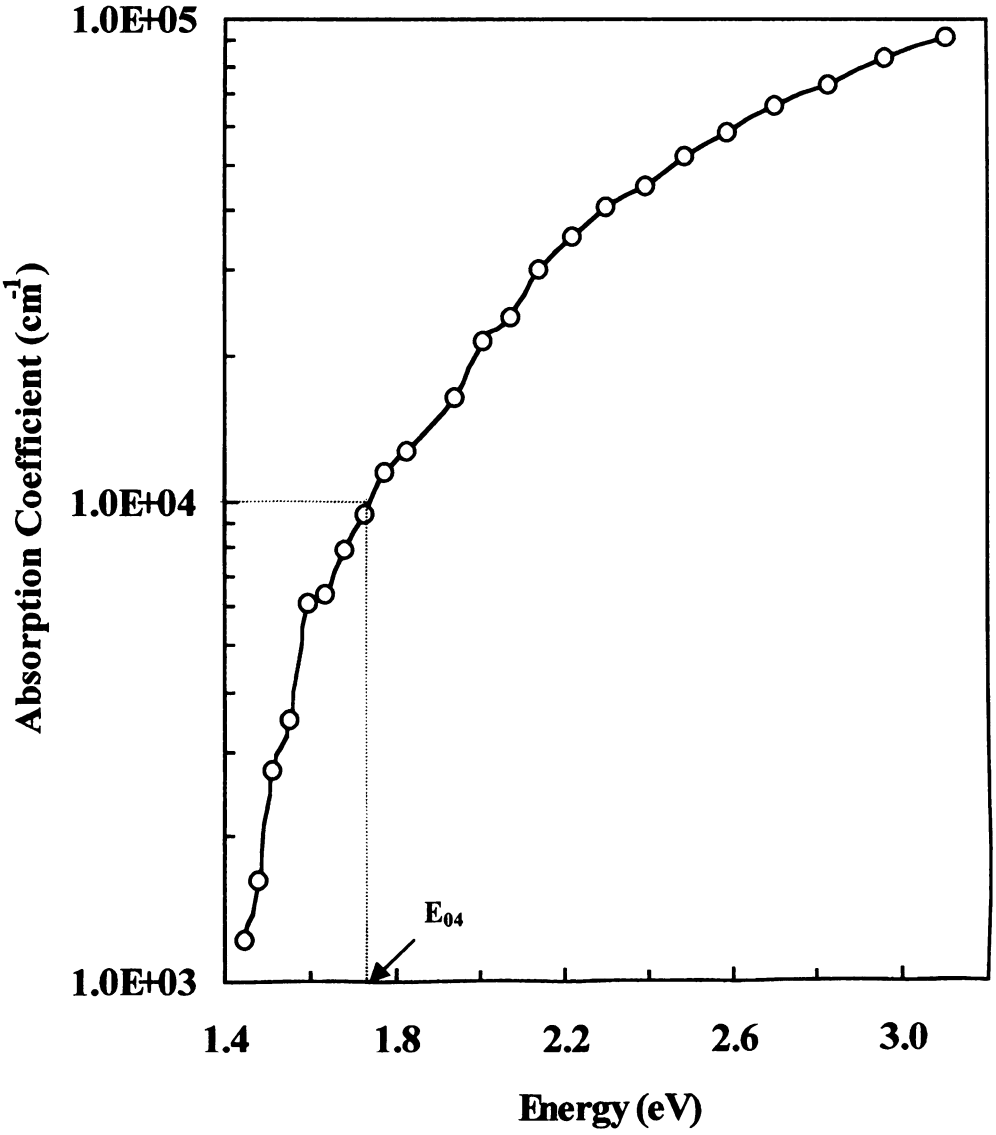

Fig. 3 - 9: Absorption coefficient of an a-C:H film versus photon energy.

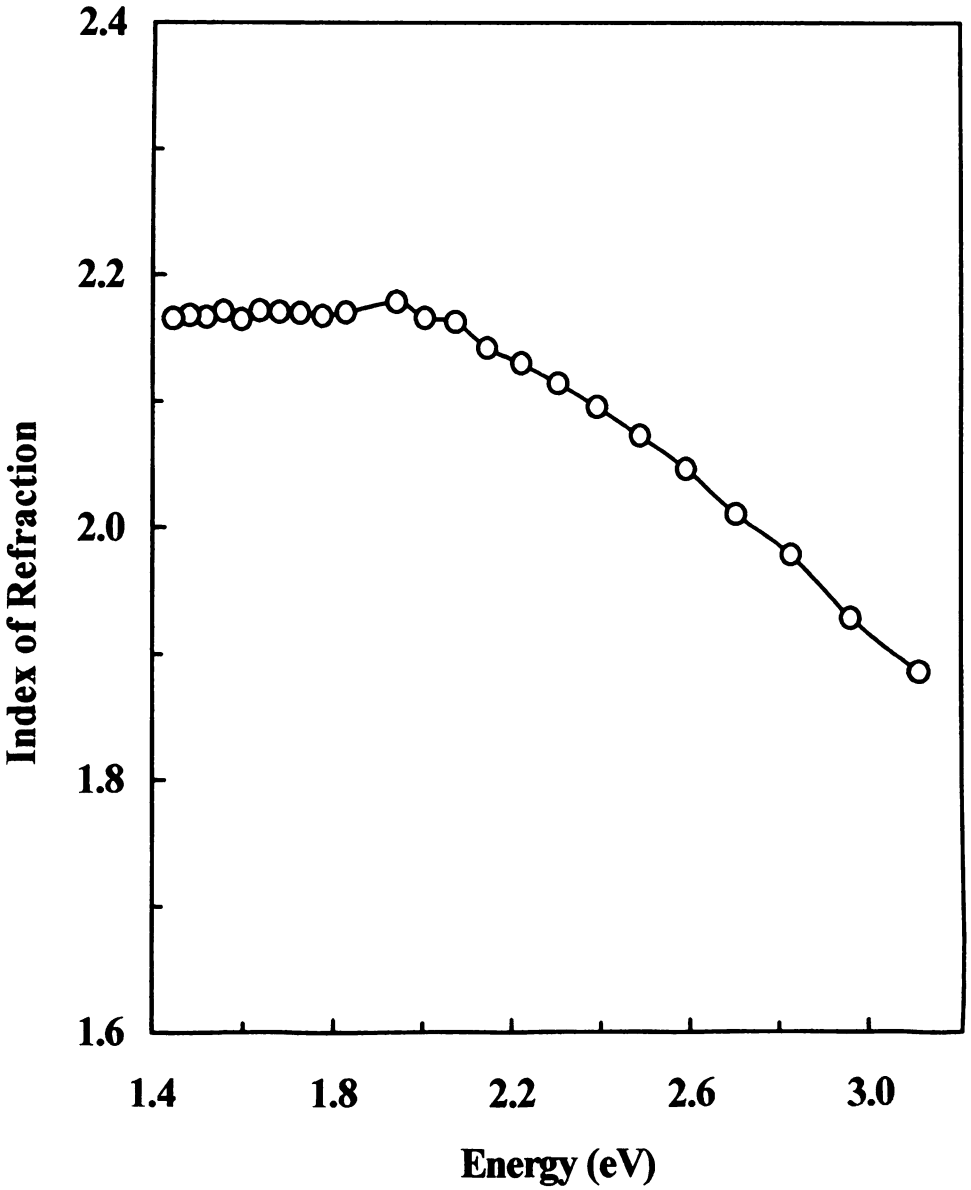

Fig. 3 - 10: Refractive index of an a-C:H film versus photon energy.

$$T = (1 - R)\exp(-\alpha d) \qquad (3 - 12)$$

where d is film thickness. The index of refraction is found using the amplitude of reflectance in Fig. 3-7 and the below equation.

$$R = \left(\frac{n_2 - 1}{n_2 + 1}\right)^2 \qquad (3\text{-}13)$$

The index of refraction, thus, is an average value over the light frequency of the measurement.

The E_{04} bandgap is determined by reading the photon energy at $\alpha=10^4$ cm^{-1} in the absorption versus photon energy plot (see Fig. 3-9). Tauc optical gap is derived from the absorption coefficient using a Tauc plot [62]. It is often observed in semiconducting glasses that at high absorption levels ($\alpha>10^4$ cm^{-1}) the absorption constant, α, has the following frequency dependence:

$$h\nu\alpha = A(h\nu - E_{tauc})^2 \qquad (3\text{-}14)$$

where A is a proportional constant, h is Plank's constant, ν is angular light frequency, and E_{tauc} is the Tauc optical bandgap. From the above relation the Tauc plot can be drawn as in Fig. 3-11. The Tauc optical bandgap is then the energy (1.3 eV in the Fig. 3-11 example) at the point that the linear fit meets the x-axis.

The density of the films was determined by measuring the mass difference of the virgin substrate before deposition and the film deposited substrate after deposition using a Denver Instrument M-220D balance. The balance has 31 g of maximum capacity, 1.0 mg of minimum capacity and 0.01 mg of readibility. The glass substrate samples used for mass measurements were 1.4 cm^2 and 0.17 mm thick. The mass change was typically

0.15-0.3 mg for the films deposited at pressures in the millitorr range. The mass density was determined from the measured mass of the film and its volume. Since both the thickness measurement and the mass measurement have uncertainties of 5-10 %, the uncertainty in the mass density measurement is 10-20 %.

For determination of the hydrogen content of a-C:H films, the infrared spectra for the region from 2800 cm^{-1} to 3200 cm^{-1} was obtained by using a Beckman IR 4220 spectrometer. The infrared absorption coefficient is derived from the transmission spectra and thickness data with equation (3-12). The typical absorption coefficient as function of wavenumber is shown Fig. 3-12. The peak C at 2956 cm^{-1} is due to sp^2-CH_2 (olefinic) bonds, the peak B at 2920 cm^{-1} is due to the sp^3-CH_2 asymmetric stretching mode bonds, and the peak A at 2870 cm^{-1} is due to the sp^3-CH_3 symmetric stretching mode bonds [63]. The infrared absorption coefficient is used to determine the bonded hydrogen content of the a-C:H films using the equation [64],

$$n_H = A\int\frac{\alpha}{\omega}d\omega \qquad (3\text{-}15)$$

where n_H is hydrogen content in cm^{-3}, A is equal to $(1.35 \pm 0.3) \times 10^{21}$ cm^{-1} [65], α is the absorption coefficient and ω is the infrared light frequency. The hydrogen content in atomic percentage was obtained from the hydrogen content and the mass density of the film as follows:

$$\rho = \frac{X_H + X_C}{N_a} \qquad (3\text{-}16)$$

$$H = \frac{X_H}{X_H + X_C} \times 100 \qquad (3\text{-}17)$$

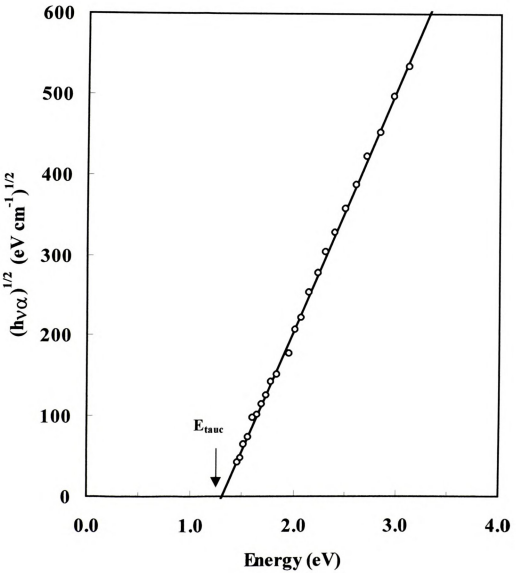

Fig. 3 - 11: Tauc plot of an a-C:H film.

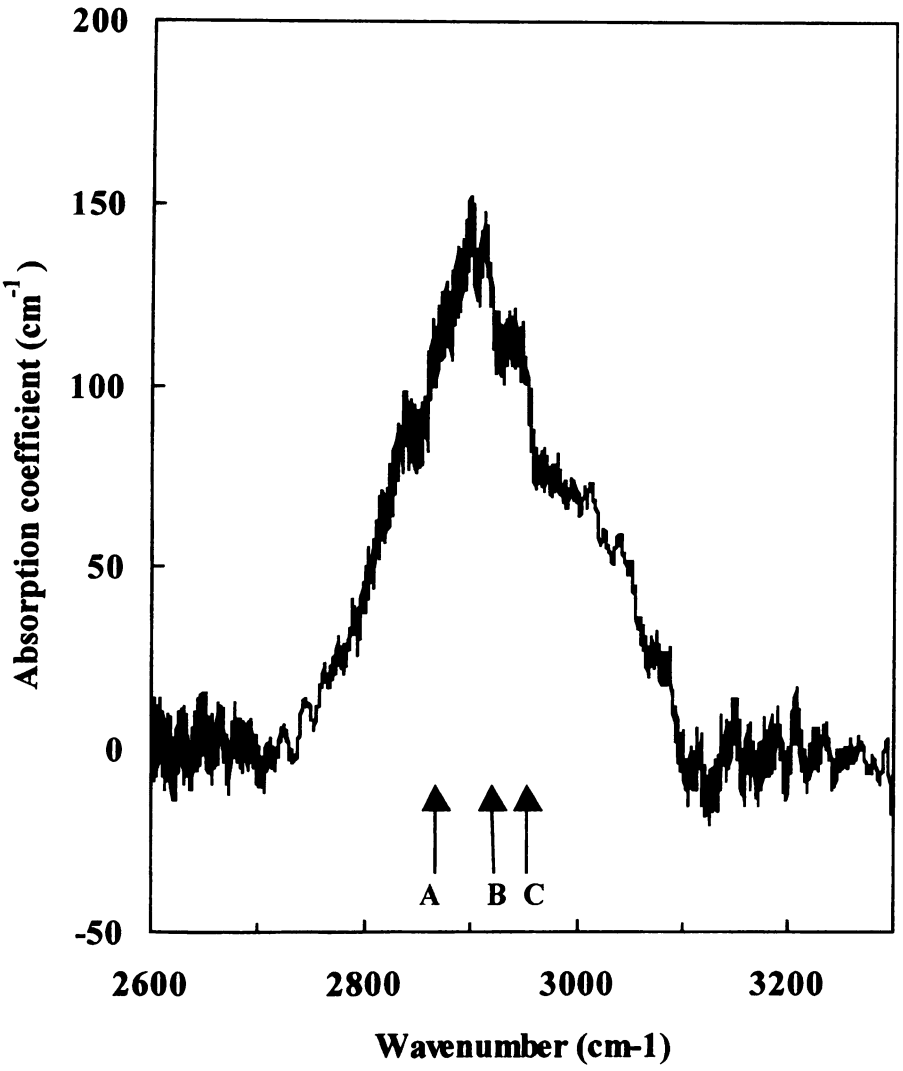

Fig. 3 - 12: An example IR absorption spectra.

where X_H and X_C are atomic concentration of hydrogen and carbon, respectively, N_a is Avogadro number, ρ is mass density and H is atomic percentage of hydrogen. X_H and ρ are determined by the measurement described previously, thus X_C can be obtained with equation (3-16) and atomic percentage of hydrogen H in a-C:H films is obtained with equation (3-17). It should be noted that this method only detects the hydrogen bonded to carbon in the film and not free hydrogen trapped in the film.

Chapter 4

4. Films Deposited from Acetylene Discharges at Pressurs in the Submillitorr Range

4.1. Introduction

Hydrogenated amorphous carbon films were deposited at pressures in the submillitorr range, and the dependence of the film properties on the ion impacting energy and the ion flux to neutral flux ratio onto the substrate during deposition are investigated in this chapter. According to the subplantation model of deposition as discussed in Chapter 2, the film has a maximum sp^3 ratio when it is deposited with approximately 100 eV of impacting ion energy per carbon and with high ion flux to neutral flux ratio onto the substrate.

In this chapter, the objectives are to deposit high sp^3 carbon-carbon bonded ta-C:H or diamond-like films using a microwave ECR plasma reactor at high deposition rate and to understand the deposition process of the films by investigating the effects of ion energy, ion flux to neutral flux ratio, deposition temperature and hydrocarbon flow rate. The rf induced substrate bias was varied from -80 V to -300 V to give variation of the ion energy onto the substrate. The deposition pressure was reduced as low as the deposition system could operate to maximize the ion flux to neutral flux ratio onto the substrate. The films were mostly deposited at 0.2 mTorr for about 45 seconds of deposition time at a substrate temperature near room temperature using acetylene gas in most cases. Acetylene was selected as the source gas of the films because it forms mostly $C_2H_2^+$ ions in low pressure plasmas [3]. Thus, the acetylene discharge at low pressure can give relatively uniform impacting ion energy per carbon onto the substrate. The typical flow

rate of acetylene gas was 7 sccm. The typical incident microwave power was 600 W. The reflected microwave power was high (about 350 W) when compared to other gas mixtures that contain inert gas under similar pressure conditions, and it varied with deposition condition such as pressure, substrate distance below the base plate and gas mixtures. The typical net absorbed microwave power for the acetylene gas discharges was about 250 W. The above deposition conditions will be termed to be the nominal deposition condition of low pressure deposition, hereafter in this chapter. The substrates are 0.17 mm thick glass and are mounted on a substrate holder with a heat sink compound, i.e. thermally conducting paste, to keep the temperature of the substrate near room temperature during the deposition process. Before film deposition, the substrates were cleaned in methanol using an ultrasonic cleaner and sputtered in an argon discharge for 30 seconds to further clean the substrate surface. After the deposition the films were again cleaned in methanol with a ultrasonic cleaner to remove the heat sink compound.

The input variables were varied to develop an understanding of the film properties in relation to the deposition conditions. Some specific relationships studied and reported in the following sections are input variable variations of feed gas rate, ion energy, substrate temperature and ion flux to neutral flux ratio. A summary of the deposition variables used is presented in Table 4-1.

In the following sections, the discharge properties measured at pressures in the submillitorr range are first presented and discussed. In particular they will be used to provide some explanation to the film properties versus variation of the input variables. Next, the effects of the ion energy and the ion flux to neutral flux ratio are shown and

discussed. Lastly, the effects of the deposition temperature and the flow rate of source gas are investigated.

Table 4-1: The deposition variable space.

Input Variables	Nominal Value	Variable Range
Acetylene Flow Rate (sccm)	7	4 - 35
Pressure (mTorr)	2.0	0.2 - 0.6
RF Induced Substrate Bias (-V)	200	80 - 300
Absorbed Microwave Power (W)	250	170 - 400
Substrate Position (cm)	3.5	3.5, 6.0
Substrate Thickness and Type	0.17 mm glass	0.17 or 1.0 mm glass
Helium Flow Rate (sccm)	0	0.0 - 2.5

4.2. Discharge Properties at Pressures in the Submillitorr Range

Selected discharge properties at pressures in the submillitorr range were measured using a double Langmuir probe and partial pressure analyzer (PPA). Specifically, the double Langmuir probe was used to measure the electron temperature and plasma density. The plasma sheath thickness and ion energy onto the substrate are then estimated using the result of the Langmuir probe measurements. In another set of experiments, a PPA measured the partial pressures of exit gases out of the discharge chamber.

The electron temperature and plasma density of acetylene discharges at 0.2 mTorr were measured for three different discharge conditions as indicated in Table 4-2. During the measurements the discharges coated the Langmuir probe with a-C:H films very quickly so the voltage on the probes was swept fast, i.e. within 30 seconds. The results of

the Langmuir probe measurements are presented in Table 4-2. The discharge pressure was 0.2 mTorr and the flow rate of acetylene gas was 7 sccm for the measurements. The electron temperatures vary about 8 eV and the plasma densities are similar to one another in Table 4-2. The fluctuation of the electron temperatures is considered due to the unstable measurement caused by the coating effects of a-C:H films on the probes.

Table 4 - 2: Double Langmuir probe measurements for electron temperature and plasma density.

Microwave Power (W) : Incident/Reflected (Net Input Power)	Saturation Ion Current (mA)	Electron Temperature (eV)	Plasma Density (x 10^{10} cm^{-3})
600/400 (200)	0.12	8.1	2.1
600/350 (250)	0.12	8.8	2.2
600/350 (250)	0.12	7.7	2.2

Using the double Langmuir probe measurements, the plasma sheath thickness and the energy of ions onto the substrate surface can be estimated as discussed in Section 3.4.2 of Chapter 3. The a-C:H films presented in this chapter were usually deposited with 250 W of net input microwave power. Thus, the averages of the electron temperatures and plasma densities at 250 W of input microwave power are used for the calculation of the plasma sheath thickness and the potential at the surface of the substrate. These average values are 8.3 eV for the electron temperature and 2.2 x 10^{10} cm^{-3} for the plasma density. The floating potential (ϕ_w in equation (3-5) in Section 3.4.2) is calculated to be 41 V. The potential difference (ϕ_{diff} in Section 3.4.2) between the floating potential at the substrate location and the chamber walls was measured to be 2-10 eV and is chosen to be 6 V as the representative value. Then the plasma sheath thickness and the acetylene ion

energy at the surface of the substrate can be calculated by using equations (3-6) and (3-7). The ion energy can be influenced by the collisions in the plasma sheath thickness. But the collisions are not considered significant in the discharge pressure regime of 0.2 mTorr. The mean free path for argon is estimated with the equation of $\lambda=1/165p$ cm where p is in Torr [51], giving the mean free path λ= 30 cm at 0.2 mTorr. The mean free path is much larger than the plasma sheath thickness. If the mean free path of acetylene is assumed to be the same order as the argon case, the collisions of an acetylene ion in the sheath thickness can be ignored and the ion energy is determined by only the potential difference between plasma and the surface of a substrate. The results of ion energy calculations are shown in Table 4-3 for several different rf induced substrate biases (ϕ_{rf}). The sheath thickness of plasma is larger than the thickness of the substrate (0.17 mm) in theses cases.

Table 4 - 3: The sheath thickness and acetylene ion energy at variations of rf induced substrate bias.

RF Induced Substrate Bias, ϕ_{rf} (-V)	Sheath Thickness (mm)		Acetylene Ion Energy (eV)	
	by Matrix Sheath	by Child Law Sheath	by Matrix Sheath	by Child Law Sheath
100	1.09	1.24	107	121
150	1.26	1.55	148	169
200	1.41	1.84	192	217
250	1.55	2.12	236	263
300	1.68	2.39	246	315

The values of ion energy are similar to those of the rf induced substrate bias. The ion energy onto the surface of the substrate, for example, is approximately 200 eV at the nominal rf induced substrate bias of -200 V.

Fig. 4-1 and Fig. 4-2 show the PPA data of acetylene gas with the discharge on and discharge off. The discharge off data in Fig. 4-1 shows standard cracking patterns of acetylene gas by electron impact ionization in the PPA unit. The acetylene gas in the chamber exit flow decreases drastically with the plasma ignition in the deposition chamber as seen in Fig. 4-2. The ratio of acetylene partial pressure (mass:26 amu) with discharge on to acetylene partial pressure with discharge off is 0.09. This fact suggests that the species containing carbon atoms in the discharge on case are activated by excitation, dissociation or ionization and come to have a high sticking coefficient, and then most of them are adsorbed on the surface of the substrate or the walls of discharge chamber. Another observation is that the hydrogen molecule concentration increases significantly with the ignition of plasma. This is believed to occur due to the fragmentation of acetylene gas. In the discharge case, the chamber pressure is largely supported by hydrogen gas, and the partial pressure of hydrocarbon species is not high compared to the other species. Thus the neutral carbon flux to the substrate will not be high compared with fluxes of other species. The water vapor increased in the case of discharge on and seems to be originating from the water molecules that had been adsorbed on the chamber walls and have escaped away from the walls by ignition of the discharge.

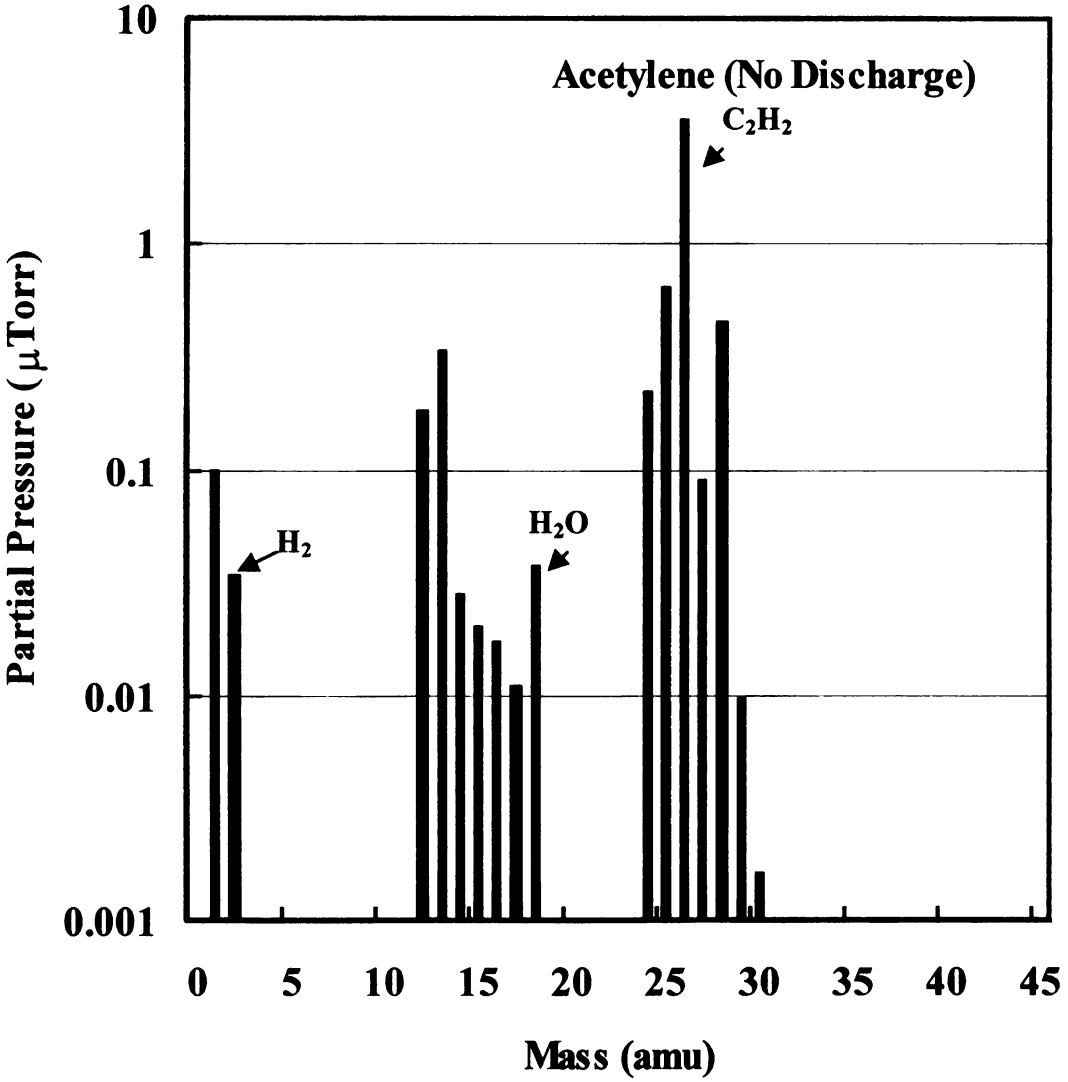

Fig. 4 - 1: Partial pressure analysis for acetylene gas with the system off (no discharge).

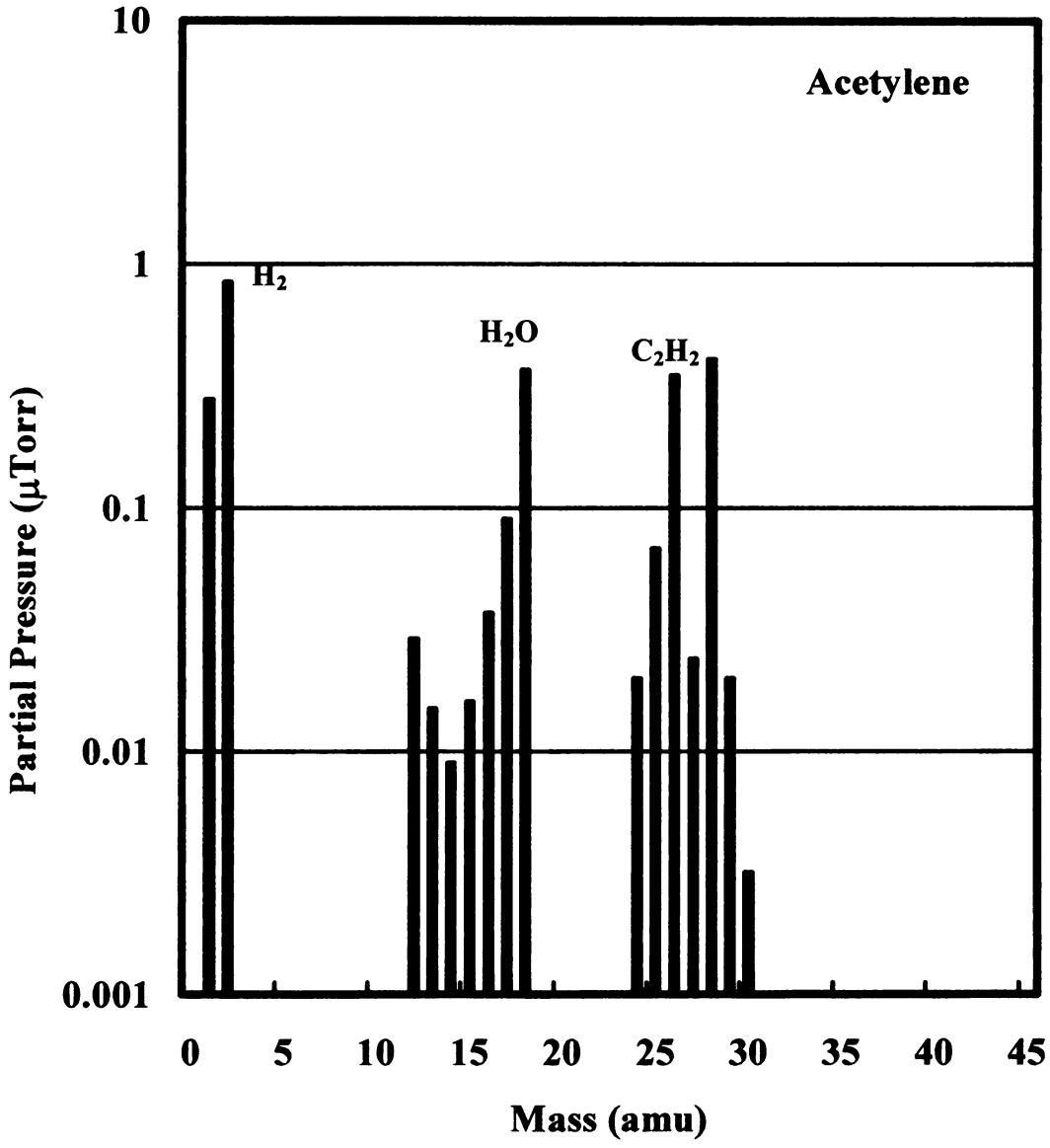

Fig. 4 - 2: Partial pressure analysis for acetylene gas with the system discharge on.

4.3. The Effect of Ion Energy (RF Induced Substrate Bias) on Film Properties

The impacting ion energy per carbon atom onto the surface of growing films and high values of ion flux as compared to neutral flux to the growing films are crucial factors for the deposition of tetrahedral (hydrogenated) amorphous carbon film as discussed in Section 2.3. In this section, the effect of ion energy on the properties of the films will be investigated.

Fig. 4-3 shows the optical bandgap (E_{04} and E_{tauc}) of the deposited films versus variation of rf induced substrate bias. The optical bandgap is high at low magnitude of induced substrate bias, and also has extreme values of 1.77 eV for E_{04} and 1.34 eV for E_{tauc} at -200 V of rf induced substrate bias (ϕ_{rf} in Table 4-3). The bars at the peak values shows the range of the optical bandgaps obtained from repeated experiments. The acetylene gas plasma has a relatively simple ionization and fragmentation pattern at low pressure and the major ion species is the $C_2H_2^+$ ion in the plasma [3], giving a uniform ion bombardment energy at a fixed rf induced substrate bias. The plasma sheath thickness and the ion energy for several rf induced substrate bias as were shown earlier in Table 4-3. The -200 V of rf induced substrate bias corresponds to approximately 200 eV, 192 eV by matrix sheath theory and 217 eV by Child Law sheath theory. Thus the optimum energy of the ion flux to the substrate is about 200 eV ion energies and the energy per carbon atom is about 100 eV as other literature has cited [3, 40]. These other research results were obtained using a filtered ion beam deposition method [16] for ta-C and a plasma beam source with a tungsten ion extraction grid [3]. In our experiments, the peak

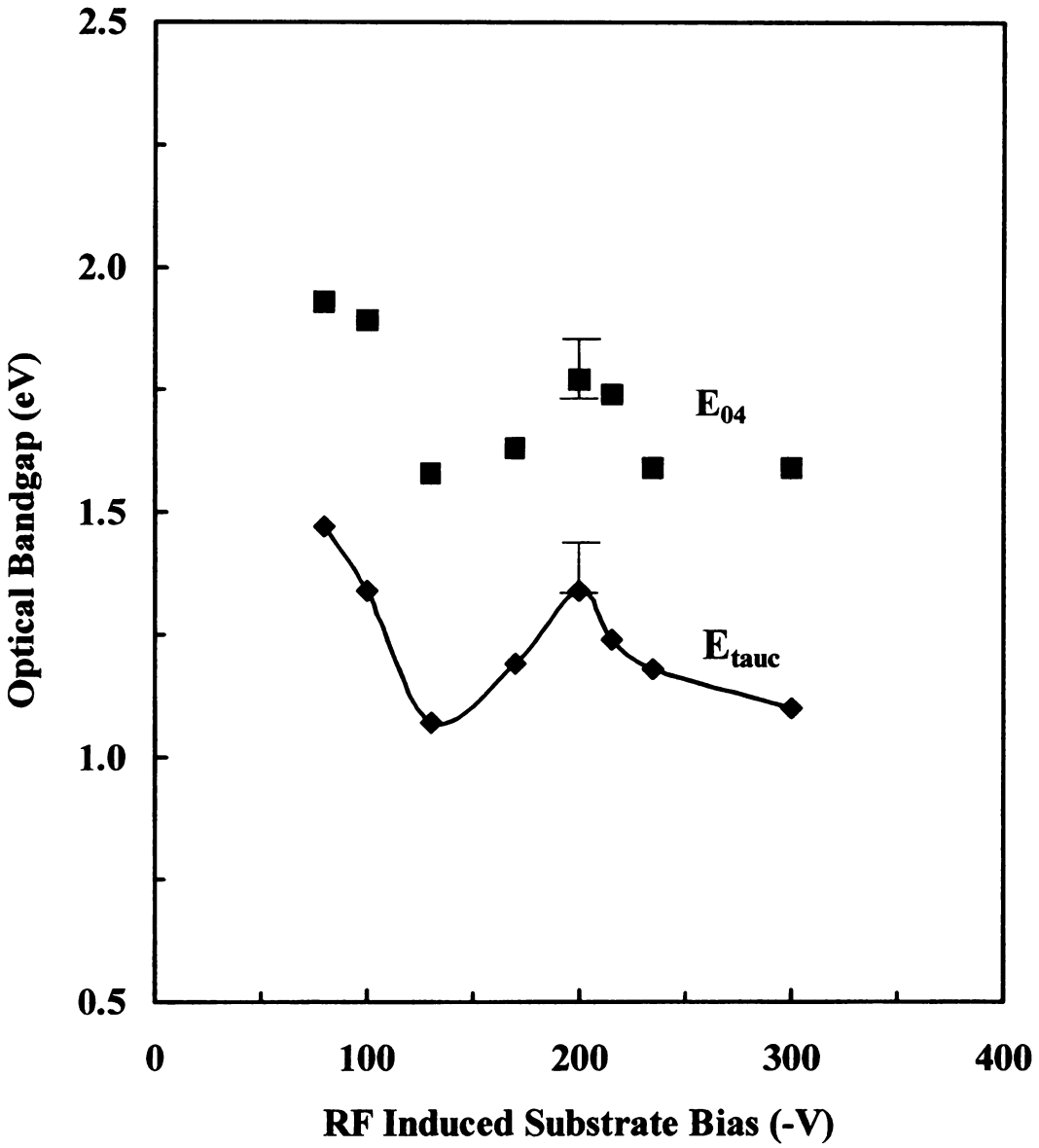

Fig. 4 -3: Optical bandgap (E_{tauc} and E_{04}) versus rf induced substrate bias for the films deposited from acetylene gas feed at 0.2 mTorr discharge pressure. The bars at the peaks show the range of measurement values of the optical bandgaps for the films deposited repeatedly with the same deposition condition.

value of the optical bandgap at 100 eV per carbon atom is obtained with a deposition system that does not have any structure of ion filtering or ion extraction grid.

The films deposited at near -200 V of rf induced substrate bias are considered to be tetrahedral hydrogenated amorphous carbon films. Even if the film structure properties like mass density or sp^3 bonding ratio to sp^2 bonding has not been characterized in this investigation, the occurrence of a peak of optical bandgap at -200 V substrate bias strongly suggest the films are ta-C:H when compared with other results published [3, 16, 40]. The optical bandgap of the films is dependent on the density of sp^3 sites and the distortion of sp^2 rings or chains [37, 38]. The peak of optical bandgap at -200 V occurs owing to high formation of sp^3 sites at the corresponding carbon ion bombardment energy and matches very well with the model by Robertson [40] and the results of others [3, 16]. The low values of optical bandgaps at ion energies just below the induced substrate biases of -100 V are attributed to low carbon ion energy onto the growing films. The low energy of these carbon ions have a lower penetration probability in the growing film that results in a smaller increase of the local mass density and a low sp^3 fraction. In the region of ion energy exceeding the optimum rf induced substrate bias of -200 V, the excess ion energy induces relaxation of the diamond-like film structure according to the subplantation model of Robertson discussed in Section 3 of Chapter 2. The high values of optical bandgap at lower magnitude of the rf induced substrate biases are considered to be related with the high hydrogen content at these biases [66, 67]. The sp^3 carbon bond is characterized by a lower binding energy than sp^2 bonds, while unpaired electrons in dangling orbits of amorphous carbon create states in the energy gap between bonding and antibonding states. Hydrogen removes these states from the gap by closing dangling

bonds and reduces the density of graphite states [68]. Low energy of the ions could not dehydrogenated the films because the ions have insufficient energy to break carbon-hydrogen bonds liberating hydrogen from the film structure. Thus, the film's optical bandgap is high at the region of low ion energy. The higher hydrogen content can hinder formation of sp^2 sites by the preferential formation of sp^3 carbon- hydrogen bonds. Thus the sp^2 carbon - carbon bondings will not be high for films deposited at low carbon ion energies. The relationship between the hydrogen content and optical bandgap will be discussed in more detail in the next chapter which deals with the films deposited at pressures in the millitorr range.

The infrared active hydrogen content of the films was measured for the samples deposited. The absorptance present in the FTIR spectra of films in the region of 2700 to 3100 cm^{-1} were measured as discussed in the previous chapter. The film's substrates used for the measurement of hydrogen content were thick pieces of glass (~ 1 mm) to remove a coherent interference effect between the reflected IR beams and the transmitting IR beams that occur for thin substrates. The result is shown in Fig. 4-4. The unit of hydrogen content is not presented using atomic percentages (at.%) because the density of the films has not been measured. Thus the hydrogen content with the unit of cm^{-3} does not necessarily present the film's percent hydrogen composition. The hydrogen content shows a slight decrease with increasing magnitude of the rf induced substrate bias. The trend is expected because the higher implanting ion energy will expel more hydrogen atoms from the films resulting in less hydrogen content. The film thickness is very thin (~60 nm) so slight surface contamination of the substrates can affect the hydrogen

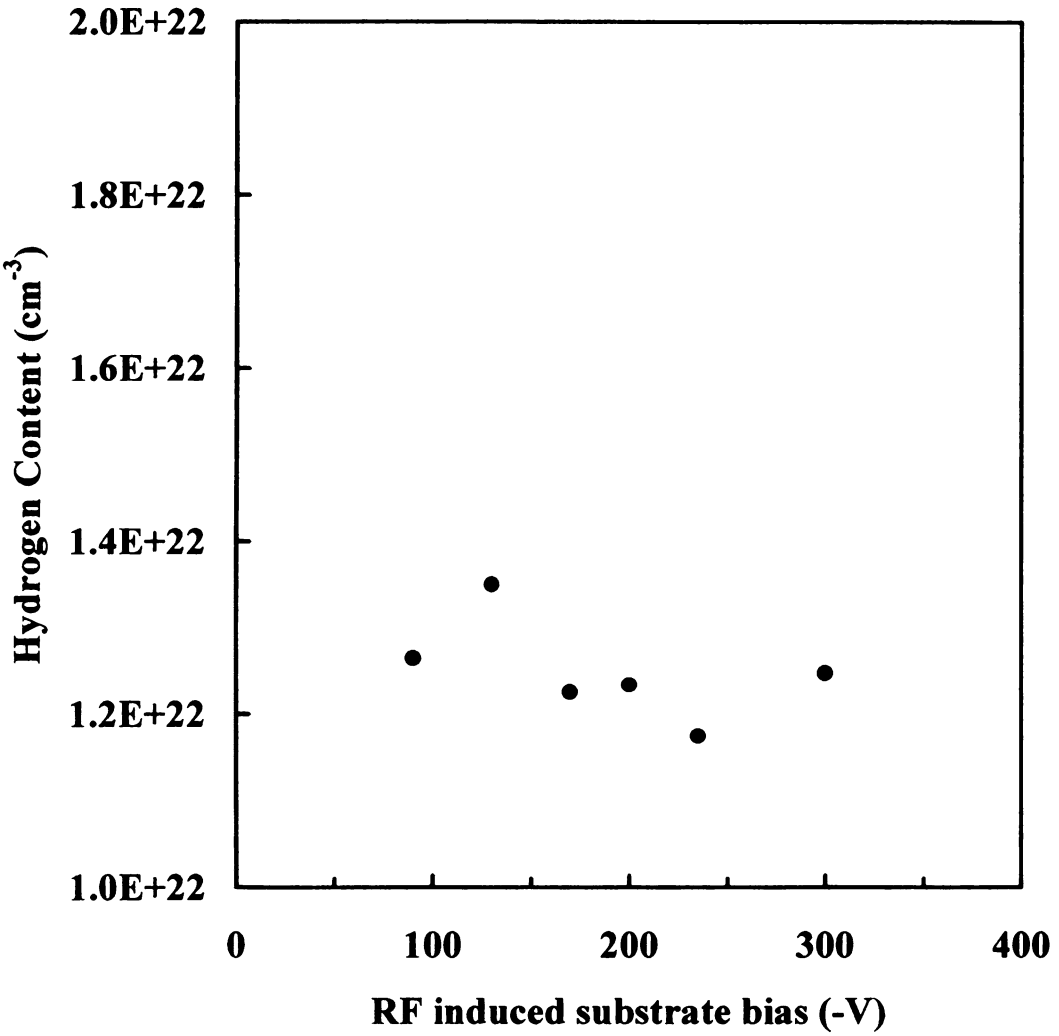

Fig. 4 - 4: Hydrogen content versus rf induced substrate bias for films from acetylene gas feed at 0.2 mTorr discharge pressure.

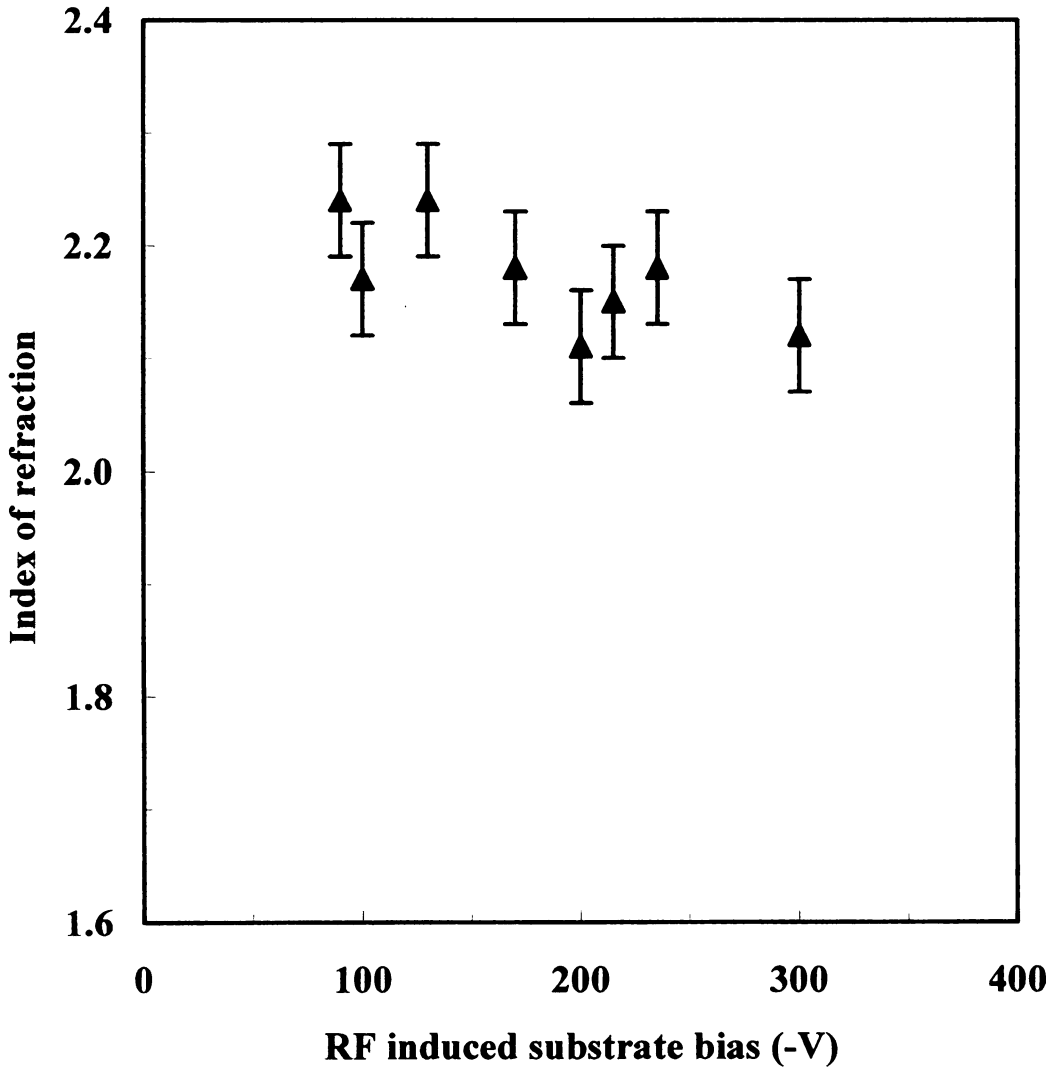

Fig. 4 - 5: Index of refraction at 633 nm versus rf induced substrate bias for films from acetylene gas feed at 0.2 mTorr discharge pressure. The bars present the standard deviation of the measurements for the films.

content measured for the films, which will give partial explanation of the fluctuation of the hydrogen content shown in the figure.

Fig. 4–5 shows the index of refraction of the films versus variation of rf induced substrate bias. The values do not show significant variation and are all about 2.2. The fluctuation of the values is almost within the standard deviation of the measurements which is about 0.05. The trend shows a slight decrease with increasing magnitude of the rf induced substrate bias and is similar to that of hydrogen content and not to the that of optical bandgap. Therefore the index of refraction is not considered as sensitive as optical bangap to the sp^3 fraction of the films.

Fig. 4-6 shows the deposition rate of the films versus variation of rf induced substrate bias. The deposition time was in the range of 45-60 seconds and was measured within ± 5 seconds. The deposition rate is not significantly varying with the variation of rf induced substrate bias. The fluctuation of the deposition rates will be partially explained by the measurement error of the deposition time. The average of the deposition rates is 90 nm/min. The deposition rate at 7.0 sccm of acetylene flow rate in the nominal deposition condition is much higher than the other filtered ion beam and plasma beam deposition systems used for tetrahedral (hydrogenated) amorphous carbon film depositions as in Table 2-1.

4.4. The Effect of Ion Flux to Neutral Flux Ratio

In section 4.3, the effect of the ion energy on the film properties is shown and discussed. In this section, the effect of ion flux on the film properties is investigated. To

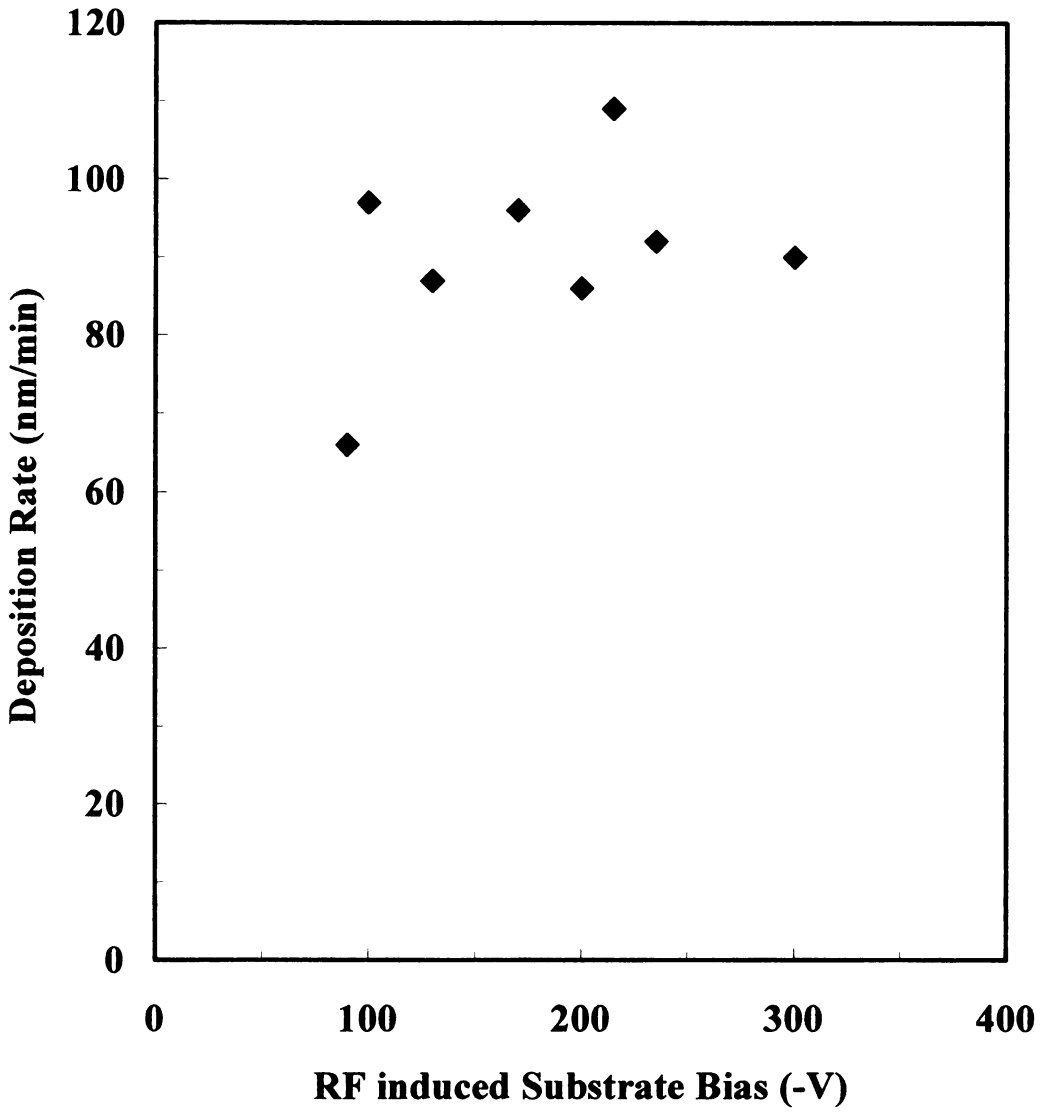

Fig. 4 – 6: Deposition rate versus rf induced substrate bias for the films deposited from acetylene discharges.

see the effect of ion flux onto the surface of growing films in this investigation, several kinds of experiments were performed including variation of pressure, absorbed microwave power, and vertical position of the substrate. The variation of the deposition conditions is expected to change the ion flux to neutral flux ratio. The ratio of ion flux to neutral flux of species that contains carbon atoms onto the substrate is estimated for the case of this ECR deposition process.

The fluxes of neutrals and ions are estimated first for the nominal deposition condition to compare the ion flux to neutral flux ratios of the discharges for the various off-nominal deposition conditions. The nominal deposition condition was previously defined with a deposition pressure of 0.2 mTorr, an absorbed microwave power of 250 W, a 7 sccm flow rate of acetylene gas and a substrate position of 3.5 cm. The radical and neutral flux onto the surface of the substrate is estimated from the pressure and gas temperature of a discharge. The ions and neutrals are all assumed to be those of acetylene in the estimation. The gas temperature of the discharges is assumed to be 600 K. The neutral flux is obtained using equation (3-8), $\Gamma_n=(1/4)n_g\langle v\rangle$. The equation, $n_g=p/kT_g$ gives a neutral flux of $3.22\text{x}10^{18}$ m^{-3} at 0.2 mTorr and 600 K. The mean velocity of neutrals is 697 m/s at 600 K for acetylene molecules using the equation, $\langle v\rangle=(8kT_g/\pi m)^{1/2}$. Thus, the neutral flux is 5.61×10^{16} $cm^{-2}s^{-1}$ at 0.2 mTorr and 600 K for acetylene molecules. The ion flux of species that contains carbon atoms onto the substrate is estimated by measuring the ion current density to the conducting substrate holder with varying DC bias. The substrate holder area is 54 cm^2 inside the acetylene gas discharge. The current density is shown in Fig. 4-7. The current density is near linear versus the variation of DC bias and is about 0.9 mA/cm^2. This current density

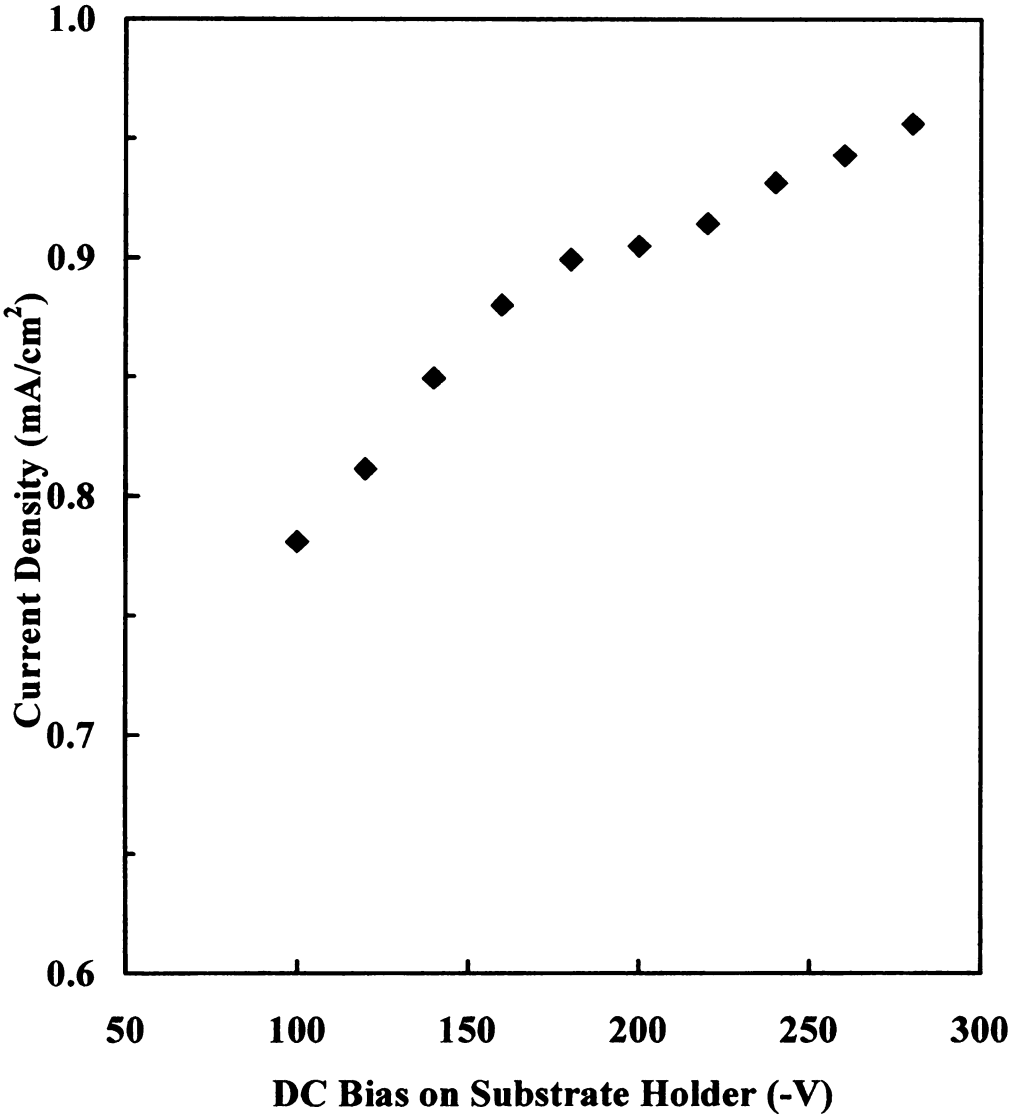

Fig. 4 - 7: Current density on the substrate versus dc bias on the substrate holder for acetylene discharge at pressure of 0.2 mTorr and substrate posion of 3.5 cm.

corresponds to $6.0x10^{15}$ cm^{-2}-s^{-1} of ion flux onto the substrate at -200V DC substrate bias. In this estimation of neutral flux and ion flux, the neutrals and ions of hydrogen molecules are all regarded as those of acetylene. Then, the rough estimation of the ratio of ion flux to neutral flux onto the substrate holder is about 10 %, which is smaller than the value of the filtered ion beam (~ 100%) [16] and plasma beam source with tungsten ion extraction grid (95%) [3]. This fact shows the tetrahedral hydrogenated amorphous carbon films can be deposited with a 0.1 ratio of ion flux to neutral flux onto a substrate in a ECR plasma reactor that has a rf biased substrate holder operating at low pressure.

4.4.1 The Effect of Pressure

The molecular flux onto the surface of a container is proportional to the pressure at a certain temperature so the discharge pressure of a deposition system determines the fluxes of neutral species to the surface of the substrate in the deposition chamber. The plasma density also increases as the discharge pressure increases but does not as quickly as the density of neutral species. The effect of pressure variation in the deposition process, therefore, can indicate the effect of the variation of ion flux to neutral flux ratio onto the surface of the substrate. To investigate the effect of pressure variation, films were deposited on pieces of thick glass with the nominal deposition condition cited above in the introduction part of this chapter except for the pressure variation. The pressure was varied from 0.22 mTorr to 0.6 mTorr by adjusting the gate conductance valve of the deposition system. The pressure effects on the film properties are shown in Fig. 4-8 and Fig. 4-9. The current density onto the surface of the substrate was measured with –200 V

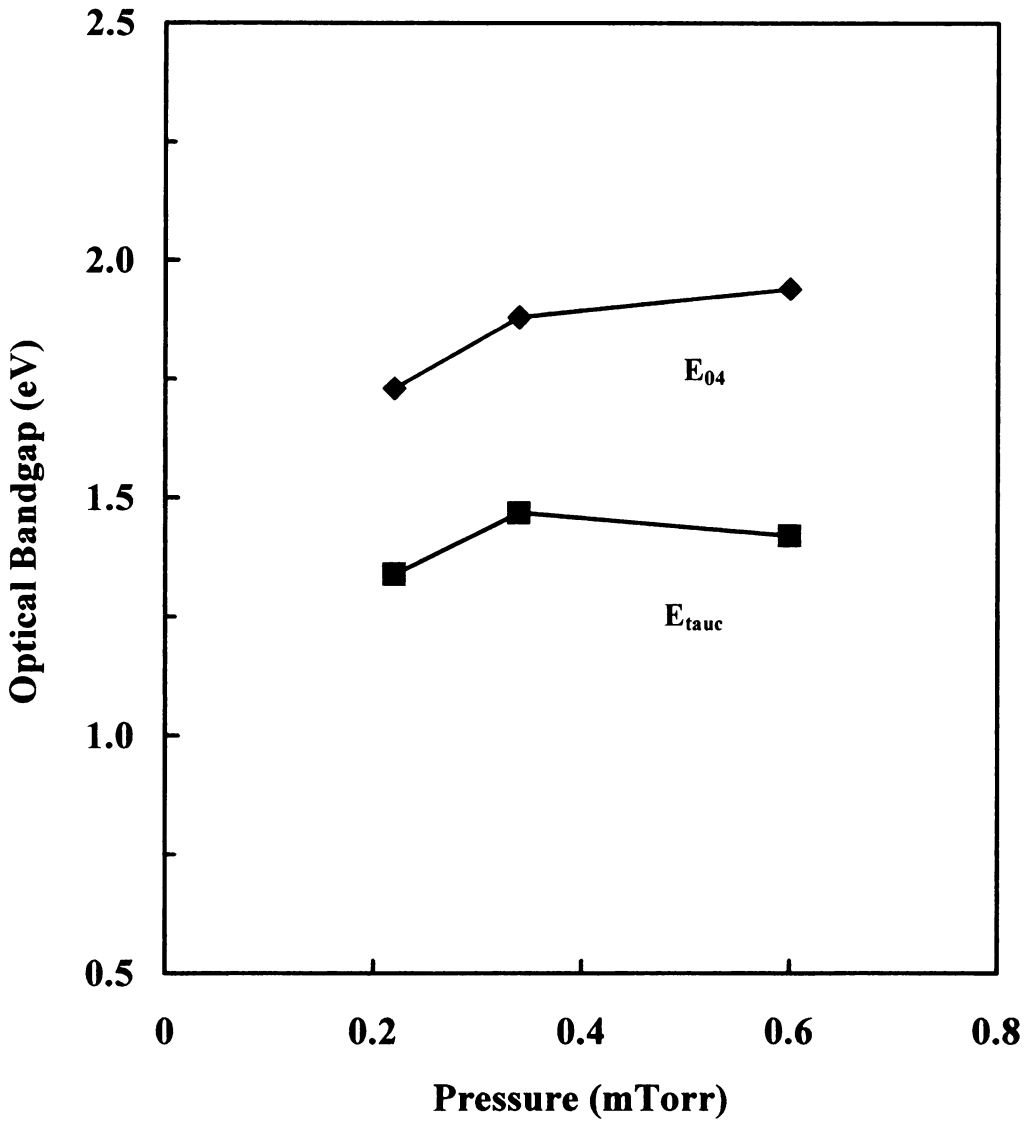

Fig. 4 - 8: Optical bandgap (E_{tauc} and E_{04}) versus pressure for films deposited with -200 V of rf induced substrate bias from acetylene gas feed.

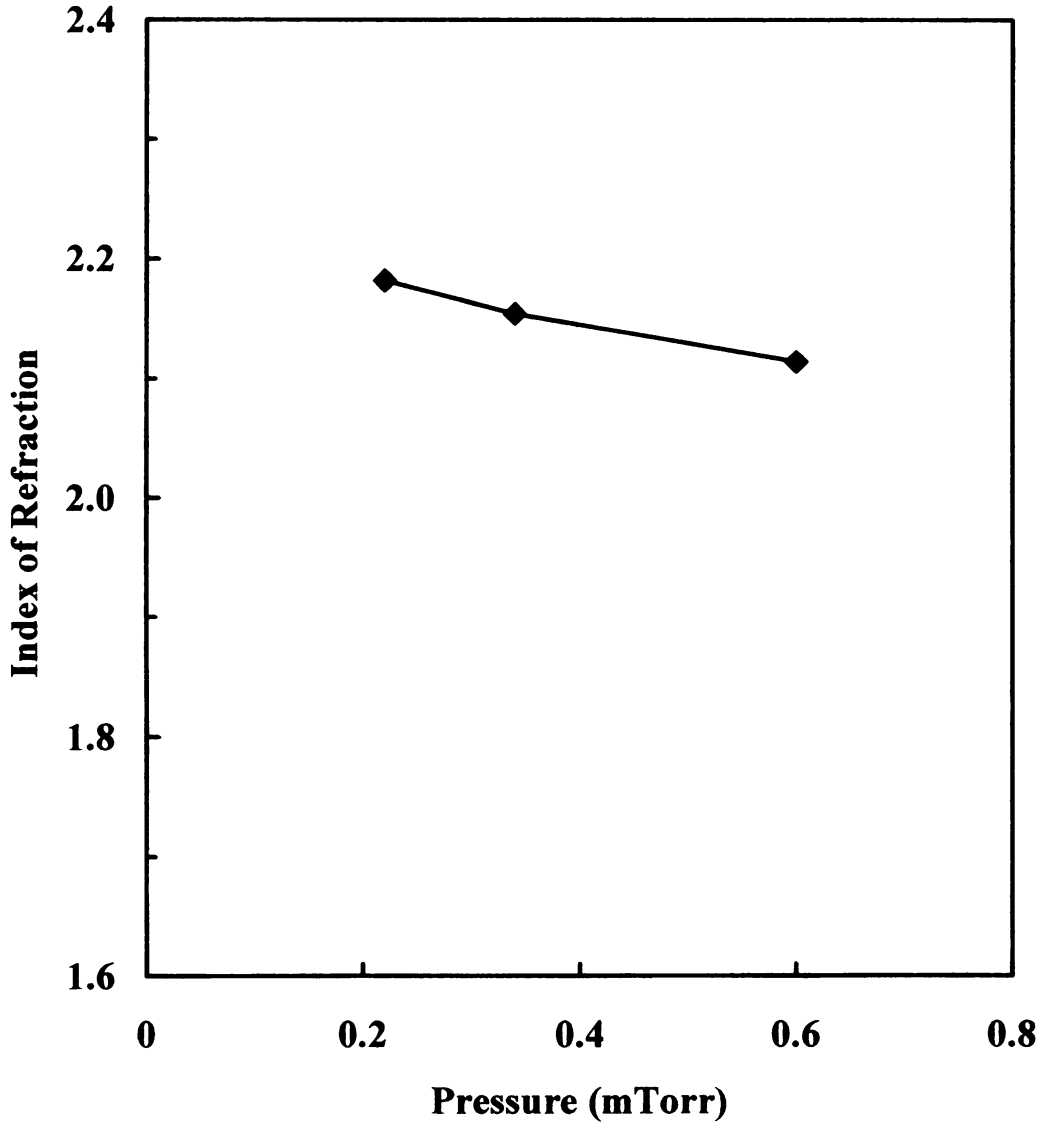

Fig. 4 - 9: Index of refraction versus pressure for films deposited with -200 V of rf induced substrate bias from acetylene gas feed.

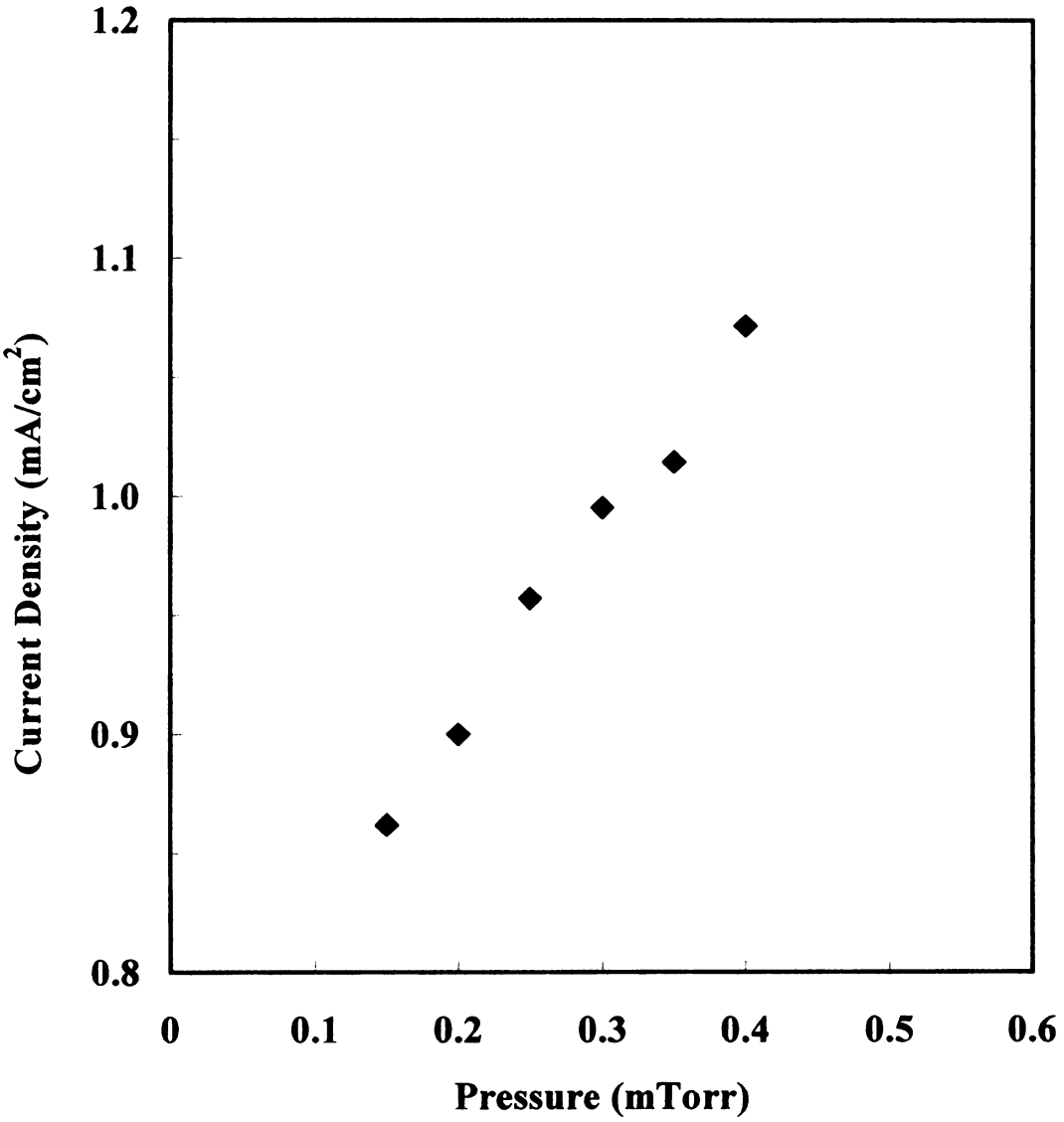

Fig. 4 - 10: Current density to the substrate versus pressure for the acetylene discharge.

of DC bias on the substrate holder and the same other deposition conditions, and it is shown on Fig. 4-10. The optical bandgap has a slightly increasing trend and the index of refraction shows a slightly decreasing trend versus increasing deposition pressure.

To interpret these results it is useful to estimate the ion flux to neutral flux ratio at various pressures. The pressure variation increases the neutral flux up to 2.7 times from the value at the nominal deposition condition because the neutral flux is directly proportional to pressure. The ion flux onto the surface of the substrate can be estimated from the current density of Fig. 4-10. The current density increased 1.3 times as it varied from 0.9 mA/cm^2 to 1.2 mA/cm^2 across the range of variation of the pressure, hence so did the ion flux. Thus the ion flux did not increase as much as the neutral flux in the variation of the pressure. Therefore, the nominal ion flux to neutral flux ratio decreased by 50 % (=1.3/2.7) as the pressure increased in the range. The increase in the pressure can also be expected to alter the composition of the species fluxes to the deposition surface. Based on the PPA results presented earlier in Section 4-2, the dominant neutral flux is expected to be hydrogen. With a fixed flow rate of acetylene gas, the hydrocarbon species are activated in the discharge and subsequently stick on the surface of the substrate or the chamber walls, that is, are consumed in the chamber, thus do not contribute significantly to the increase of total pressure in the deposition chamber. But the hydrogen gas is not consumed in the chamber and the partial pressure of hydrogen gas is higher than the hydrocarbon gas and hence hydrogen forms the large part of the total pressure of the deposition chamber. Therefore, the ratio of the ion flux to the neutral flux of hydrocarbon species does not change significantly with the variation of the deposition pressure with the fixed feeding of acetylene gas. Thus, the variation of deposition pressure changes the

hydrogen flux primarily and therefore the pressure variation shows only a small affect on the film properties across the 0.2-0.6 mTorr range. The slight increasing trend of optical bandgap and decreasing trend of index of refraction are considered to be due to the effect of increasing hydrogen content of the films with the increasing deposition pressure. In the other literature, the pressure showed a big influence on the properties of the ta-C:H films prepared by rf plasma deposition by increasing the plasma density using a magnetic field [69]. It is because the ion flux to neutral flux ratio and the ion energy are affected significantly with variation of the deposition pressure in rf discharges.

4.4.2. The Effect of Microwave Power

The absorbed microwave power also increases the plasma density of the discharge according to the global model of plasma discharges [51], thus, it is expected that microwave power changes will affect the ratio of ion flux to neutral flux onto the substrate. The absorbed power was varied from 170 W to 410 W in the experiments to investigate the effect of the absorbed microwave power on the properties of films. The films were deposited on the pieces of 0.17mm thick glass attached to the substrate holder using a heat sink compound in the nominal deposition condition. The properties of optical bandgap and index of refraction did not show significant variation with the changing absorbed microwave power as seen in Fig. 4-11 and Fig. 4-12. The current density with the microwave power variation is presented in Fig. 4 - 13. The current density is 0.9 mA/cm^2 at the nominal deposition condition (250W), 0.8 mA/cm^2 at 170 W and 1.12

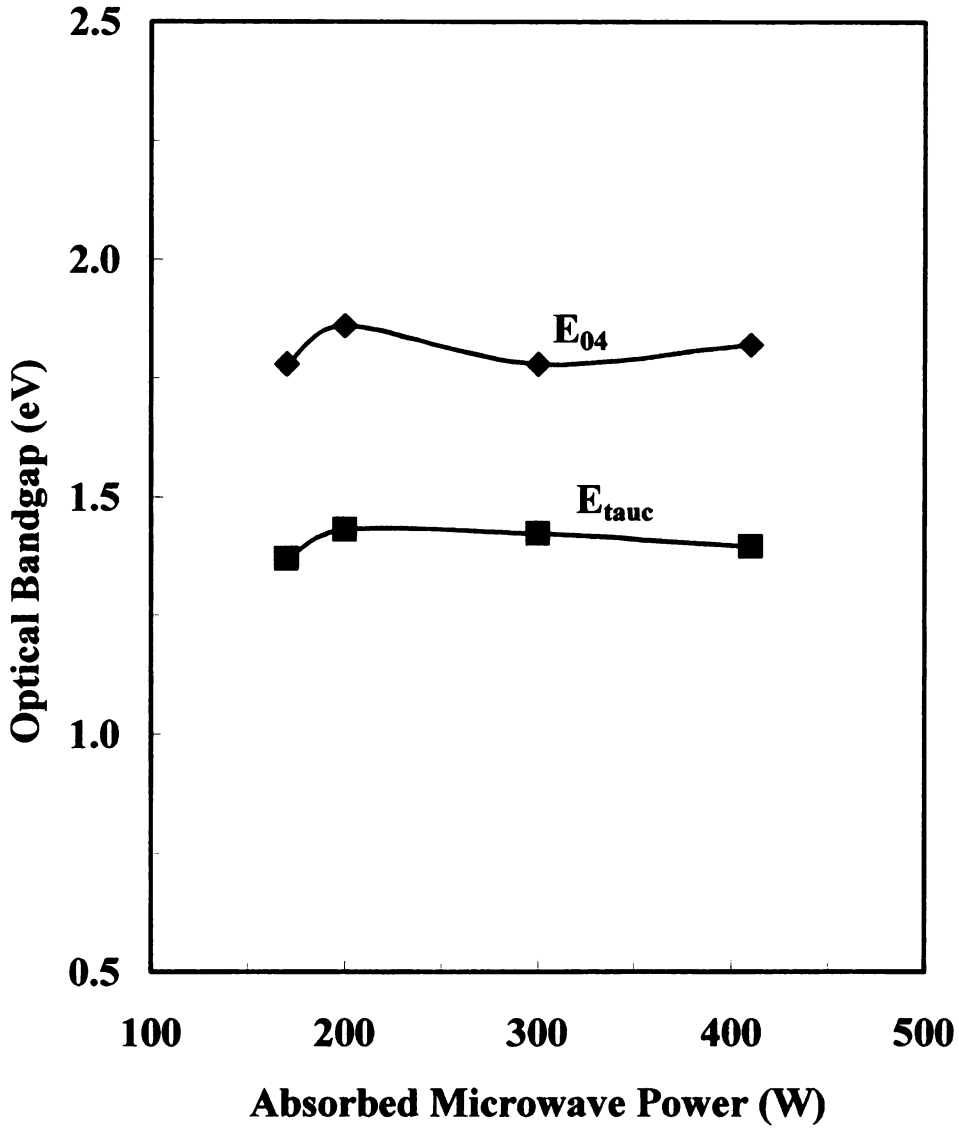

Fig. 4 - 11: Optical bandgap (E_{tauc} and E_{04}) versus absorbed microwave power for films deposited with 200 V of rf induced substrate bias from acetylene gas feed at 0.2 mTorr discharge pressure.

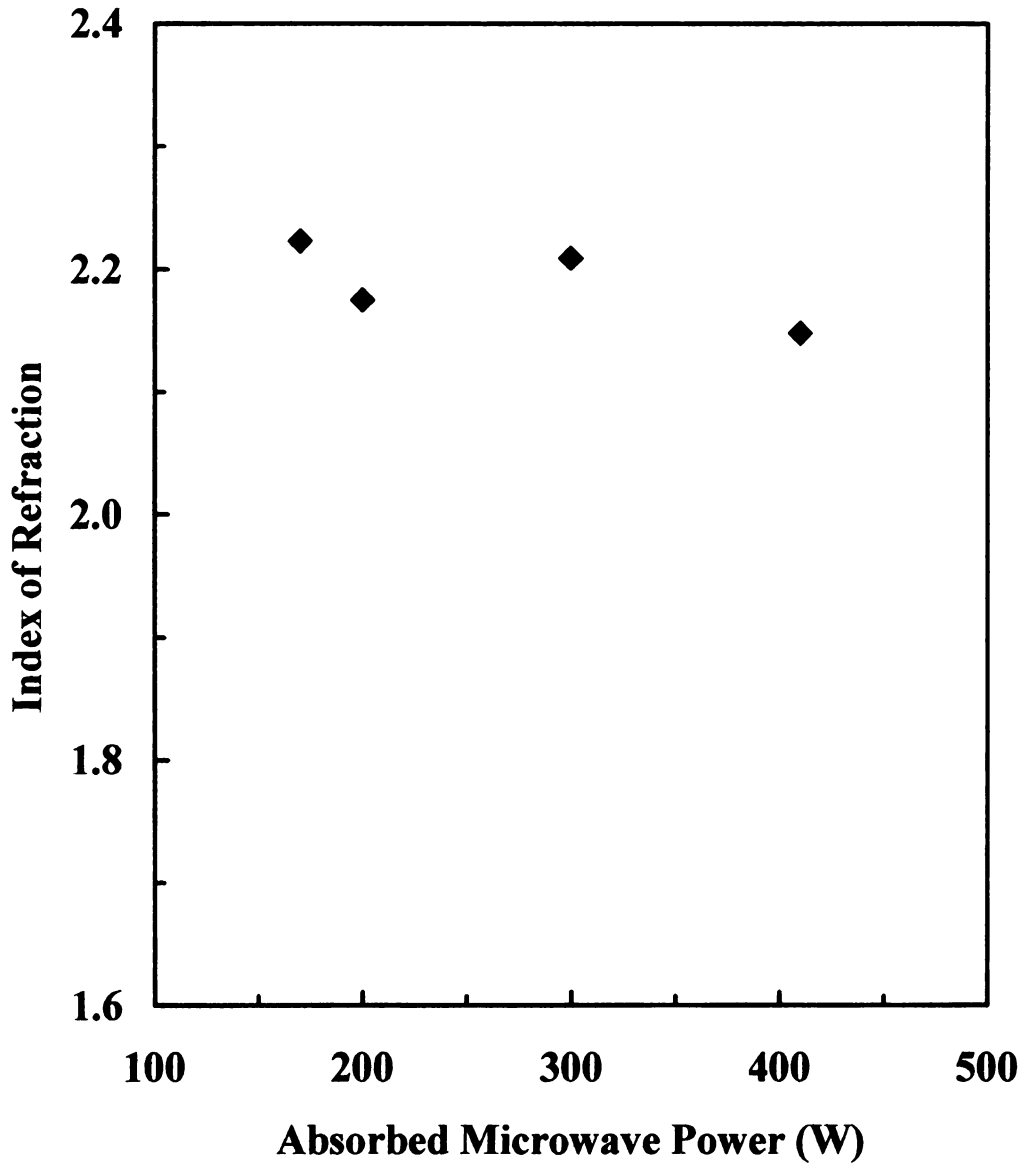

Fig. 4 - 12: Index of refraction versus absorbed microwave power for films deposited with 200 V of rf induced substrate bias from acetylene gas feed at 0.2 mTorr discharge pressure.

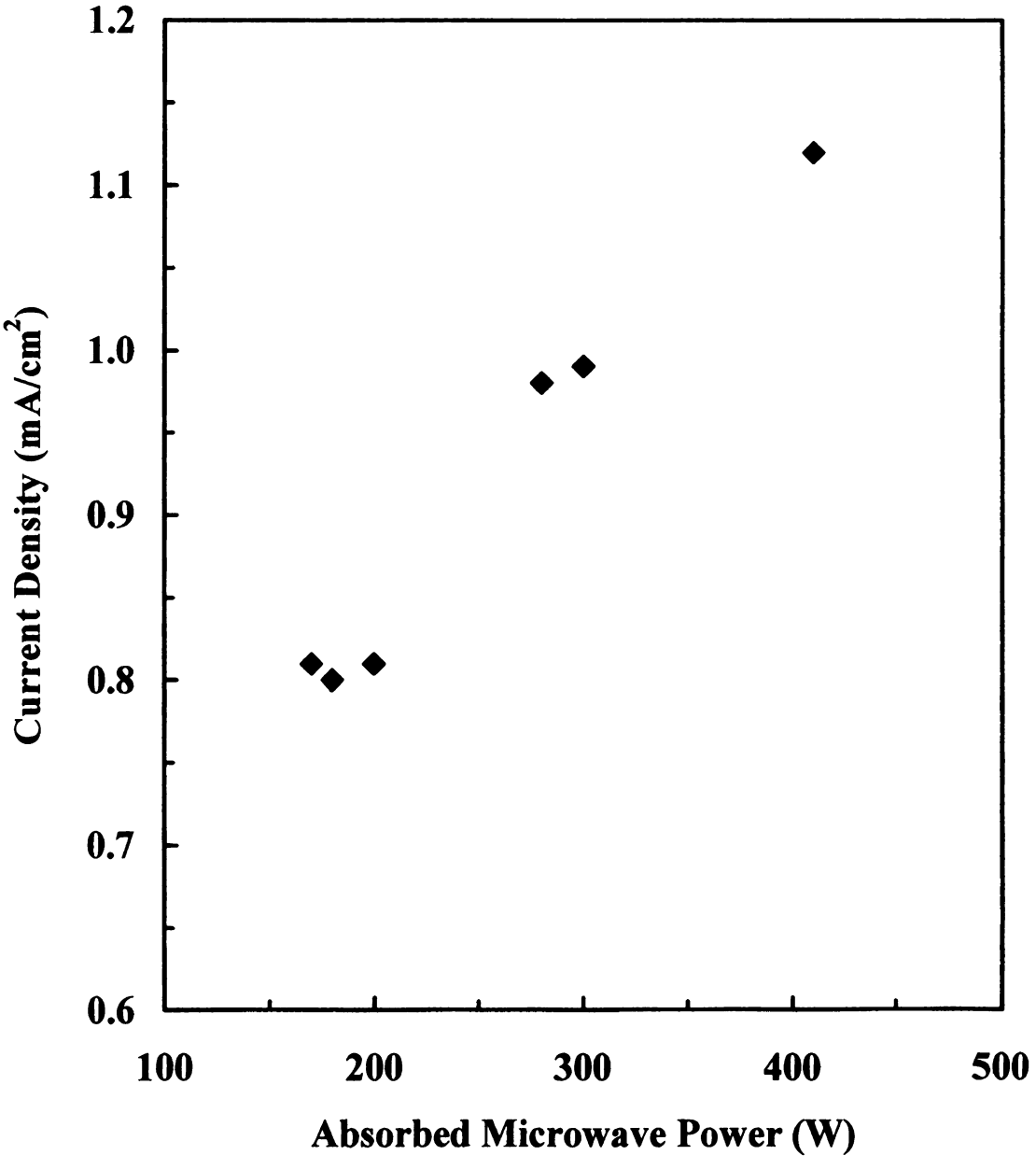

Fig. 4 - 13: Current density to the substrate holder versus absorbed microwave power for an acetylene discharge at 0.2 mTorr pressure.

mA/cm^2 at 410 W. Thus, the ion flux to neutral flux ratio decreased 11 % at 170 W and increased 24 % at 410 W from the value at the nominal deposition condition. The optical properties of the films did not show significant variation within the variation of the ion flux to neutral flux ratio onto the surface of the substrate for –11 % and 24 % variation about the nominal deposition condition. In rf deposition of ta-C:H films by increasing the plasma density using a magnetic field, the increased rf power increased the optical bandgap and the hardness [69].

4.4.3. The Effect of Substrate Position

The plasma density decreases exponentially in an argon discharge with increasing distance from the center of the discharge region for the discharge reactor of this investigation [70]. With the motivation from this fact, the a-C:H films were deposited at two different positions of the substrate. The substrate positions were 3.5 cm or 6.0 cm below the base-plate of the discharge chamber. One group of films was deposited at 3.5 cm and another group at 6.0 cm with a variation of rf induced substrate bias and with the nominal deposition values for other input variables. The results of the optical properties of the films are presented in Fig. 4-14 and Fig. 4-15. The current density was again measured at the two different positions versus variation of the rf induced substrate bias to estimate the ion flux to the surface of the substrate, and it is shown in Fig. 4-16. The optical bandgap shows very different trends for the two different substrate positions. The curve for 3.5 cm substrate position has a peak value of the optical bandgap at -200 V of rf

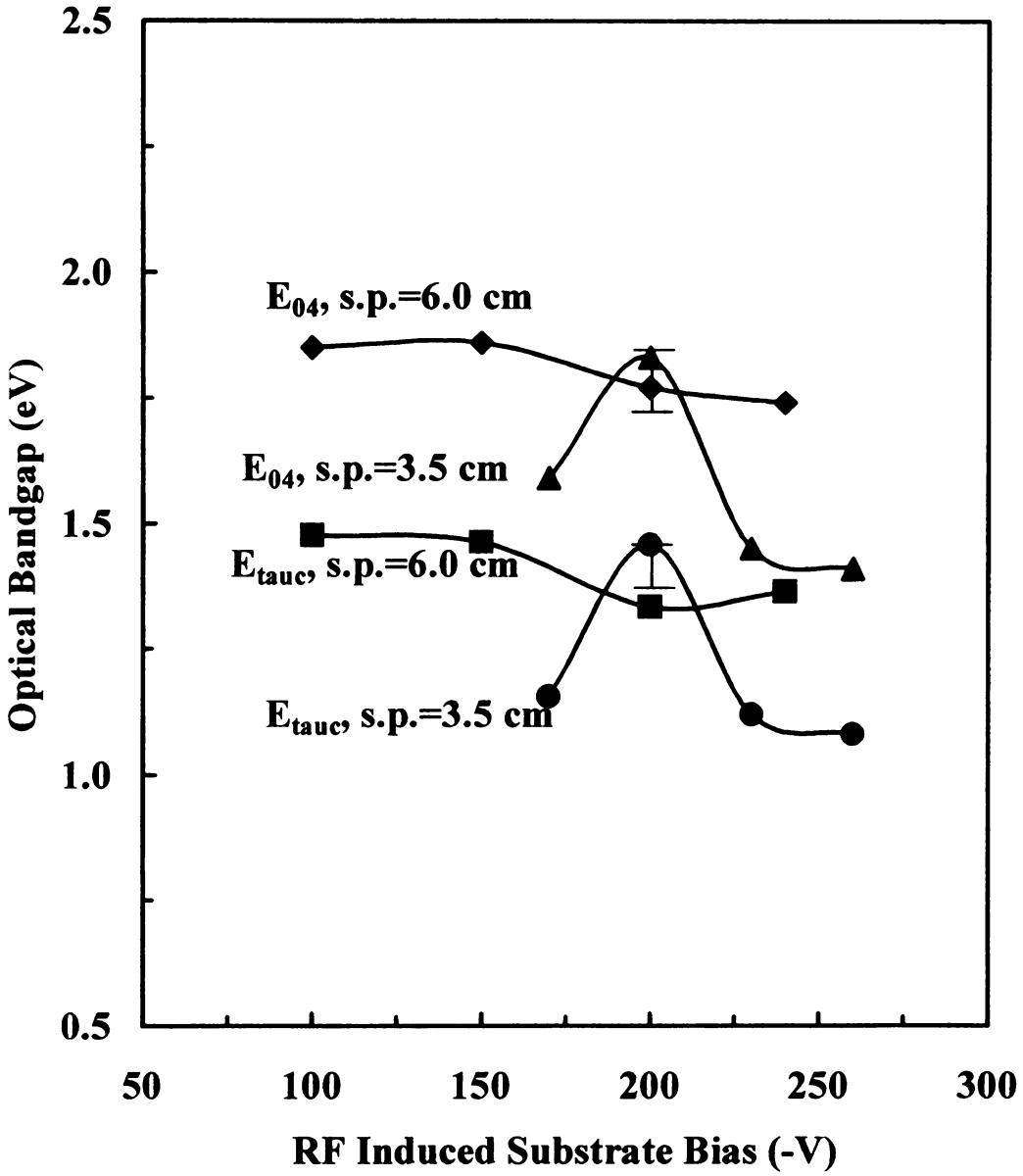

Fig. 4 - 14: Optical bandgap (E_{tauc} and E_{04}) versus rf induced substrate bias for films deposited from acetylene gas feed at 0.2 mTorr discharge pressure with substrate positions (s.p.) of 3.5 cm and 6.0 cm. The bars at the peaks show the range of measurement values of the optical bandgaps for the films deposited repeatedly with the same deposition condition.

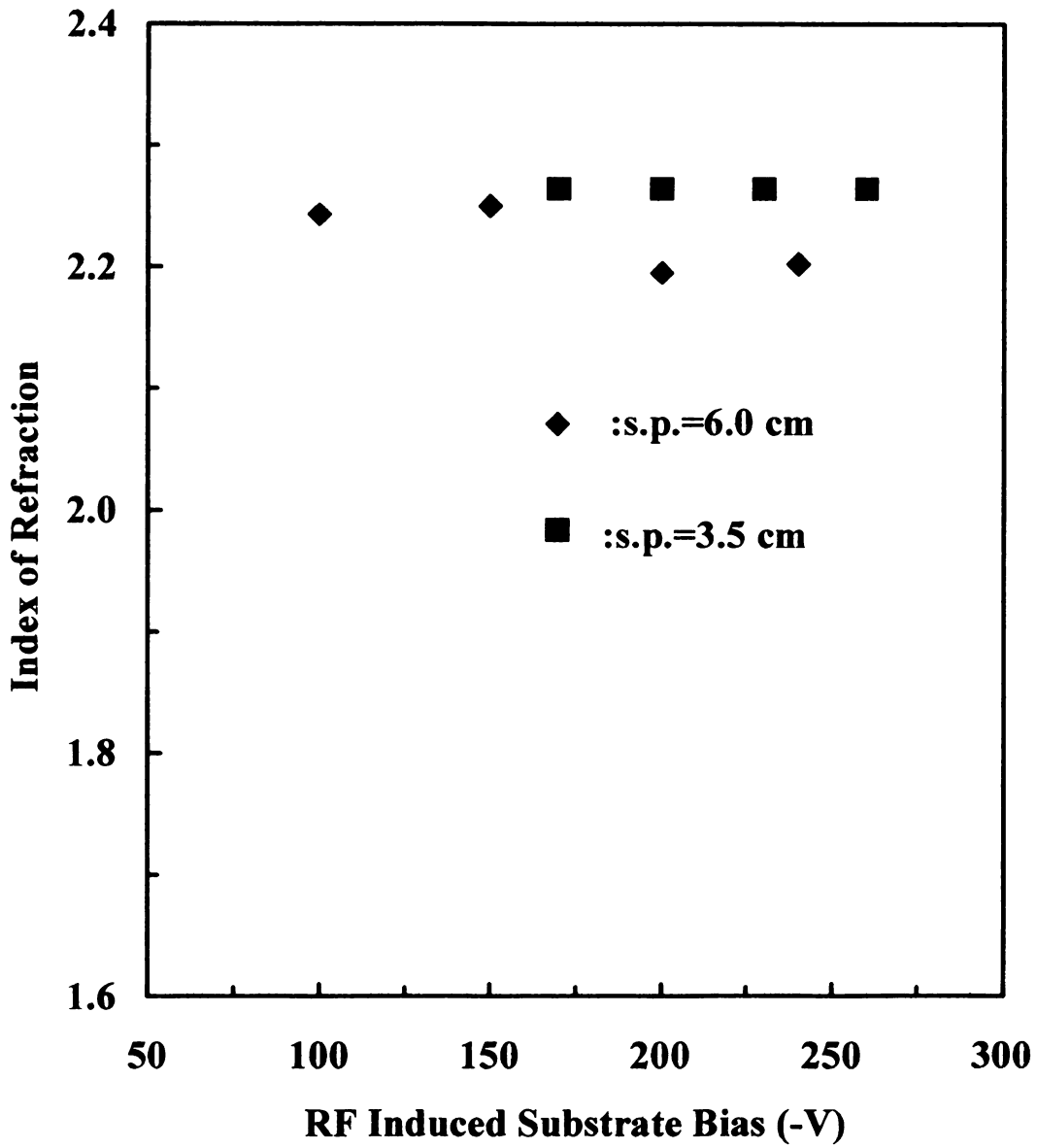

Fig. 4 - 15: Index of refraction versus rf induced substrate bias for films deposited from acetylene gas feed at 0.2 mTorr discharge pressure with substrate positions (s.p) of 3.5 cm and 6.0 cm.

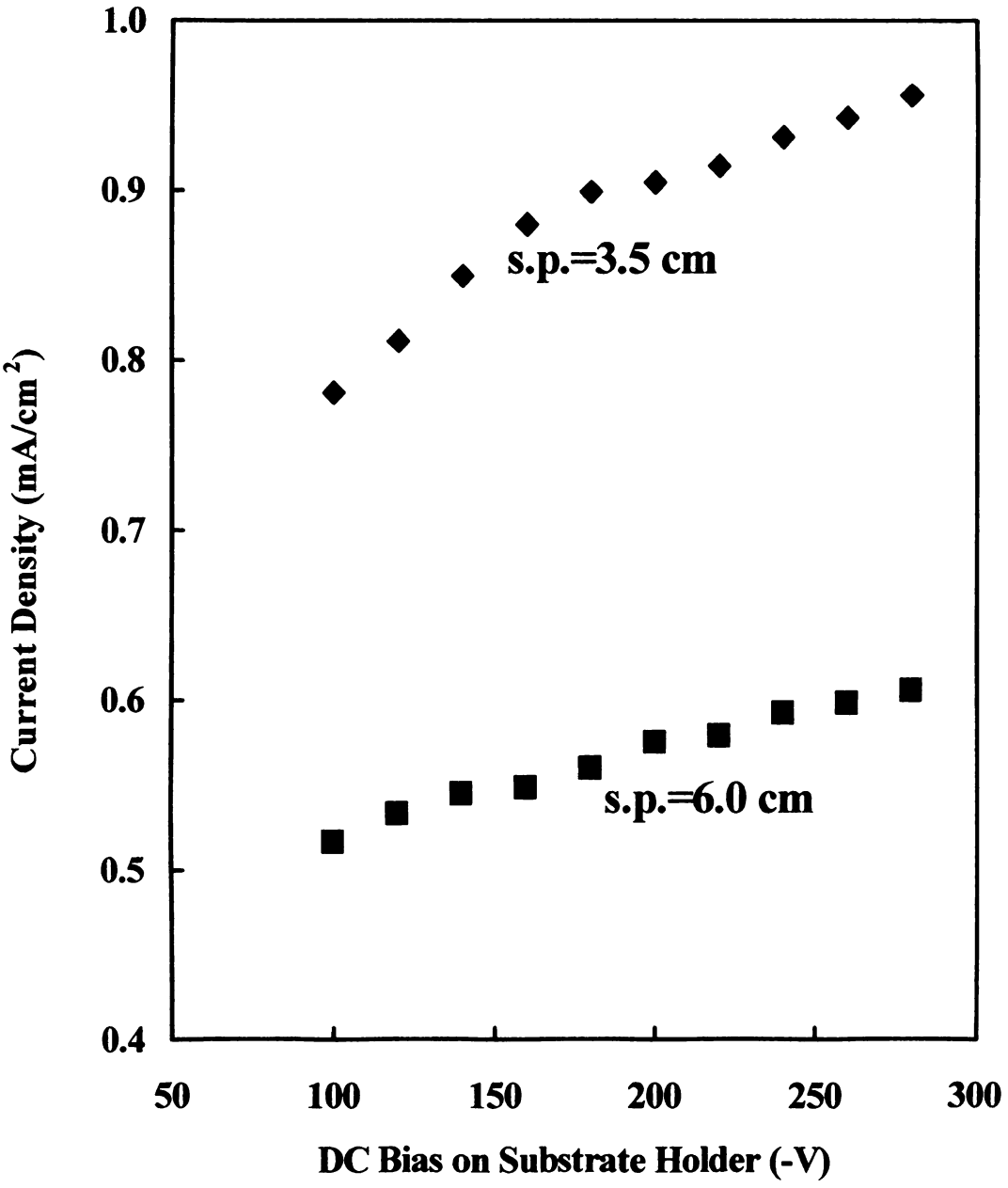

Fig. 4 - 16: Current density on the substrate versus dc bias on the substrate holder for acetylene discharge at 0.2 mTorr pressure at substrate positions (s.p) of 3.5 cm and 6.0 cm.

induced substrate bias. The bars at the peak of optical bandgaps show the range of the optical bandgaps obtained from the repeated experiments. This observation was already shown earlier in Fig. 4-3 and it repeats here again. The variation of optical bandgap near the peak value is considered to be due to the variation of sp^3 fraction in the film composition and the film deposited at –200 V rf induced substrate bias is considered to be ta-C:H films as discussed in Section 4.3. On the other hand, the curve with 6.0 cm substrate position is almost flat not showing the peak value. The index of refraction at 3.5 cm substrate position is slightly higher than the value at 6.0 cm substrate position. The current density at 3.5 cm substrate position (0.9 mA/cm^2) is significantly higher than that at 6.0 cm substrate position (0.57 mA/cm^2). Thus, the ion flux to neutral flux ratio at 6.0 cm substrate position decreased about 40 % from the value with the nominal deposition condition. The facts that the films of 6.0 cm substrate position have relatively high and flat values of optical bandgap and the ion flux is lower than the nominal case suggest that the films are hydrogenated amorphous carbon films with lower carbon-carbon sp^3 fraction. The low value of ion flux onto the growing films at 6.0 cm substrate position could not expel the hydrogen atoms in the films enough to lower the optical bandgaps as discussed in the effect of rf induced substrate bias in Section 4-3.

Fig. 4-17 shows the optical bandgap, E_{tauc}, as a function of the ion flux to neutral flux ratio. 'I/N' stands for the ion flux to neutral flux ratio. The data for I/N=0.95 is from the literature [3] and the data for I/N=0.1 and 0.06 is from Fig. 4-14 of this investigation. The optical bandgap shows a high peak value for the films deposited with I/N=0.95 and a

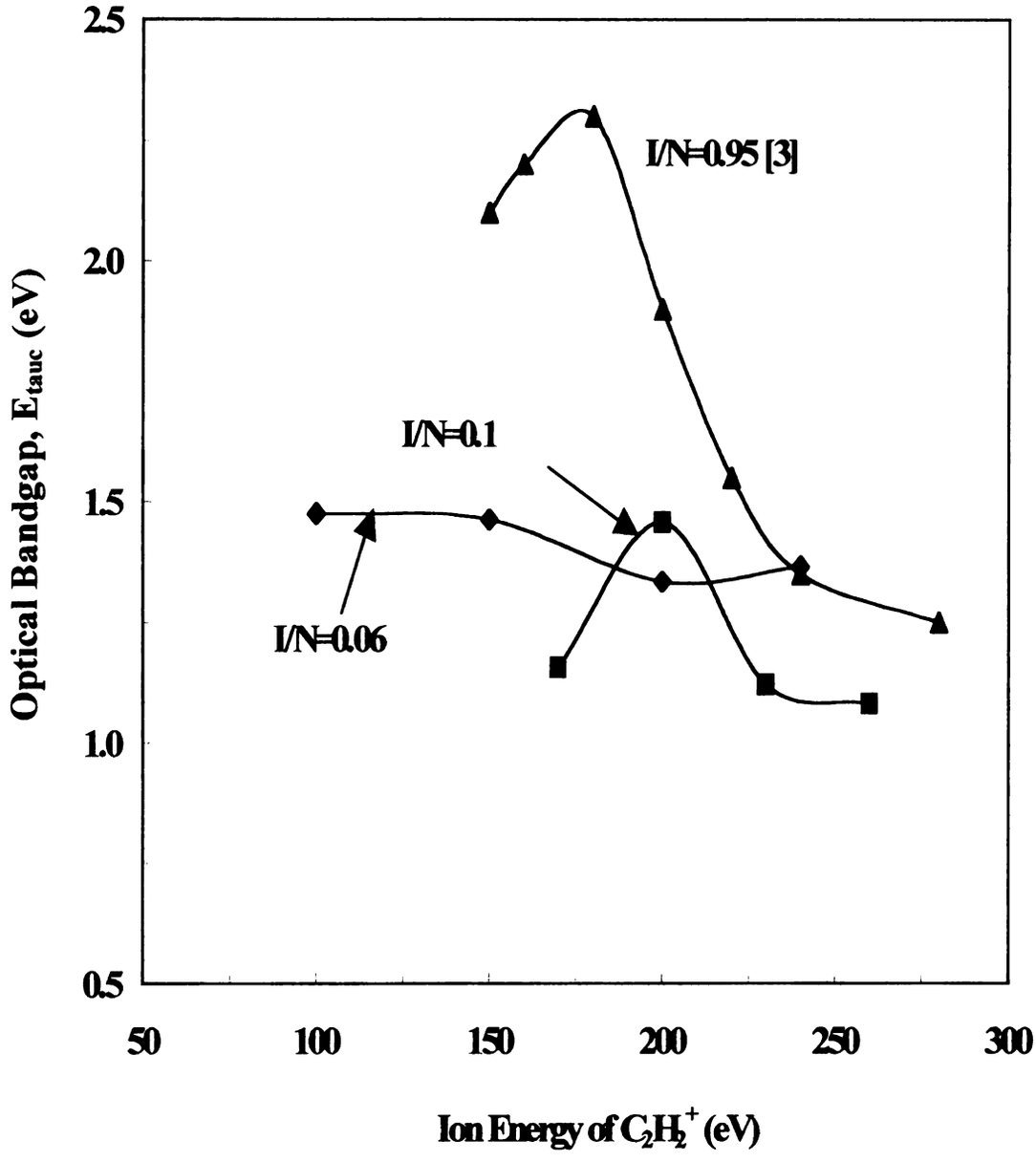

Fig. 4 - 17: Optical bandgap as a function of ion flux to neutral flux ratio

low peak value with I/N=0.1 but does not show any peak value with I/N=0.06. Therefore the threshold ratio of ion flux to neutral flux for depositionof ta-C:H films is found to be in the range of 0.06-0.1 in this investigation.

4.5. The Effect of Deposition Temperature

The deposition temperature is considered an important factor in the deposition of tetrahedral amorphous (hydrogenated) carbon films as discussed in Section 2.4 [19]. A high deposition temperature induces the relaxation of bonding structure from diamond-like carbon films to graphite-like carbon films. In this study a comparison was done between depositions at two different temperatures. The temperature difference was achieved by using a thermally conducting paste for attaching the substrate to the substrate holder, while other substrates were not thermally attached. The thermally conducting paste (heat sink compound) makes a good thermal contact between the substrate and the substrate holder so that heat arriving at the substrate can be quickly transferred to the substrate holder keeping the temperature of the substrate near the temperature of the substrate holder. The film with heat sink compound is the deposited at a lower deposition temperature than the film without heat sink compound. The result is presented in Table 4-4.

Table 4 - 4: The effect of temperature effect on optical bandgaps (E_{tauc} and E_{04}) and index of refraction (n).

Sample	E_{tauc} (eV)	E_{04} (eV)	n
Film with heat sink compound	1.45	1.80	2.27
Film without heat sink compound	1.19	1.59	2.27

The sample with the heat sink compound gave the higher value of optical bandgap of 1.44 eV than the other's 1.19 eV of optical bandgap. The lower optical bandgap of the sample deposited at the higher temperature (no thermally conducting paste) is likely due to higher sp^2 content in the film (i.e., more thermal relaxation of the bonding structure has occurred in the film without heat sink compound). The index of refraction was the same for the two samples at 2.27. Thus, the effect of deposition temperature can be demonstrated by attaching the substrate to the substrate holder using the heat sink compound. Because of this temperature influence, most experiments in this chapter were performed with the substrates thermally attached to the substrate holder by using the heat sink compound.

4.6 The Effect of Addition of Helium Gas

In the deposition process most of the hydrocarbon species are activated and subsequently stick on the surface of the substrate or the walls of deposition chamber, thus, they do not contribute significantly on the total pressure of the chamber as discussed based on the PPA data in Section 4.2. The hydrogen gas has the biggest partial pressure in the chamber of the acetylene discharge. In this section the effect of partial replacement of the hydrogen gas by helium gas in the deposition chamber is investigated by adding helium gas to the acetylene feed gas going into the chamber. The deposition condition was the same as the nominal deposition condition except for the addition of helium gas into the feed gas. The flow rate of helium gas was varied from 0.5 sccm to 2.5 sccm. The films were deposited on the thin substrates that were just put on the substrate holder

without using the heat sink compound. The optical properties of the films are presented in Fig. 4-18 and Fig. 4-19. The films show almost no or minimal influence of the variation of helium flow rates on the optical bandgap and index of refraction. The index of refraction does not show any significant variation with the variation of flow rate of helium and has similar values to those of other films such as films in Table 4-4. However, the optical bandgaps ($1.25< E_{tauc}$ (eV) <1.45) of the films prepared with the addition of helium are a little higher than the values (1.19 eV for E_{tauc} as listed in Section 4.5) of films deposited without either the heat sink compound and helium. One group of samples done with helium addition was deposited on the substrates attached to the substrate holder using heat sink compound. Unfortunately, the films were completely peeled off in the process of ultrasonic cleaning in methanol for removal of heat sink compound before optical characterization was performed. The peeling-off did not occur in films with the nominal deposition condition without helium. From the above facts, the films deposited with addition of helium gas seem to have different film structure and possible more internal stress (hence the peeling) compared to the films deposited with the standard deposition condition.

4.7. The Deposition Rate as a Function of the Acetylene Flow Rate

The flow rate of acetylene gas into the deposition chamber was varied and the films were deposited with other external deposition conditions fixed. The deposition rate almost linearly increases with the increasing flow rate as shown in Fig. 4-20. This result suggests that the flow rate of acetylene source gas is the rate limiting process to form and grow the films. The neutrals, radicals and ions of acetylene gas are considered to have a

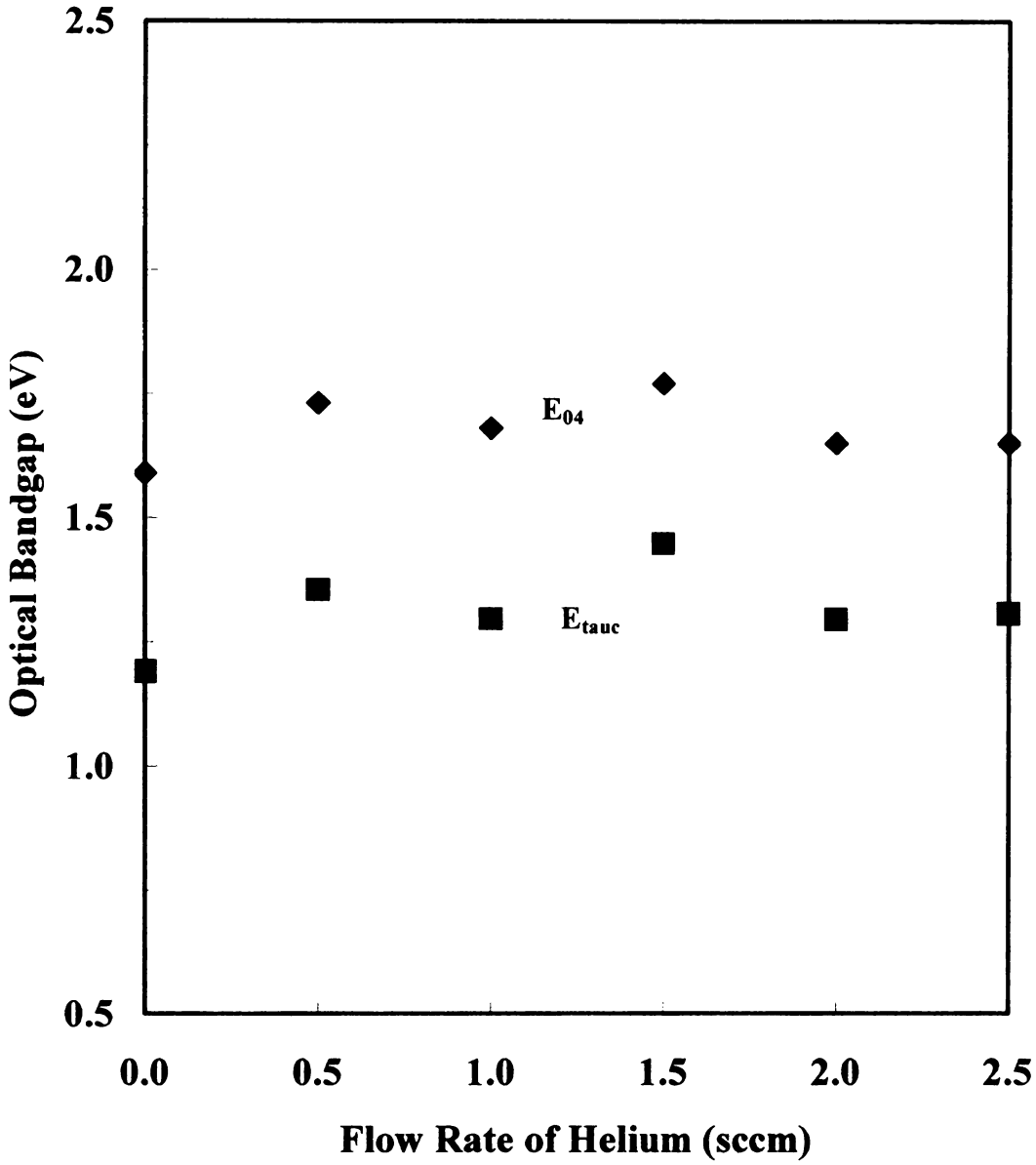

Fig. 4 - 18: Optical bandgap (E_{tauc} and E_{04}) versus flow rate of helium for films deposited from acetylene and helium gas feed with 200 V of rf induced substrate bias.

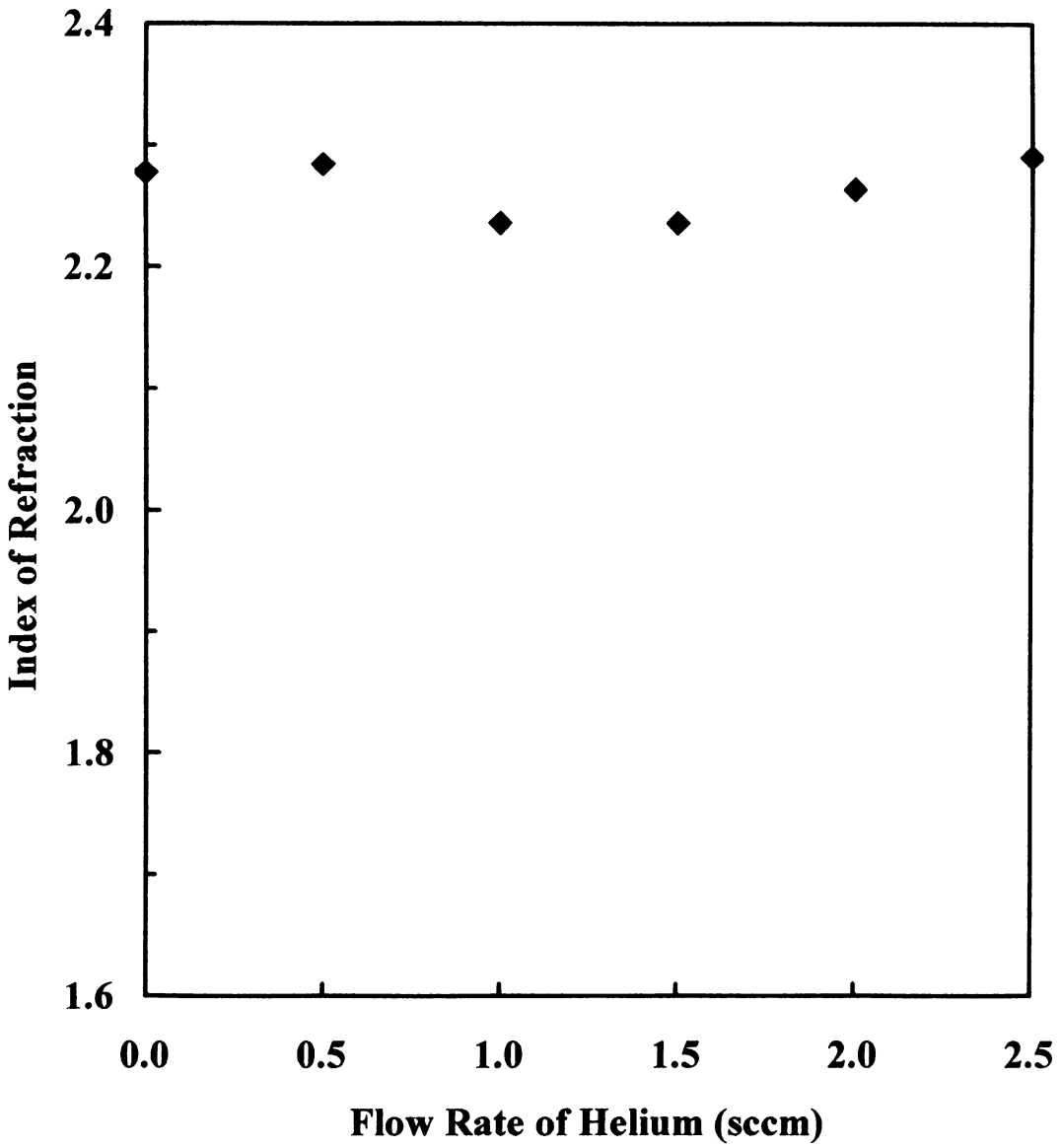

Fig. 4 - 19: Index of refraction versus flow rate of helium for films deposited from acetylene and helium gas feed with 200 V of rf induced substrate bias.

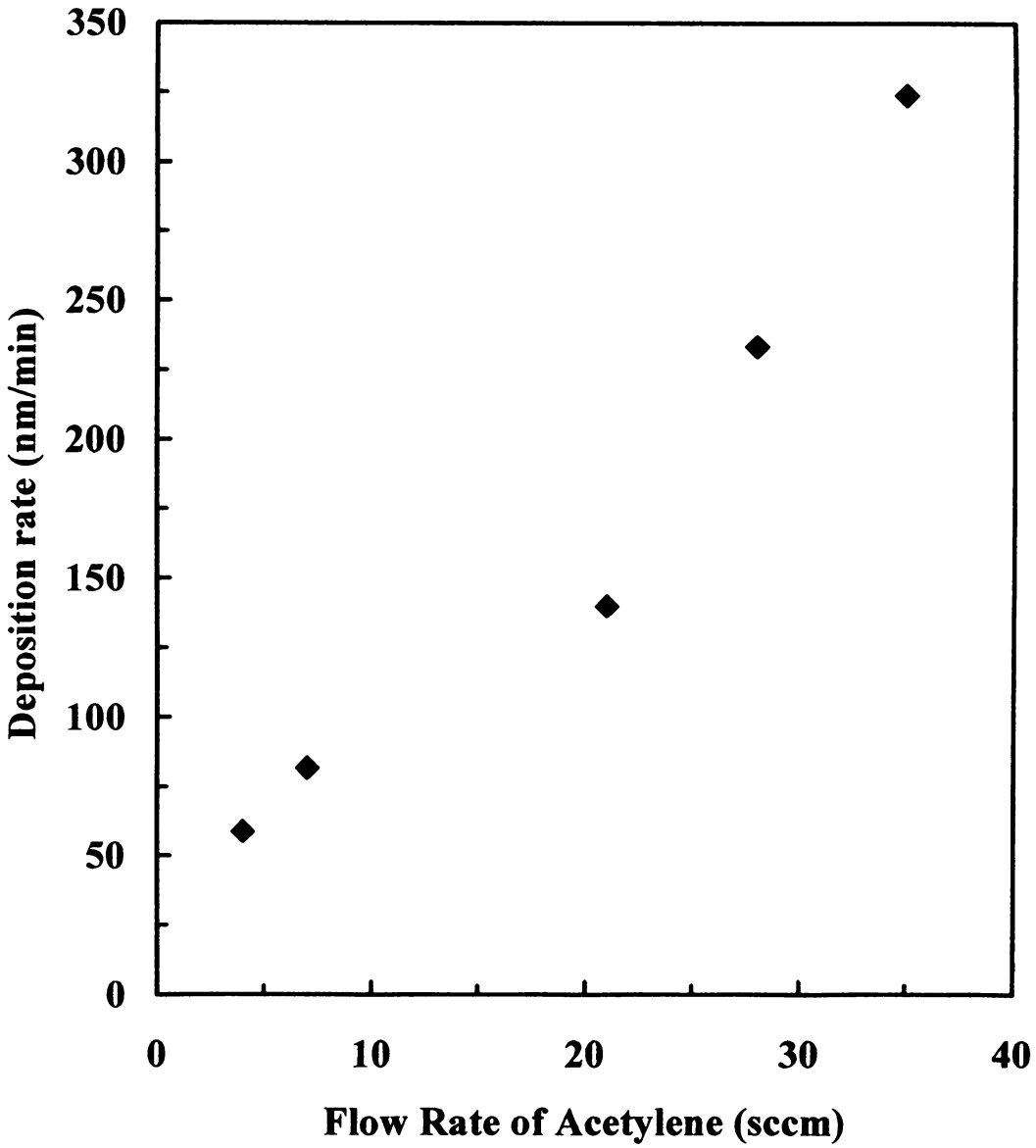

Fig. 4 – 20: The deposition rate of a-C:H films versus the flowrate of acetylene gas into the discharge. The pressure of the discharges varied from 0.2 mTorr to 0.45 mTorr as the acetylene flow rates increased from 4 sccm to 35 sccm

high sticking coefficient in the deposition process from this result. The PPA data also support that they have high sticking coefficient, which was shown in earlier discussion in Section 4.2. The deposition rate (~90 nm/min) at 7.0 sccm of acetylene flow rate in the nominal deposition condition is much higher than the other filtered ion beam and plasma beam deposition systems used for tetrahedral (hydrogenated) amorphous carbon film depositions as discussed in Section 4.3.

4.8 Summary

Hydrogenated amorphous carbon films were deposited at pressures in the submillitorr range and room temperature with the variation of rf induced substrate bias from 80 to -300 V using acetylene source gas. The flow rate of acetylene gas was 7 sccm and the net absorbed input microwave power was about 250 W.

The optical bandgap of the films has a peak value (1.34-1.44 eV for E_{tauc} and 1.77-1.83 eV for E_{04}) at -200 V of rf induced substrate bias, which corresponds to 100 eV of ion energy per carbon atom. The occurrence of a peak value of optical bandgap at -200 V of rf induced substrate bias is in good agreement with the results in the literature and matches well with the subplantation model of ta-C:H films described in Section 2-3. Thus, the films deposited at near -200 V of rf induced substrate bias are considered to have the maximum ratio of carbon sp^3 bonding to sp^2 bonding. Further, the index of refraction does not vary much and the hydrogen content is almost uniform over the experimental range of rf induced substrate bias.

Maintaining a low deposition temperature was critical to obtain the peak value of optical bandgap at -200 V of rf induced substrate bias. The optical bandgap was lowered

to 1.19 eV for E_{tauc} at a higher deposition temperature from 1.44 eV for E_{tauc} at a lower deposition temperature. The effect of ion flux to neutral flux ratio on the properties of films was not present as the films were deposited with the variation of absorbed microwave input power. But the effect appeared as the films were deposited with a variation of substrate position and move weakly with variation of pressure. Thus, the optical bandgap had the peak at -200 V of rf induced substrate bias for the films deposited at 3.5 cm substrate position, but did not show the peak for the films deposited at 6.0 cm substrate position. The ion flux to neutral flux ratio is smaller by 40 % at 6.0 cm substrate position as compared at 3.5 cm substrate position. Thus, the effect of ion flux to neutral flux ratio on the properties of a-C:H films is demonstrated as the subplantation model predicts. The estimated ion flux to neutral flux ratio at 3.5 cm deposition position is approximately 10 %, which is much smaller than the usual ta-C:H film deposition systems of plasma beam systems and filtered ion beam systems in literature. Hence, the observation of a peak in the optical bandgap can occur at ion flux to neutral flux ratio as low as 10 % and the threshold ratio of ion flux to neutral flux for the deposition of ta-C:H films is found to be in the range of 0.06-0.1 at –200 Vrf induced substrate bias.

The deposition rate increased almost linearly with the increasing acetylene flow rate, which suggests the carbon species in the discharge have a very high sticking coefficient in the deposition process. This fact is supported by the data of partial pressure analysis of the exit gas from the deposition chamber, which shows there are few carbon species in the exit gas. Thus, the flow rate of acetylene gas acts as rate-limiting process of the film deposition. The deposition rate (~90 nm/min) at 7.0 sccm of acetylene flow rate

in the nominal deposition condition is much higher than the other filtered ion beam and plasma beam deposition systems used for tetrahedral (hydrogenated) amorphous carbon film depositions.

Chapter 5

5. Films Deposited from Acetylene-Argon and Methane-Argon Discharges at Pressures in the Millitorr Range

5.1. Introduction

In this chapter, a-C:H films are deposited and characterized at higher pressure conditions than those of the previous chapter. The objectives in Chapter 5 are to establish the variation of film properties possible by depositing the films using different hydrocarbon/argon feed gases at different deposition conditions and to understand the deposition process of the films by investigating the effects of rf induced substrate bias, pressure and argon flow ratio. The deposition pressure is increased up to the millitorr range from the submillitorr range, and the typical pressure is 3mTorr. Many plasma-assisted CVD investigations for a-C:H deposition have been run at pressures in the millitorr range as discussed in Section 2.4. At this range of pressures, the films are sometimes deposited with the addition of inert gases or hydrogen gas [20, 25-28, 30, 71-73]. Work by Mutsukura and coworkers have studied the influence of noble gases He, Ne, Ar, Kr and Xe on methane plasmas used for the deposition of a-C:H films [74-76]. Their work done using a rf plasma deposition system showed that He, Ne, Ar and Kr can all work to enhance the hydrocarbon ion flux to the deposition surface. The source gases used in this study for the films were acetylene gas and methane gas, and argon gas was used as the inert gas. The usual deposition time was 5 minutes for acetylene-argon discharge and 10 minutes for methane-argon discharge. The incident microwave input

power was about 250 W and the reflected power was very small when compared with the incident power, thus the reflected power was neglected. The rf induced negative substrate bias was varied from 0 to -60 V for 0.17 mm thick glass substrate and from 0 to -100 V for 1 mm thick glass substrate. The substrates used were mounted on the metal substrate holder without thermally conducting paste (heat sink) and placed at 3.5 cm below the baseplate. Thus, the substrate temperature was higher than room temperature because of the heating from the discharge. The substrate temperatures were measured to be around 80-100 C after 5 minutes of deposition time at 3mTorr with the method discussed in Section 3.4.3.

The deposition pressure and the argon flow rate were also varied for the deposition of several films to see their effects on the properties of the films. This variation of deposition condition in this chapter produces a variation of the film properties. Specific properties studied include deposition rate, density, hydrogen content, index of refraction and optical bandgap. The ranges of input variables are summarized in Table 5 - 1.

Table 5-1: The input variable space

Input Variables	Variable Range
RF induced substrate bias (-V)	0 - 60 for 0.1 mm thick glass substrate 0 - 100 for 1 mm thick glass substrate
Microwave power (W)	200 - 300
Pressure (mTorr)	1 - 5
Hydrocarbon gas flow rate (sccm)	7 or 8 (C_2H_2 or CH_4)
Argon flow to hydrocarbon gas flow ratio	0 - 1 (Ar/C_2H_2 or Ar/CH_4)

The discharge properties at pressures in the millitorr range are presented before the properties of the films to use the discharge properties in the discussion of the properties of the films. The discharge properties include electron temperature, plasma density measured by double Langmuir probe and partial pressure analysis of the exit gas.

5.2 Discharge Properties at Pressures in the Millitorr Range

For the investigation of discharge properties of the ECR-CVD deposition system at pressures in the millitorr range, the electron temperature and plasma density were measured using a double Langmuir probe for an argon discharge at 200 W microwave input power and 8 sccm argon flow rate versus variation of pressure. The probes were located at the place where the substrates are normally positioned. The results are shown in Fig. 5-1 and Fig. 5-2. The electron temperature decreases and plasma density increases with increasing pressure.

The double Langmuir probe was also used to measure a-C:H deposition discharges. These discharges coated the probe quickly with an insulating film, so before each measurement the probe was biased negative and sputtered clean of the a-C:H film with an argon plasma. Once cleaned, the probe could be used to take measurement for about 30 seconds before a new a-C:H insulating coating would disrupt the measurements significantly, thus requiring the probe be cleaned again. The summary of this data taken at a pressure of 3mTorr, microwave power of 270 W and argon flow rate of 8 sccm is shown in Table 5-2. The electron temperatures of acetylene-argon discharges are similar, but are slightly lower than those of the methane-argon discharges. Another observation in Table 5-2 is that the ion saturation current shows only a modest change as the gas composition varies. Specifically, the change in the ion saturation current, at a fixed

microwave power as the hydrocarbon gas flow rate is adjusted, is less than a 30% deviation from the pure argon plasma value.

Table 5-2: Langmuir probe measurement of argon, methane-argon, and acetylene-argon discharges. The argon flow rate is constant at 8 sccm.

CH_4 flow rate (sccm)	C_2H_2 flow rate (sccm)	Saturation ion current (mA/cm^2)	Electron temperature (eV)
0	0	2.33	2.0
8	0	1.67	2.8
4	0	2.11	2.7
0	8	1.96	2.3
0	4	2.96	2.6

An important variable that has a crucial influence on the film properties is the ion impacting energy onto the surface a growing film as discussed in Section 2-2. The ion energy is determined by the potential given by $|\phi_{rf}|+\phi_w+\phi_{diff}$ in the discussion in Section 3.4.2. The potential ϕ_w, as determined from equation (3-5) and T_e values of 1.8-3.0 eV from Table 5-2 and Fig. 5-1, ranges from 6 to 14 V. ϕ_{diff} measured varies from 2-10 V. So the potential difference between the plasma and the substrate holder is $|\phi_{rf}|$+(8 to 24) V. and can be written by $|\phi_{rf}|+16\pm8$. The plasma sheath thickness on the substrate holder can be estimated with ϕ_{rf} (=100 V, for example), electron density of (0.6-1.8)x10^{11} cm^{-3} from Fig. 5-2 and T_e of the values given above using equation (3-6) and (3-7) in Section 3.4.2. It has ranges of 0.33 mm-0.61 mm with the matrix sheath theory and 0.45 mm-0.99 mm with Child Law sheath theory. When the thickness of the substrate (0.17 mm) is considered, the ion energy on the surface of a substrate using the above estimation of

plasma sheath thickness on the substrate holder and a given ϕ_{rf}=100 V, has ranges of 25-64 eV with the matrix sheath theory and 54-96 eV with Child Law sheath theory.

Another factor that could influence the ion energy is collisions within the plasma sheath. The importance of collisions can be assessed by comparing the ion mean free path between collisions with the plasma sheath thickness. The plasma sheath is already estimated and is less than 1 mm. The mean free path λ_i for an argon ion moving in an argon background gas of temperature 600 K [77] is approximated as λ_i=1/(165p) cm [51] where p is the pressure in torr. For the pressure range studied in this investigation of 1-5 mTorr the mean free path ranges from 12-60 mm. Hence the mean free path is significantly longer than the sheath thickness and minimal collision occurs as the ions transit the plasma sheath. Therefore, the ion energy is well described by knowing the potential across the plasma sheath adjacent to the substrate.

The compositions of the residual gas flow at the pumping port of the chamber for 50 % / 50 % methane-argon mixtures with discharge on and discharge off are shown in Fig. 5-3 - Fig. 5-4, respectively. Acetylene-argon mixtures with discharge on and discharge off are shown in Fig. 5-5 and Fig. 5-6, respectively. The mass of various species is presented in Table 5-3 for convenience in reading the plots of partial pressure analysis.

Table 5 - 3: Table of mass

Mass (amu)	1	2	16	26	18	40
Species	H	H_2	CH_4	C_2H_2	H_2O	Ar

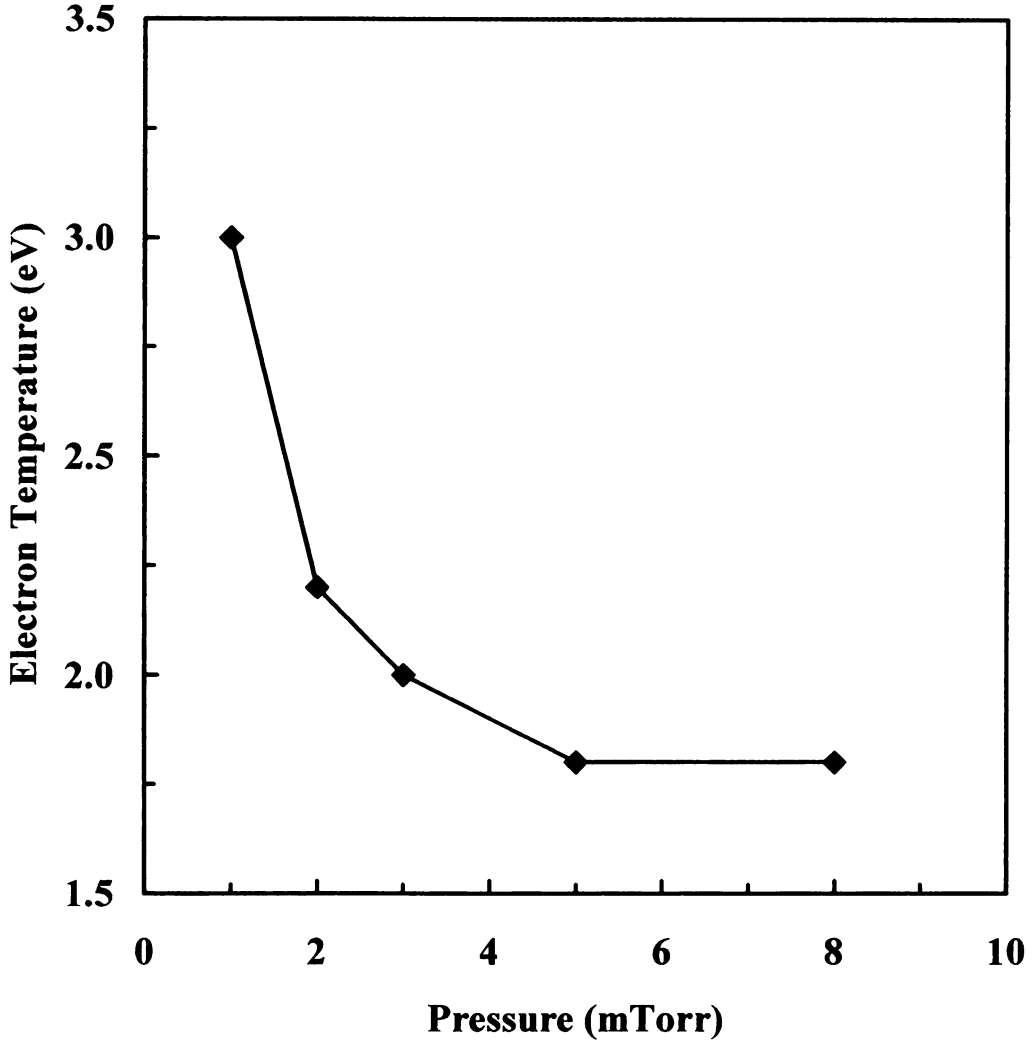

Fig. 5 - 1: Electron temperature for argon discharges versus pressure in the ECR-CVD system.

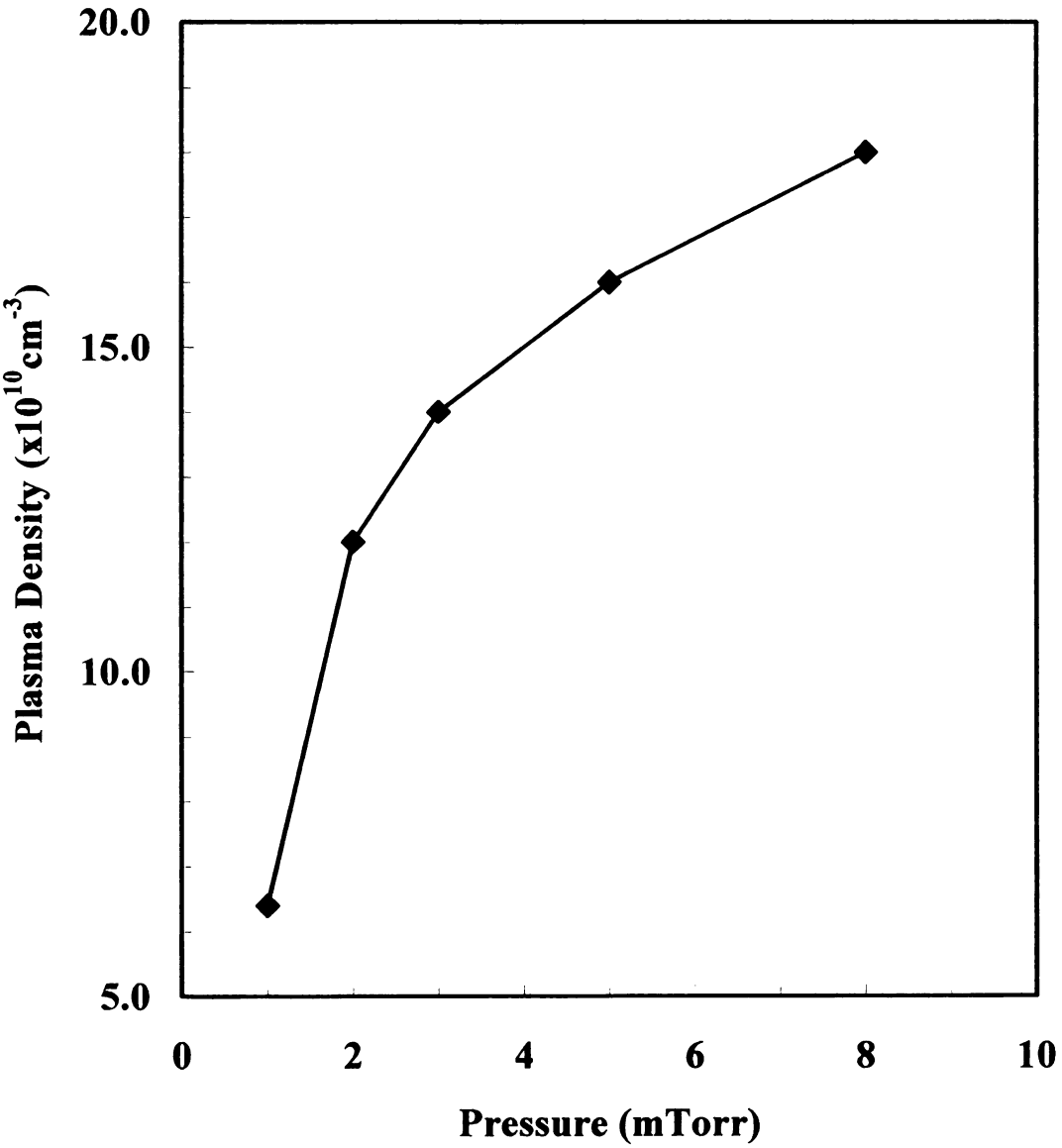

Fig. 5 - 2: Plasma density, n_p, for argon discharges versus pressure in the ECR-CVD system.

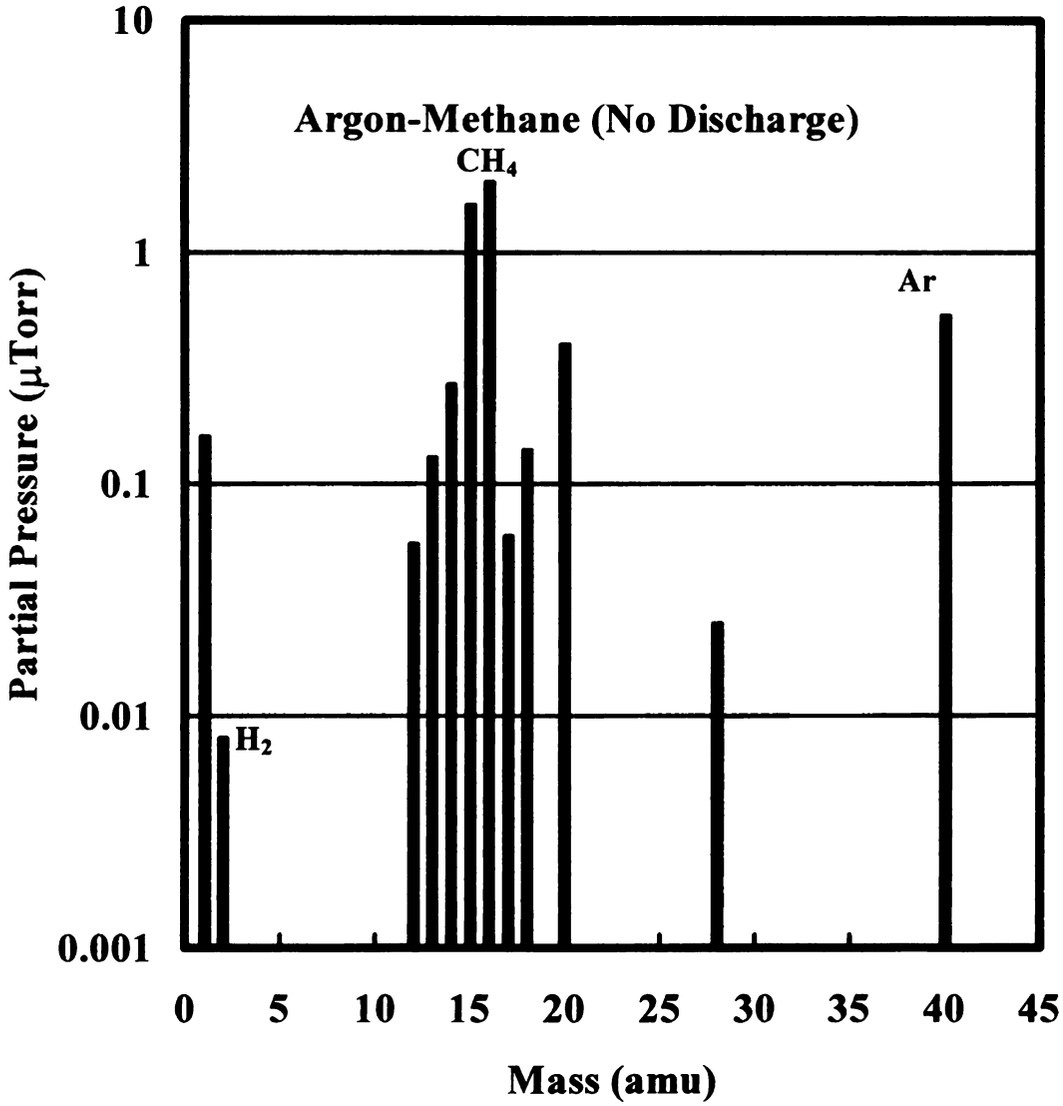

Fig. 5 - 3: Partial pressure analysis for the methane-argon gas mixture with the discharge off.

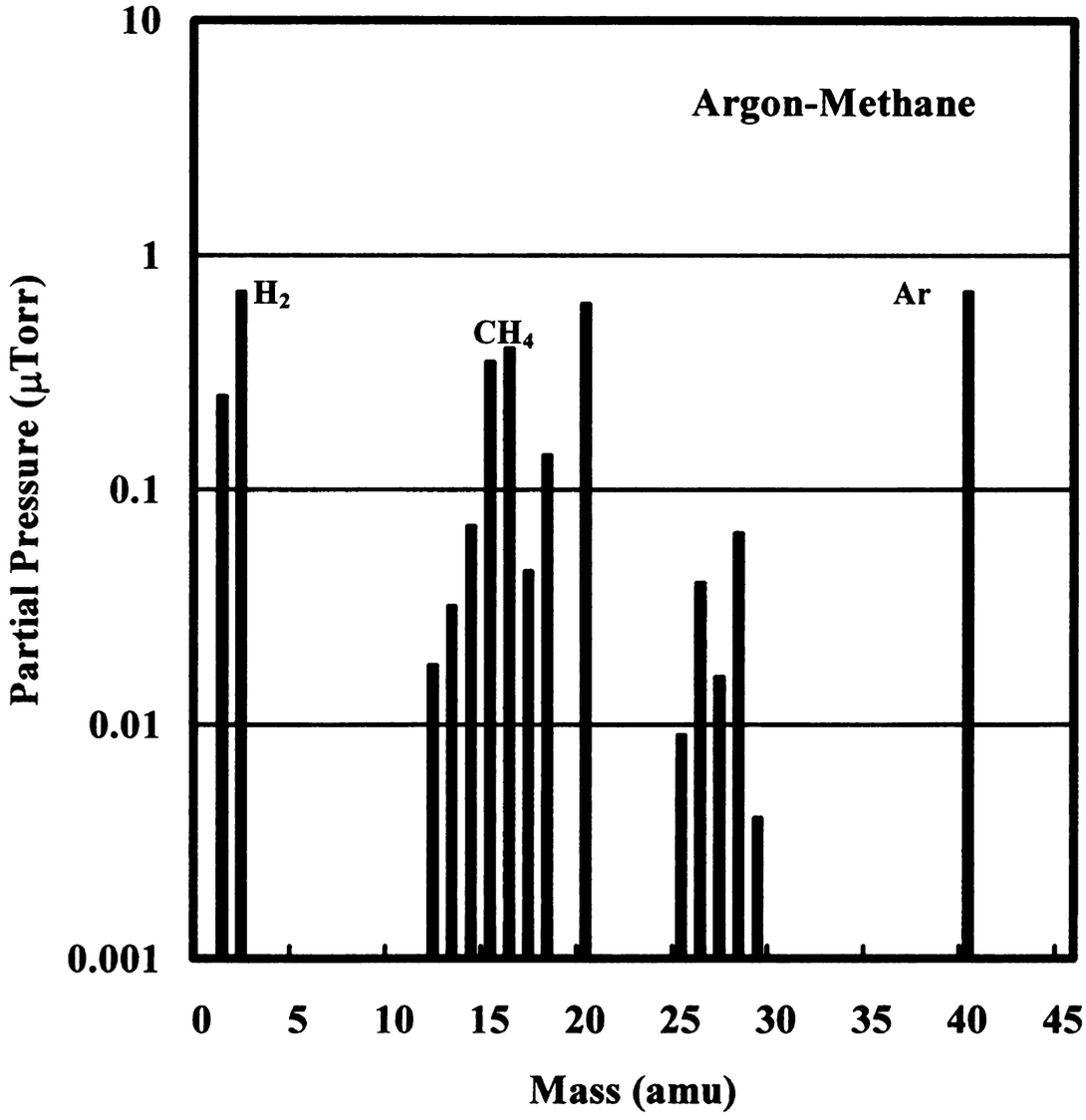

Fig. 5 - 4: Partial pressure analysis for the methane-argon gas mixture with the discharge on.

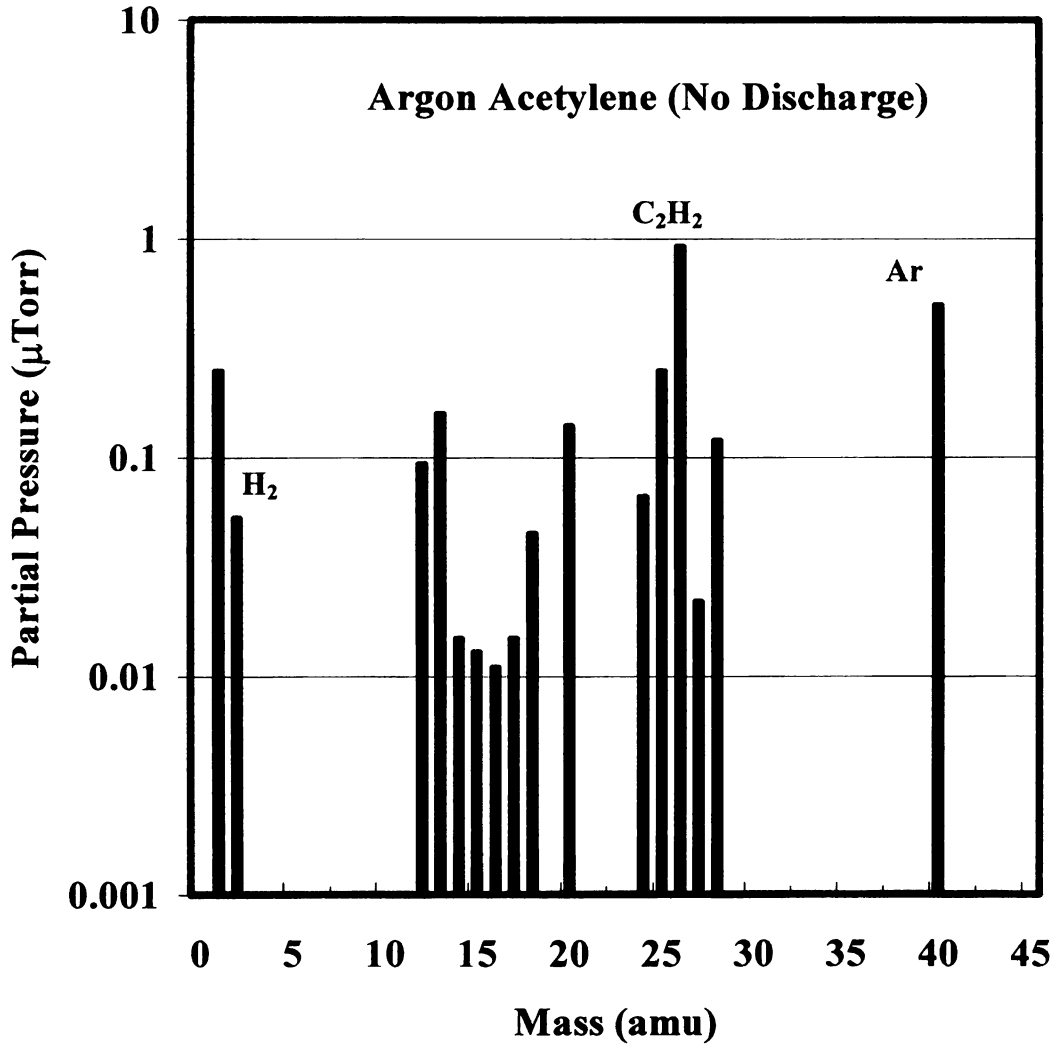

Fig. 5 - 5: Partial pressure analysis for acetylene-argon gas mixture with discharge off.

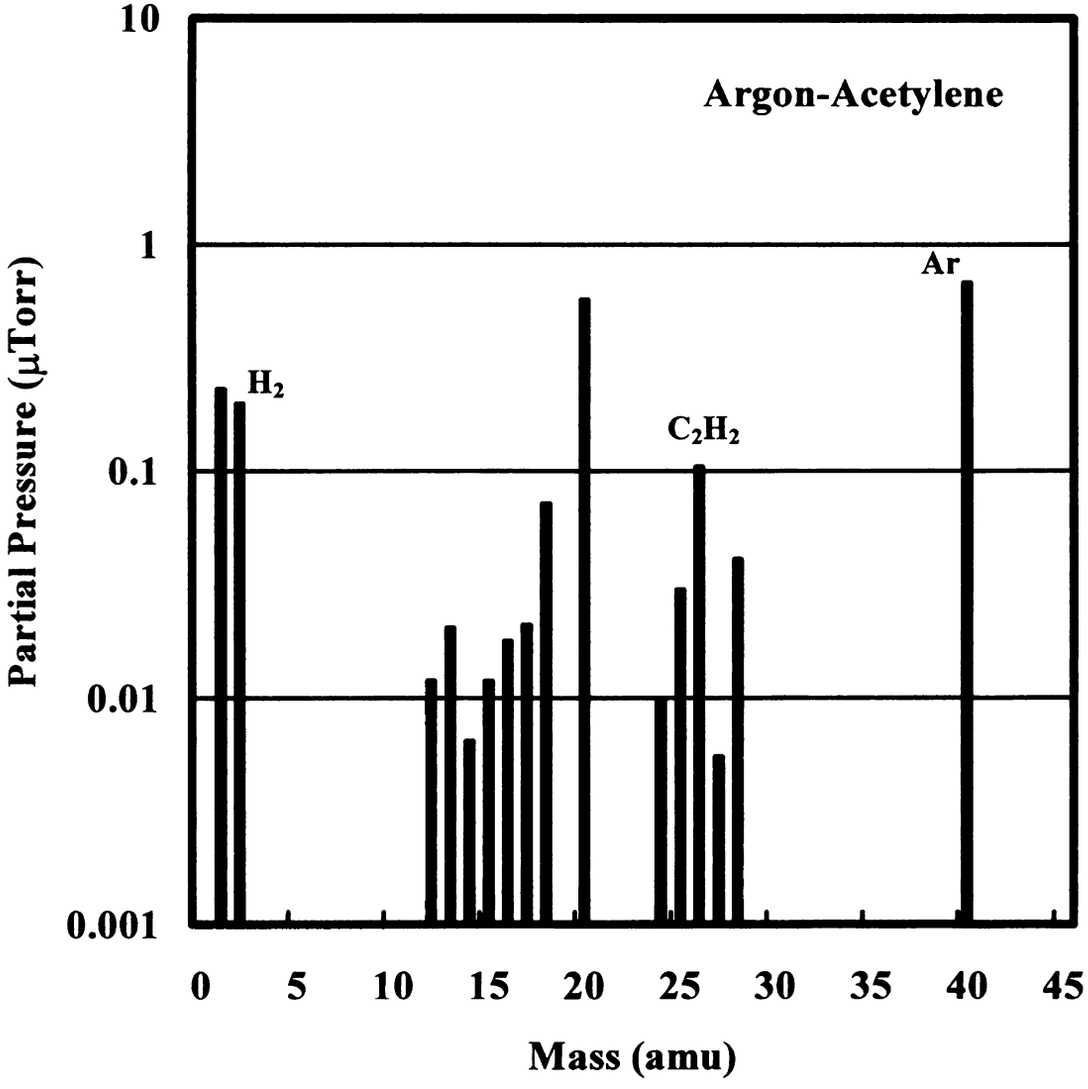

Fig. 5 - 6: Partial pressure analysis for acetylene-argon gas mixture with discharge on.

The discharge conditions for the figures were 3 mTorr pressure, 300 W microwave input power, 7 sccm flow rate of acetylene or methane, 7 sccm argon flow rate and zero rf induced substrate bias voltage. The discharge-off data in Fig. 5-3 and Fig. 5-5 shows standard cracking patterns for electron impacting ionization. The partial pressure of carbon-containing species in the exit gas flow with the discharge on is low. The ratio of methane partial pressure with the discharge on as compared to the discharge off is 0.20 for a methane-argon mixture (7 sccm-7 sccm) in Fig. 5-4. Similarly, the ratio of acetylene partial pressure with discharge on to the acetylene partial pressure with discharge off is 0.11 for an acetylene–argon mixture (7 sccm - 7 sccm) in Fig. 5-6. Hence, a substantial portion of the carbon that flows into the plasma discharge is activated by either excitation, dissociation or ionization and this carbon is deposited on either the substrate or the chamber walls. The high sticking coefficient of hydrocarbon species in acetylene discharge was also seen in Section 4-2, already. Also indicated is that the methane-argon plasma shows a substantial increase in the hydrogen present in the exit gas when the discharge is on as compared to the discharge off. It should be also noted that the source of the hydrogen for the discharge-off case in the PPA spectrum of Fig. 5-3 and Fig. 5-5 is likely dissociation of methane caused by the electron emitter in the PPA unit.

5.3 Film Properties at Pressures in the Millitorr Range

5.3.1 Absorption Coefficients

The optical absorption coefficient versus photon energy of a-C:H films deposited using a methane-argon plasma are shown in Fig. 5-7 and Fig. 5-8. Fig. 5-7 shows the absorption coefficient versus photon energy for four different rf induced substrate biases.

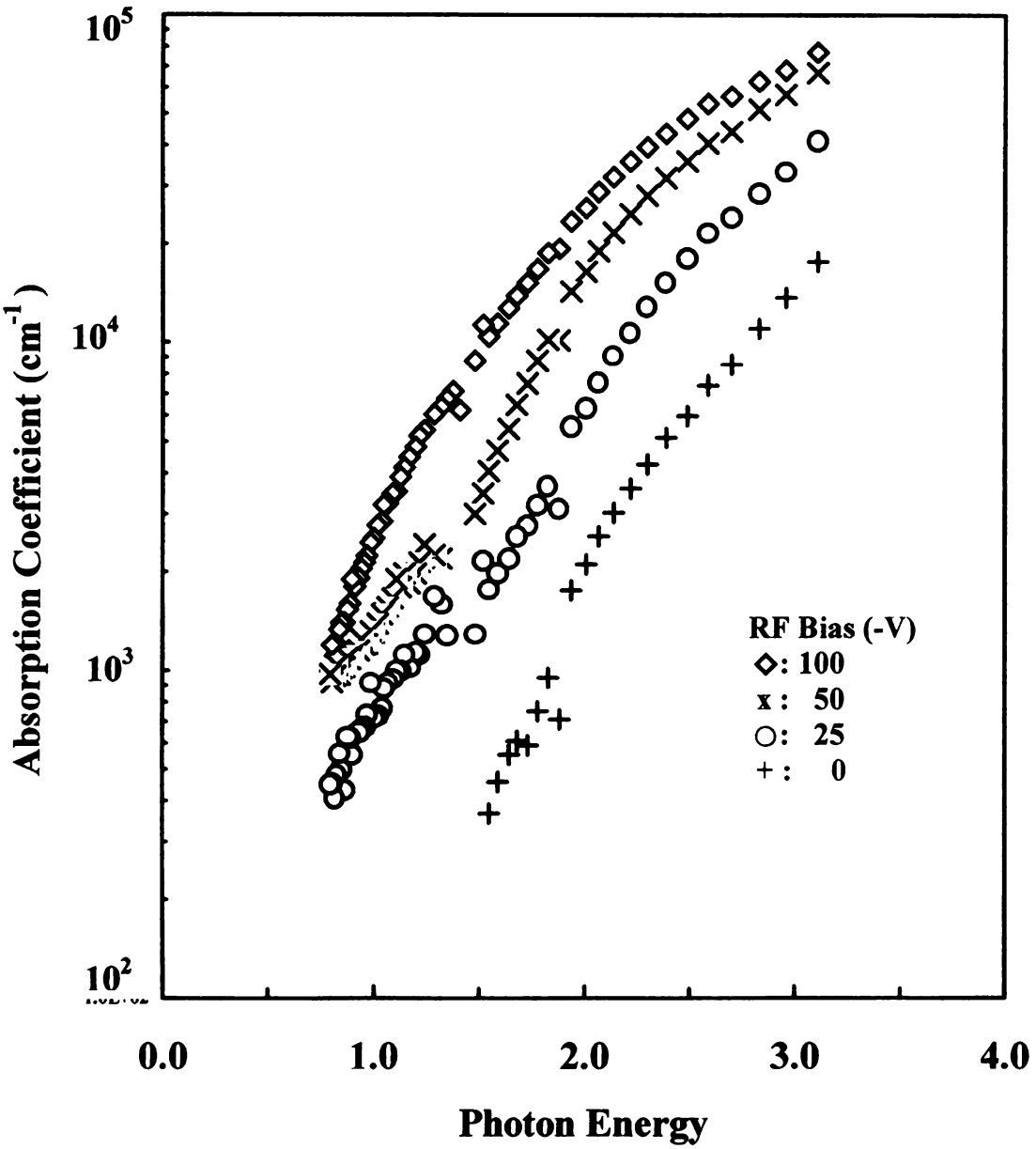

Fig. 5 - 7: Optical absorption coefficients of films deposited in methane-argon discharges. Data is plotted versus photon energy at various rf induced substrate biases.

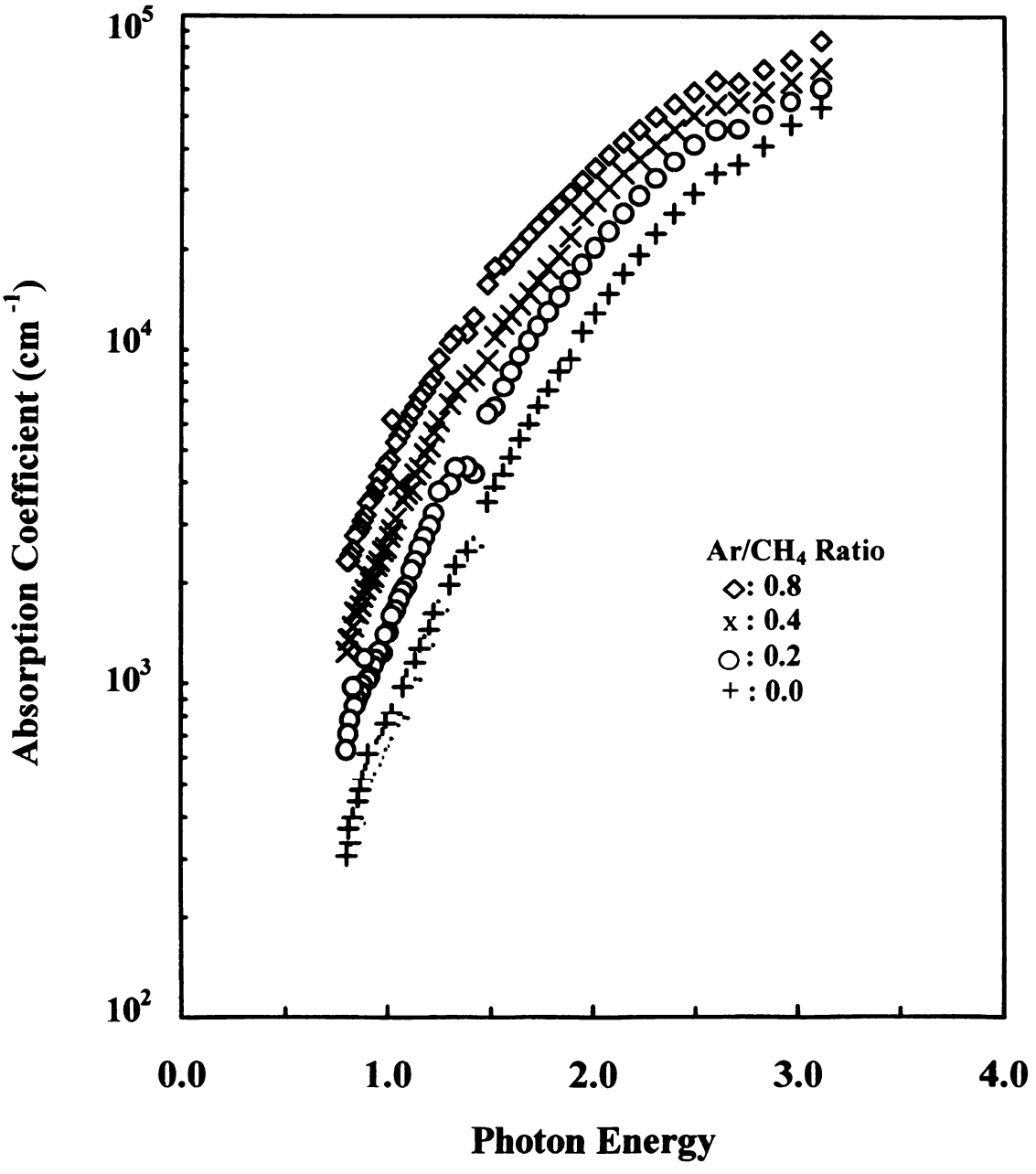

Fig. 5 - 8: Optical absorption coefficients of films deposited in methane-argon discharges. Data is plotted versus photon energy at various argon flow ratios.

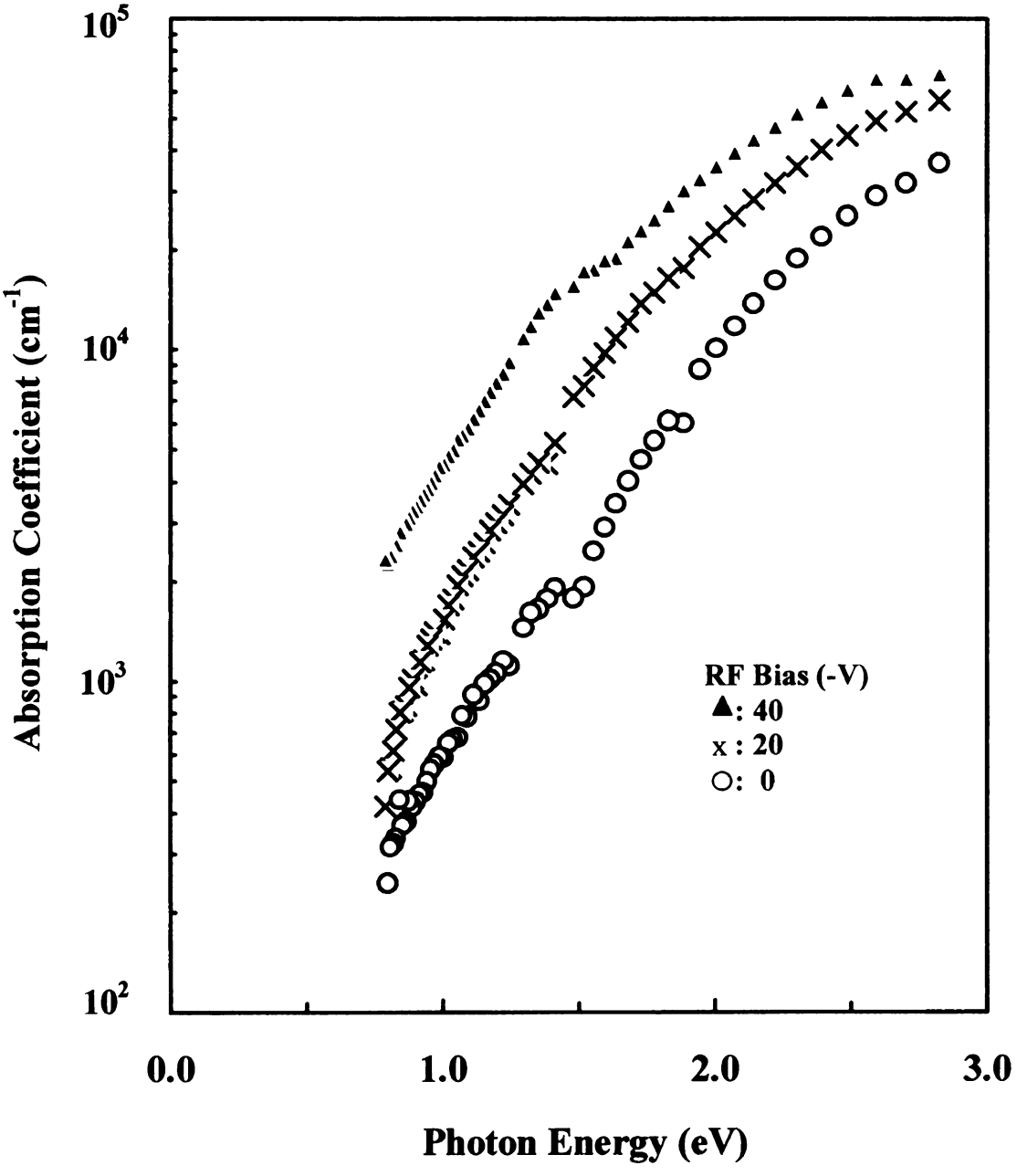

Fig. 5 -9: Optical absorption coefficients of films deposited in acetylene-argon discharges. Data is plotted versus photon energy at various rf induced substrate biases.

The deposition condition for this figure is 200 W input microwave power, 8 sccm argon, 8 sccm methane, and 3 mTorr pressure. The films were deposited on 1 mm thick glass substrates. The absorption at a given photon energy increases as the ion energy increases (i.e., the rf induced substrate bias becomes more negative). Fig. 5-8 shows the absorption coefficient for four different argon/methane flow rate ratios at the condition of 300 W microwave power, 8 sccm argon, 8 sccm methane, 3 mTorr and -50 volts induced substrate bias. The addition of argon produces films of higher optical absorption. Fig. 5-9 shows the absorption coefficient for films deposited using an acetylene-argon gas mixture. The deposition conditions include 200 W microwave power, 8 sccm acetylene, 8 sccm argon, 3 mTorr pressure, and -40, -20 and 0 V rf induced dc substrate bias. The films were deposited on 1 mm thick glass substrates. The more negative substrate biases again produced films that are more optically absorbing.

5.3.2 The Effect of RF Induced Substrate Bias

The effects of the rf induced substrate bias voltage on the film property variations are shown further in Fig. 5-10 to Fig. 5-14 at pressures in the millitorr range. All of the films in Fig. 5-10 to Fig. 5-14 were deposited at 3 mTorr, 200 W microwave input power, 7 sccm flow rate of acetylene or methane gas and 7 sccm flow rate of argon gas with a variation of rf induced dc substrate bias from 0 to -60 V (i.e., increasing ion energy). The films were deposited on 0.17 mm thick glass substrates. The films were unable to be deposited below -60 V of rf induced substrate bias in this deposition process because of delamination. The film's deposition rate decreases with increasing ion energy for both acetylene-argon and methane-argon discharges in Fig. 5-10. The films from acetylene-

argon discharges have a higher growth rate than from methane argon discharges at the same rf induced substrate bias. Film mass density increases with the increasing ion energy for depositions from both acetylene-argon and methane-argon discharges in Fig. 5-11. The mass density of films from acetylene-argon discharges is higher than from methane-argon discharges. The hydrogen content of acetylene-based films changes only slightly with the variation of rf induced substrate bias, and in contrast, the hydrogen content of methane-based films decreases greatly with ion energy increases in Fig. 5-12.

The refractive index increases quickly with the increasing ion energy for acetylene-based films and changes more slowly for methane-based films in Fig. 5-13. The Tauc optical bandgap E_{tauc} and E_{04} bandgap (energy at absorption coefficient $\alpha=10^4 cm^{-1}$) decreases with the increasing ion energy in Fig. 5-14. The optical bandgaps of the CH_4 films are consistently higher than those of the acetylene-based films.

The deposition rate of both acetylene-based and methane-based films decreases in Fig. 5-10 as the rf induced substrate bias is increased. This result agrees with the reference [73] in which the films were deposited using a rf inductively coupled plasma reactor with a rf biased substrate. The plasma deposition conditions are expected to be similar in this system as in ECR systems. In general, for ion-assisted deposition two competitive processes that determine the deposition rate include an increase in the sticking coefficient with increases in the bias voltage and an increase in the sputtering/etching with increases in the bias voltage. An increase in the sticking coefficient would increase the deposition rate [14, 21, 30], which is not observed experimentally in this investigation. Rather, the decreasing deposition rate of the films

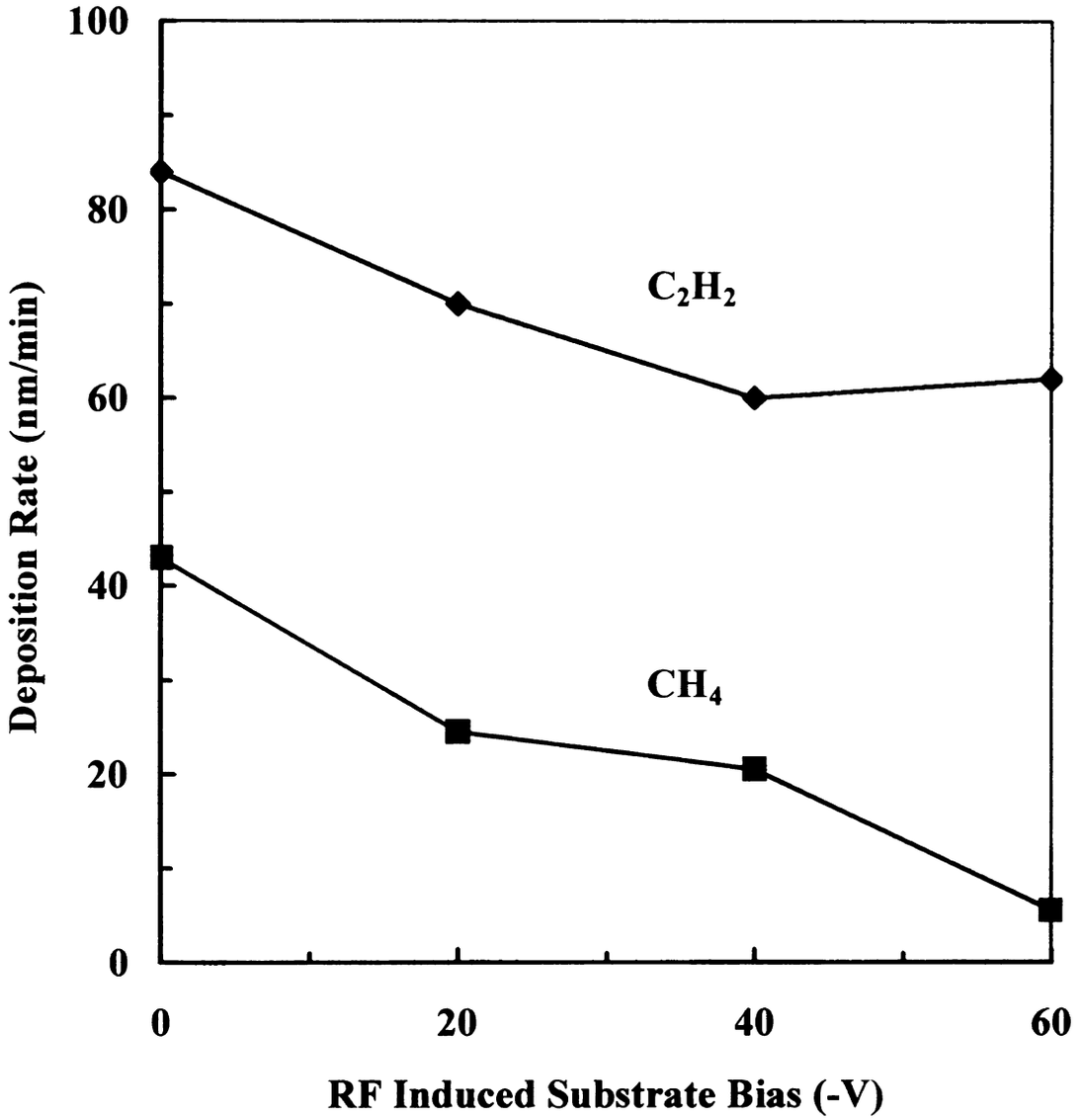

Fig. 5 - 10: Deposition rate versus rf induced substrate bias for methane-based and acetylene-based films.

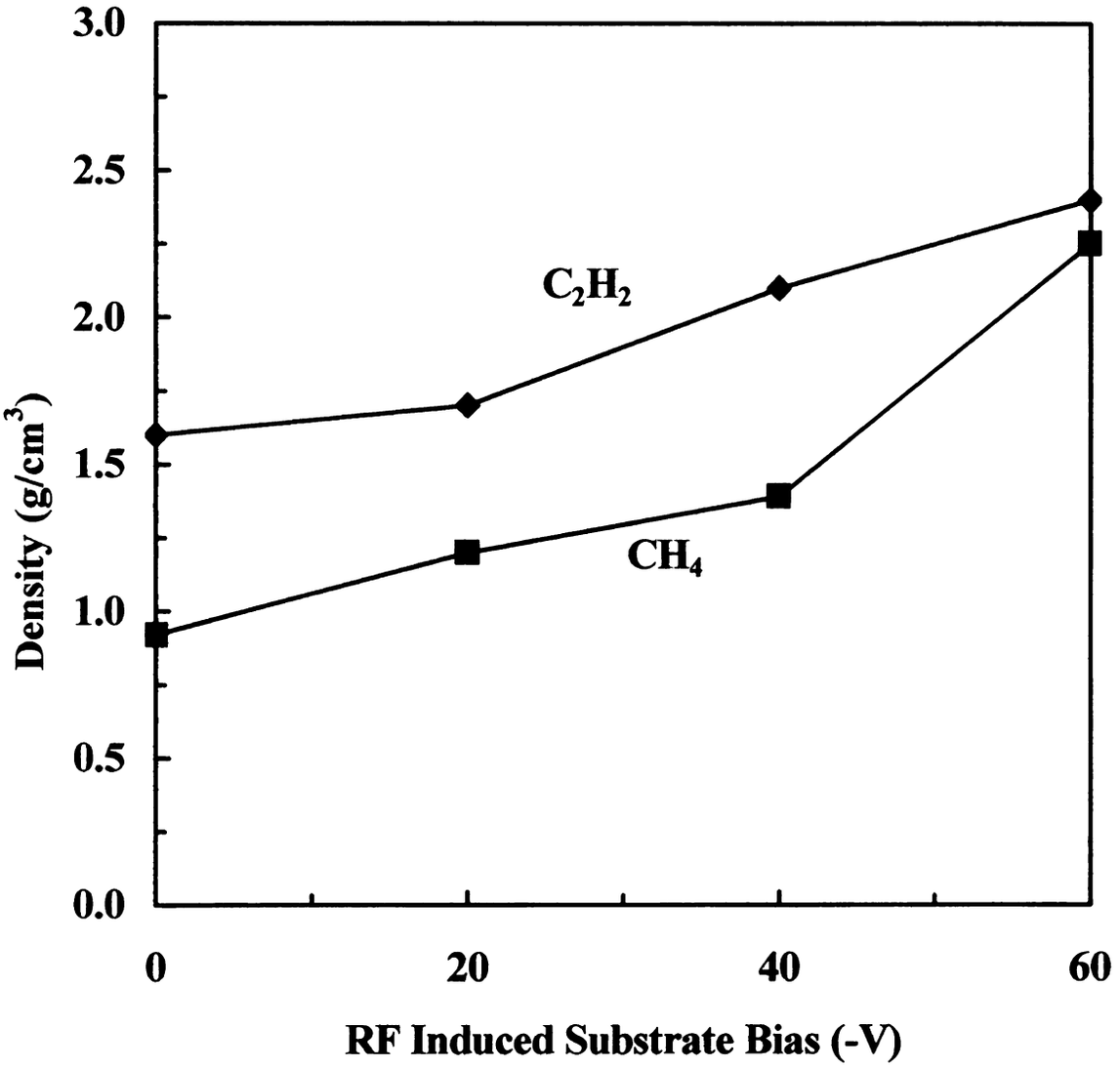

Fig. 5 - 11: Mass density versus rf induced substrate bias for methane-based and acetylene-based films.

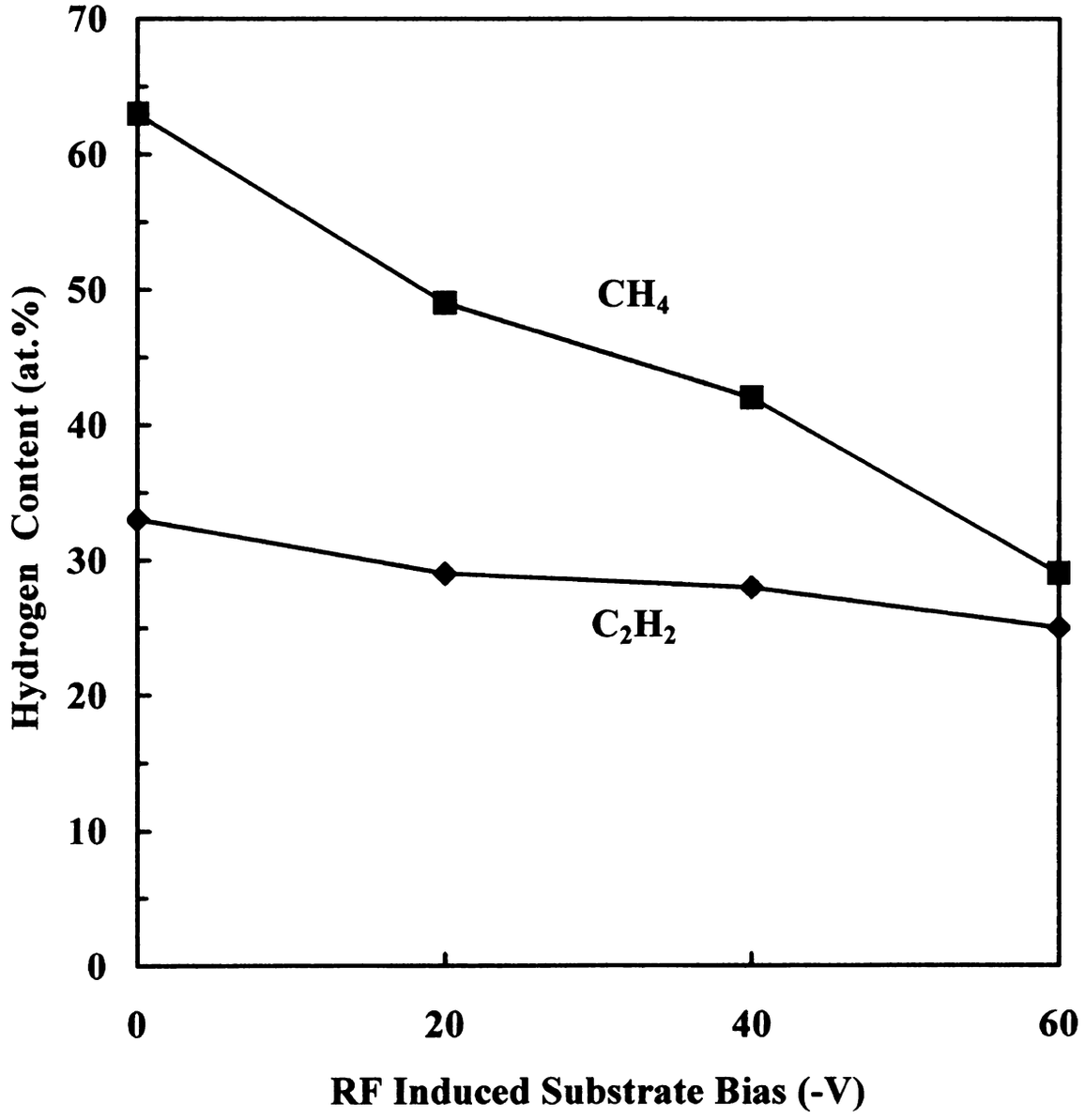

Fig. 5 - 12: Hydrogen content (at. %) versus rf induced substrate bias for methane-based and acetylene-based films.

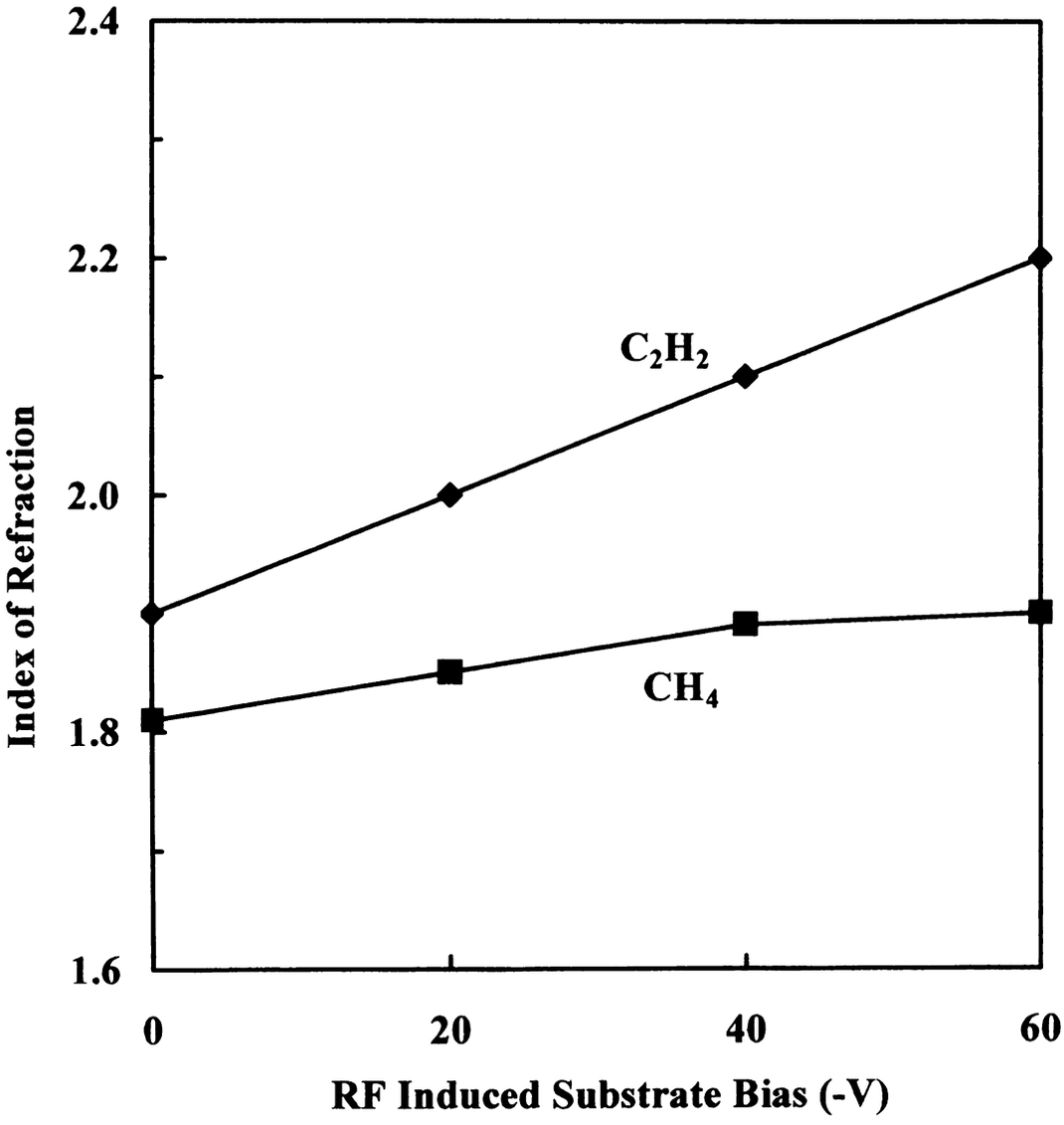

Fig. 5 - 13: Index of refraction versus rf induced substrate bias for methane-based and acetylene-based films.

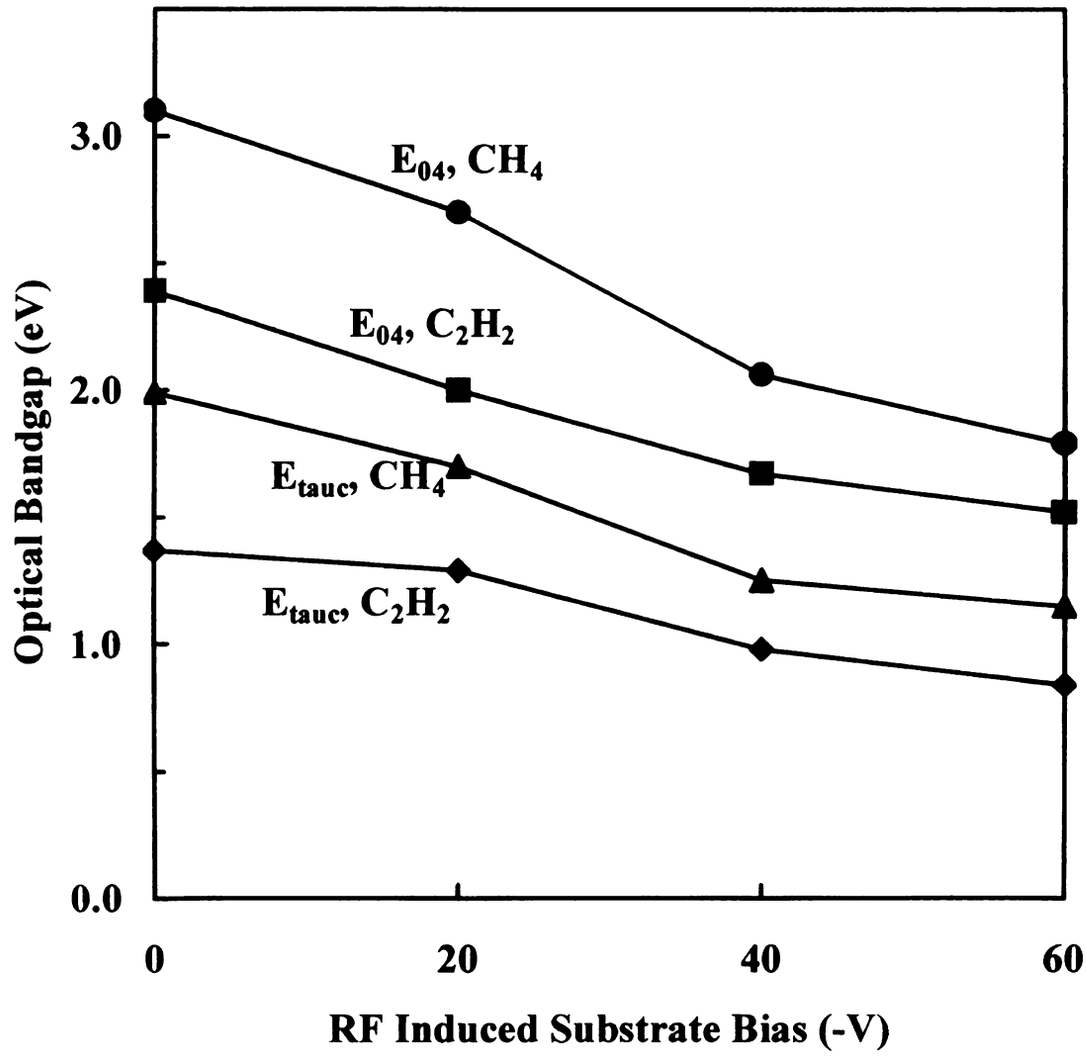

Fig. 5 - 14: Optical bandgap (E_{tauc} and E_{04}) versus rf induced substrate bias for methane-based and acetylene-based films.

with increasing bias voltage reflects the influence of a sputtering or etching effect on the films and/or densification of the films during the deposition process. The decreasing hydrogen content (Fig. 5-12) in the films and the increasing density of films (Fig. 5-11) with increasing ion energy primarily support the densification explanation. This densification with the increasing magnitude of negative induced dc bias on the substrate can be explained by momentum transfer of the bombarding argon, hydrogen, and/or hydrocarbon ions to the surface. This bombardment reduces the hydrogen in the film and also lead to more sp^2-bonded carbon [68]. It should also be noted that at higher argon/methane flow ratios (over 75% argon), argon sputter dominates and no film deposition occurs in the ECR-CVD system studied.

In Fig. 5-10, the acetylene-based films have higher deposition rates than methane-based films at a given rf induced substrate bias voltage and flow rate, indicating that the carbon flux to the deposition substrate in acetylene-argon discharges is higher than in the methane-argon discharges. The depositing flux of carbon to the surface of the substrate at a typical experimental deposition rate of 40 nm/min and a film of density 2.0 g/cm^3 is $4x10^{17}$ carbon/cm^2/min. For comparison, the peak deposition rate possible can be estimated assuming all the carbon entering the system is deposited uniformly on the surfaces defined by the substrate holder, quartz dome, and plasma source region walls. For this estimate, a flow rate of 7 sccm for the hydrocarbon gas is assumed to enter the plasma source. This flow rate is $1.8x10^{20}$ molecules/min or $1.8x10^{20}$ carbon-atoms/min for methane and $3.6x10^{20}$ carbon-atoms/min for acetylene. The surface area of the region defined by the substrate holder, the quartz dome top, and the plasma source/quartz dome sidewalls is approximately 400 cm^2 when we consider the surface to be a surface of

virtual sphere of 10 cm radius. If all the incoming methane carbon atoms are assumed to be ionized or dissociate and then to flow and stick to the walls defined by this surface area, the deposition rate for a carbon film of density 2.0 g/cm^3 would be 45 nm/min. This deposition rate is similar in magnitude to that actually deposited on the substrate, which ranges from 10-40 nm/min as shown in Fig. 5-10. This suggests that most of the methane injected into the plasma is activated and it is deposited on the substrate or walls. This is also supported by the partial pressure analyzer data in Fig. 5-3 to Fig. 5-6, in which most of the carbon in the hydrocarbon gas flows is deposited into the films or on the walls since hydrocarbon gas is found in the exit gas flow at a low levels of 10% for acetylene and 20 % for methane when the discharge is on as compared to the level with no discharge present. For the case of acetylene-based films, the deposition rate is higher because acetylene has two carbons per molecules instead of the one of methane. Hence the deposition rate is expected to be approximately two times of the rate of methane. This approximate doubling of the deposition rate is in fact observed in Fig. 5-10.

Another way to evaluate the fluxes to the deposition surface is to compare the flux of carbon to the substrate, the flux of ions to the surface, and the flux of neutral species to the surface. Here, the species consist of argon, hydrogen, and hydrocarbon molecules. The measured current density to the substrate surface at a pressure of 3 mTorr is typically in the range of 2-3 mA/cm^2 as given in Table 5-2. This corresponds to an ion flux of approximately ~10^{18} ions/min/cm^2. The neutral flux can be estimated from the neutral gas temperature and pressure using the ideal gas law and neutral diffusion Γ given by $\Gamma = n_n v_n / 4$ where n_n is the neutral density and v_n is the average neutral speed. This estimation at a pressure of 3 mTorr and a gas temperature of 600K [77] is ~10^{20}

species/min/cm^2 depending on the species' mass assumed which ranged from 1 amu to 40 amu. This simple flux counting exercise indicates that for each carbon incorporated into the film, one to a few ions arrive at the deposition surface and 100 or more neutral species arrive at the surface, some of which may be chemically active neutral radicals that are deposited.

A comparison of the film properties for methane and acetylene-based films given in Fig. 5-10 - Fig. 5-14 shows substantial differences between the two discharge types. At any selected rf induced bias, the acetylene-based films have a higher density, lower hydrogen content, higher refractive index, and lower optical bandgap as compared to the methane-based films. To interpret this difference the hydrogen content will first be examined. The acetylene-based films have a substantially lower amount of hydrogen incorporated during the deposition. First, this is what can be expected to occur because the hydrogen/carbon ratio for acetylene is 1 and the hydrogen/carbon ratio for methane is 4. Hence, more hydrogen is available in the methane discharges. An examination of the partial pressure analyzer (PPA) spectrum of Fig. 5-3 - Fig. 5-6 confirms this since it shows that the hydrogen concentration in the exit gas increases when the discharge is on for methane or acetylene as compared to the discharge being off. Further for methane, if the amplitude of the PPA mass spectrum signals for hydrogen are compared to the argon (40 amu) signal for the discharge on case, the equivalent number of hydrogen atoms flowing out of the system for methane is at most twice of the argon flow. Since the input gas flow of methane is 8 sccm (or 32 sccm equivalent hydrogen atom flow), the flow of argon is 8 sccm and the equivalent flow of hydrogen atom out of the system is at most 16 sccm (2 times of argon flow), less than half of the hydrogen that entered the system flows

out through the pumping system. This leaves more than half of hydrogen (more than 2 hydrogen atoms per carbon atom) being incorporated into the carbon on the substrate and walls.

The behavior in the acetylene-argon plasmas is different. The hydrogen content in the exit gas flow does not increase as much as the methane-argon case when the discharge is on indicating that most of the hydrogen is incorporated into the carbon film deposited on the walls and the substrate. This hydrogen incorporation rate is therefore less than 1 hydrogen per carbon because the input gas acetylene has 1 hydrogen atom for each carbon atom. Hence, the methane discharges have an abundance of hydrogen which is both incorporated into the carbon on the walls and the substrate and pumped out of the system, and the acetylene discharge has some hydrogen that is incorporated into the carbon deposited on the walls and the substrate. It should also be noted that as the bias on the substrate is made more negative the hydrogen is driven out of the films as shown in Fig. 5-12.

The density of the films increased with the increasing magnitude of the rf induced substrate bias and the acetylene-based films are denser than the methane-based films in Fig. 5-11. The less hydrogen content at higher magnitude of the rf induced substrate bias and of acetylene-based films is considered to make the films more dense. The index of refraction increases with the increasing magnitude of the rf induced substrate bias and is higher for the acetylene-based films as compared to the methane-based films in Fig. 5-13. The index of refraction of materials is dependent on the density of materials and their compositions. The variation of the index of refraction can be explained with the hydrogen content of the films such as that the less hydrogen content at higher magnitude of the rf

induced substrate bias and for acetylene-based films made denser films giving a higher refractive index.

The optical bandgap decreases with the increasing magnitude of the rf induced substrate bias for both films from acetylene and methane, and the optical bandgap of acetylene-based films has lower values than those of methane-based films for films grown with the same rf induced bias as indicated in the bandgap energy, E_{04}, data of Fig. 5-14. The optical bandgap is the material property determined by the composition of the material. In this case, the composition of the films is determined by the hydrogen content, sp^2 fraction and sp^3 fraction. The hydrogen content is considered to induce the variation of the optical bandgap variation in Fig. 5-14. This can be seen more clearly in the data that shows the E_{04} optical bandgap versus hydrogen content as shown in Fig. 5-15. A decrease in the hydrogen content produces a lower optical bandgap energy. In the material's structure this is attributed to the decreasing hydrogen content reducing the sp^3 C-H bonding leaving more graphite-like (sp^2 carbon) bonds in the films [68]. These sp^2 bonds are primarily responsible for the light absorption in the visible-near infrared spectral range [67] as it is seen that the graphite is dark and black with naked eyes.

More insight into the bonding within the films can be obtained by plotting the optical bandgap versus film mass density as shown in Fig. 5-16. In general, a-C:H films are predominantly composed of three bond types including C-C sp^3 bonds, C-C sp^2 bonds and C-H bonds. The density is a good indicator at the higher range of densities (>2.4 g/cm^3) of the sp^3/sp^2 ratio as discussed in Section 2.1 with high density films having a high sp^3/sp^2 ratio. At the lower density range (less than 2.0 g/cm^3), the density is most

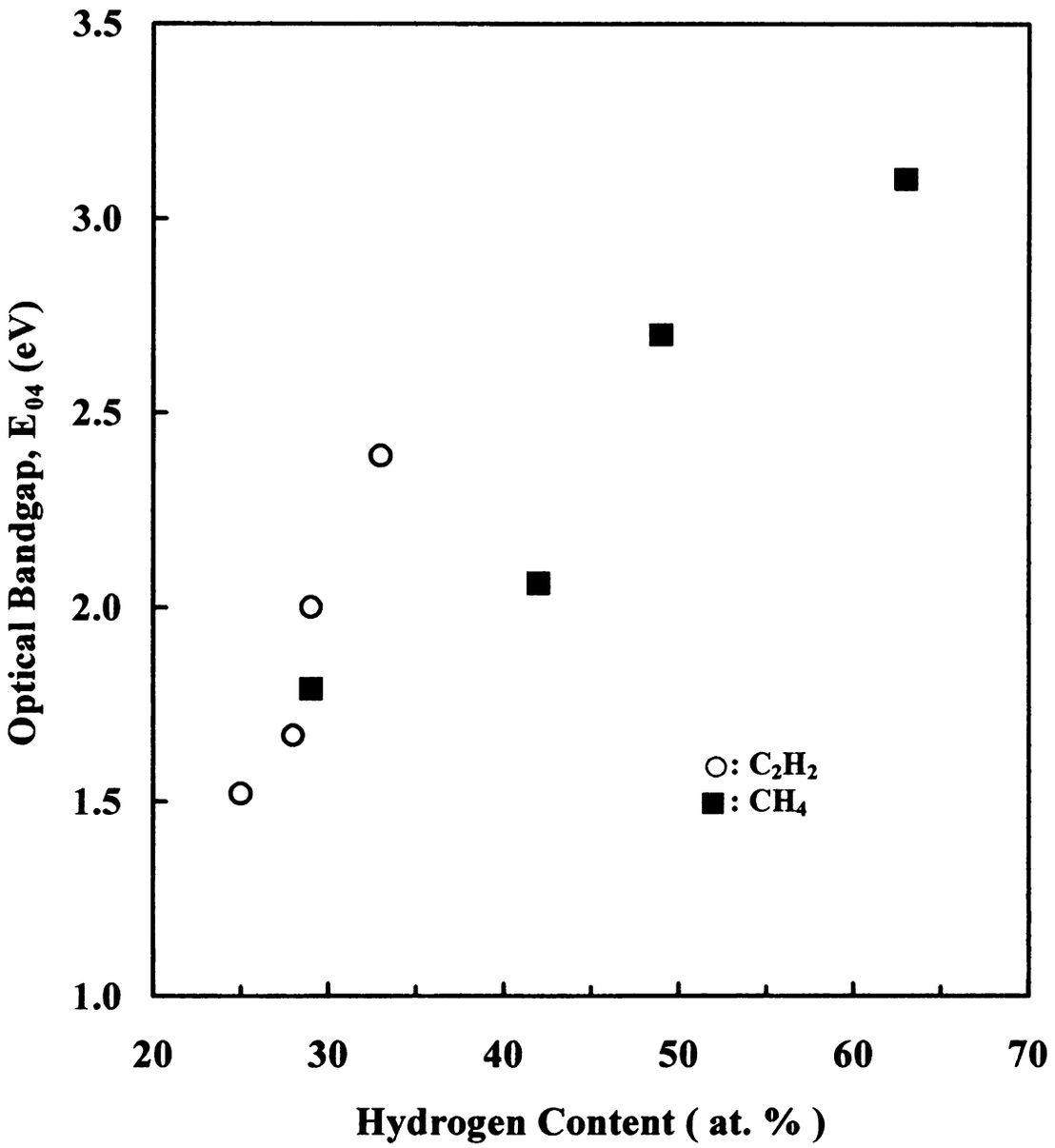

Fig. 5 - 15: Variation of optical bandgap versus hydrogen content for acetylene-based films and methane-based films.

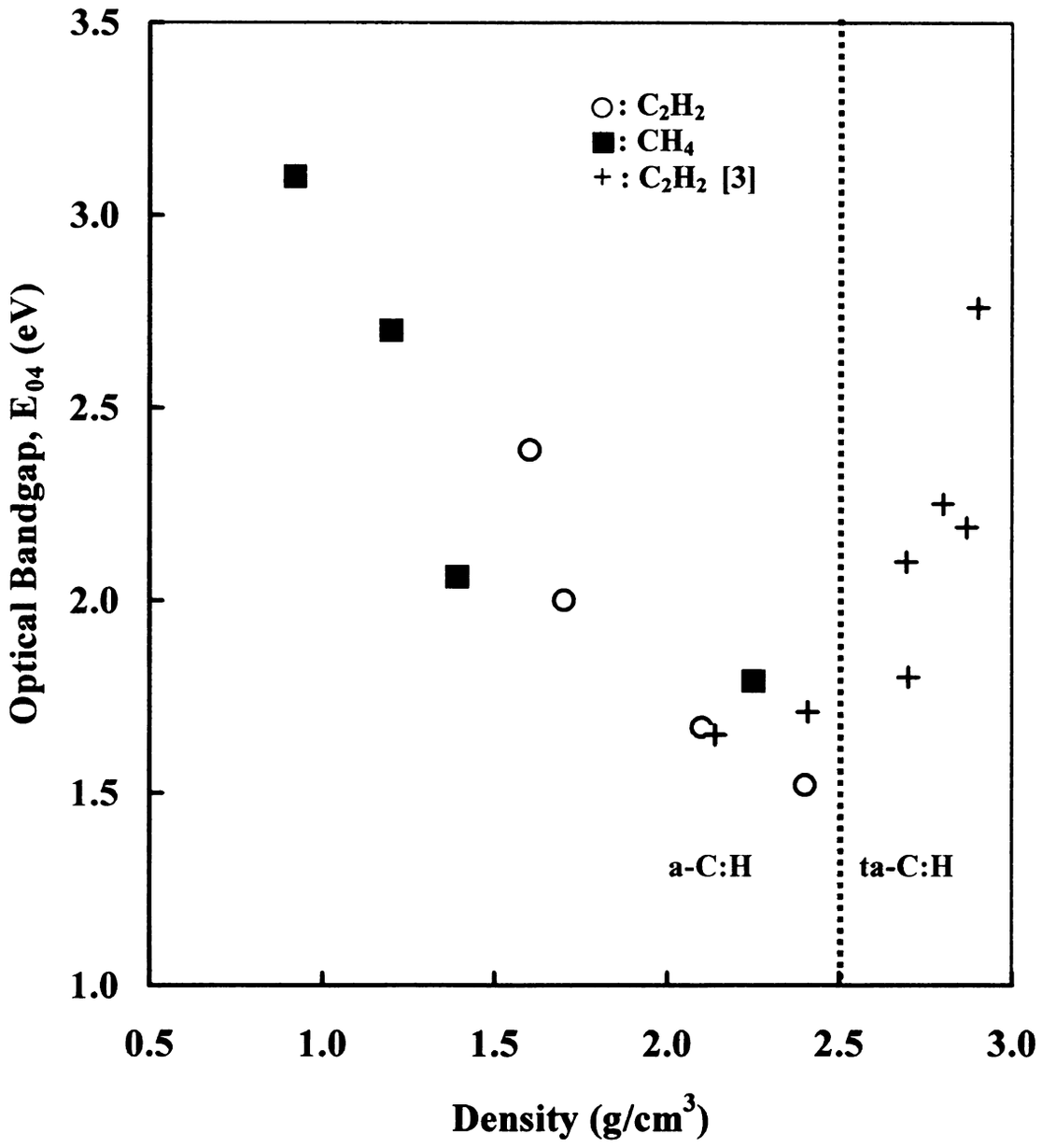

Fig. 5 - 16: Variation of optical bandgap versus mass density for acetylene-based films and methane-based films deposited in this study and in the study of Ref. [16].

dependent on the amount of hydrogen incorporated as shown in Fig. 5-11 and Fig. 5-12. Fig. 5-16, which shows both our data and data from [3, 78], can be interpreted as (1) the low density films (less than 1.5 g/cm^3) being polymer-like with high hydrogen content and many C-H bonds, (2) the intermediate density a-C:H films (2.0 g/cm^3) having a reduced number of C-H bonds and having more C-C bonds with some being of the sp^2 type, and (3) the high density ta-C:H films (greater than 2.4 g/cm^3) having few C-H bonds and an increase in the sp^3 C-C bonds and reduction in sp^2 C-C bonds. This reduced sp^2 concentration in the densest films produces the increase in the optical bandgap shown in Fig. 5-16. Thus, the optical bandgap is mainly determined by the hydrogen content for low density films and by the carbon-carbon sp3 fraction for high density films. Thus the films deposited at pressures in the millitorr range have decreasing optical bandgap with the increasing magnitude of the rf induced substrate bias because the sp^2 bondings increases with the variation of the bias. On the other hand, the films deposited at submillitorr pressure (0.2 mTorr) have a peak value of optical bandgap at -200 V of rf induced substrate bias and the occurrence of the peak is considered to be due to the variation of sp^3 fraction as discussed in Chapter 4.

5.3.3 The Effect of Pressure

The effect of pressure on the film properties including refractive index, deposition rate, and optical bandgap is shown in Fig. 5-17 - Fig. 5-19. The deposition condition in the figures is 200 W microwave input power, 8 sccm flow rate of acetylene or methane gas, 8 sccm flow rate of argon gas, -20 V rf bias for acetylene-based films or -50V for methane-based films. The two different rf induced substrate bias conditions were selected so that both the methane-based and the acetylene-based films had similar densities and

hydrogen content at a 3 mTorr deposition condition. The deposition rate of the acetylene-based films is larger than the methane-based films for all pressures considered and the rate for both discharges have the increasing trend as the pressure increases. Both the refractive index and the optical bandgap change minimally with the variation of pressure for methane-based films. When the pressure is increased, the refractive index of acetylene-based films has a decreasing trend and the optical band gap has an increasing trend. The pressure dependence given in Fig. 5-17 -Fig. 5-19 showed that the acetylene film properties including optical bandgap and refractive index are changed as a function of pressure.

The above results for the pressure variation suggest the ion bombardment effect decreases with the increasing discharge pressure and changes significantly for argon-acetylene discharge cases, and changes minimally for argon-methane discharge cases. The decreasing trend of ion bombardment effect with the increasing pressure is expected because the ion density does not increase as fast as neutral flux as the discharge pressure increases (as seen in Fig. 5-1) resulting in the decrease of the ratio of ion flux to neutral flux onto the substrates. To estimate this change in flux ratio, the argon discharge data shown in Fig. 5-1 will be used. This data first indicates a drop in the ion density at 1 mTorr to 40 % of the ion density at 8 mTorr. Next, for this same pressure variation the neutral density and hence neutral flux would change by a factor of 8 giving a value at 1 mTorr that is less than 15% of the value at 8 mTorr. Combining these two observations gives that the ion-flux to neutral flux ratio would then increase by a factor of about 3 when the pressure drop from 8 to 1 mTorr. The changed film properties at lower

pressures are therefore produced by the higher percentage of ions compared to neutral species reaching the substrate.

The acetylene-based films responded more sensitively to the variation of discharge pressure. This is explained with a significant fraction of the ions being heavier ions in argon-acetylene discharges. The momentum of ions is proportional to the square root of ion's mass when the ions have the same energy. And the ions onto a substrate are supposed to have the same energy because they have traveled through the same sheath potential regardless of the ion types. Thus, heavy ions like argon and acetylene have bigger momentum and transfer bigger momentum onto the growing films (i.e. bigger ion bombardment effect) than light ions like hydrogen molecules. Table 5-4 shows the momentum of several ion types normalized by the momentum of an atomic hydrogen ion under the condition of the same ion energy.

Table 5-4: The dependence of momentum on mass. The momentum of several ion types is normalized by that of an atomic hydrogen ion under the condition of the same ion energy and it is designated by M_x/M_H.

Ion type	H^+	H_2^+	CH_4^+	$C_2H_2^+$	Ar^+
Mass (amu)	1	2	16	26	40
M_x/M_H	1	1.4	4.0	5.1	6.3

The argon-acetylene discharges have a higher fraction of the heavier argon ions than hydrogen ions as compared to argon-methane discharges. This higher concentration of argon was shown by the PPA measurements. Hence the ion bombardment effect is much more significant for the acetylene-based films. Further, as the pressure is reduced, the ion flux to neutral flux ratio is increased showing significant film property changes for

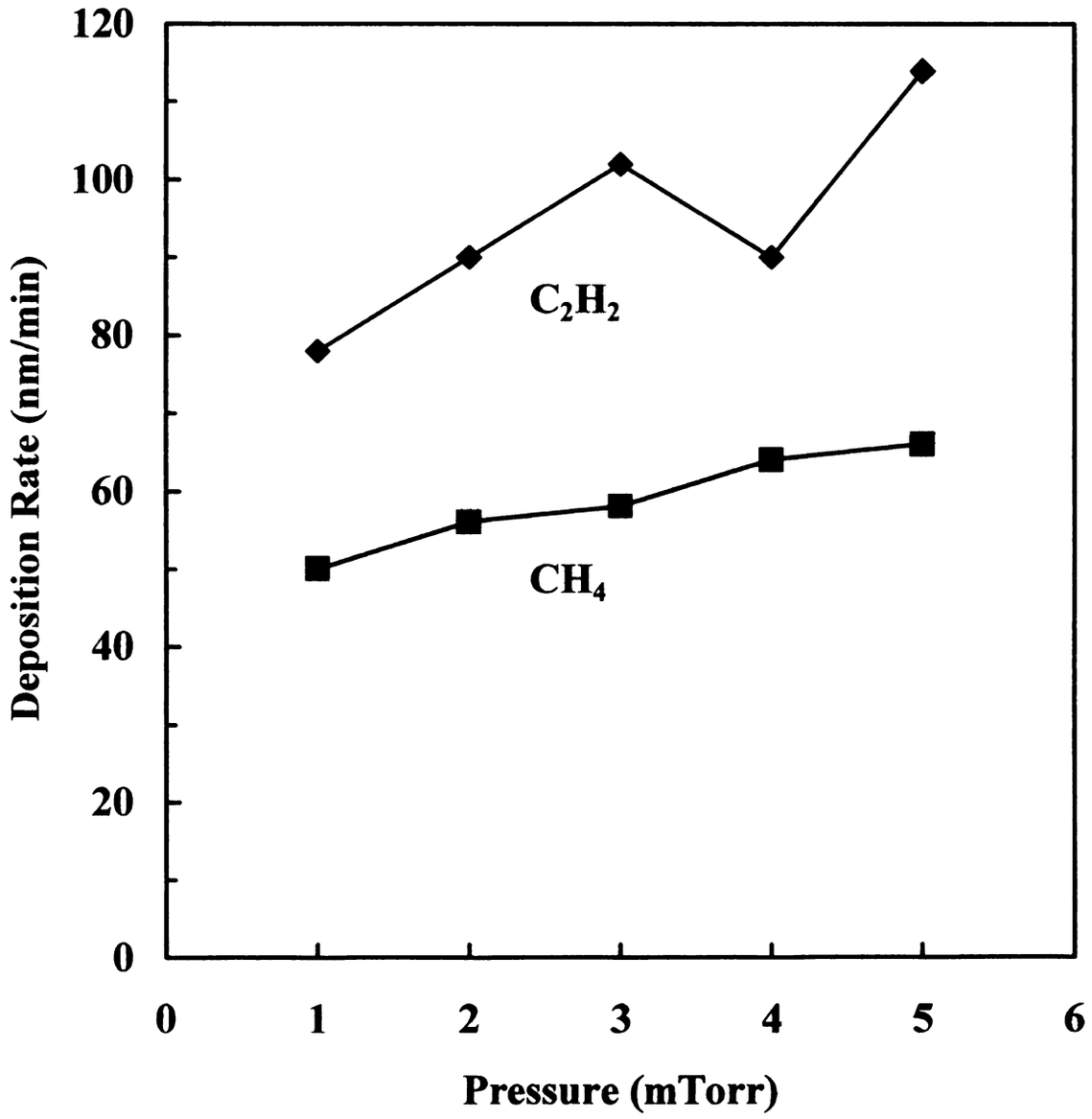

Fig. 5 - 17: Deposition rate of methane and acetylene-based films versus deposition pressure.

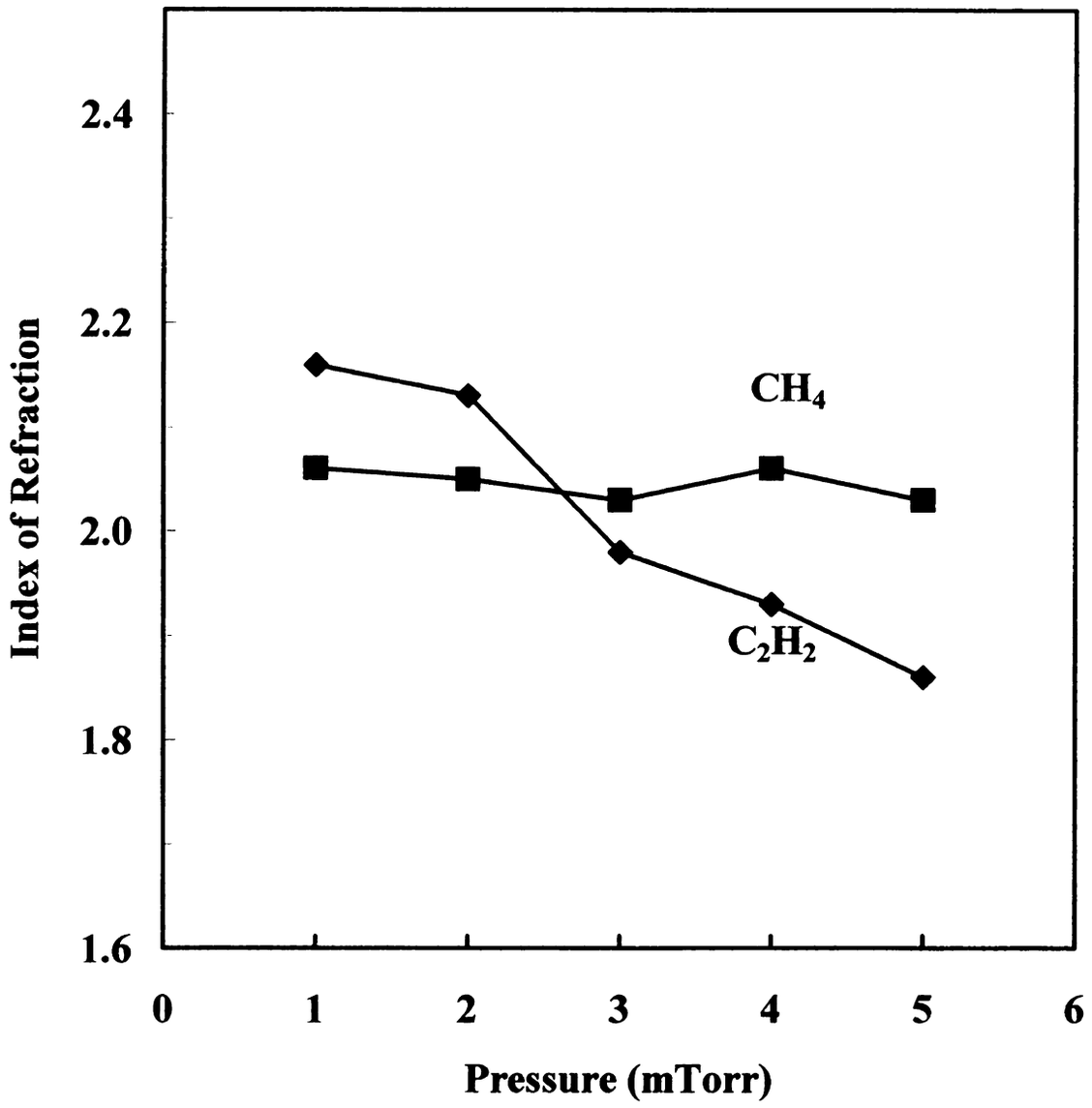

Fig. 5 - 18: Index of refraction of methane and acetylene deposited films versus deposition pressure.

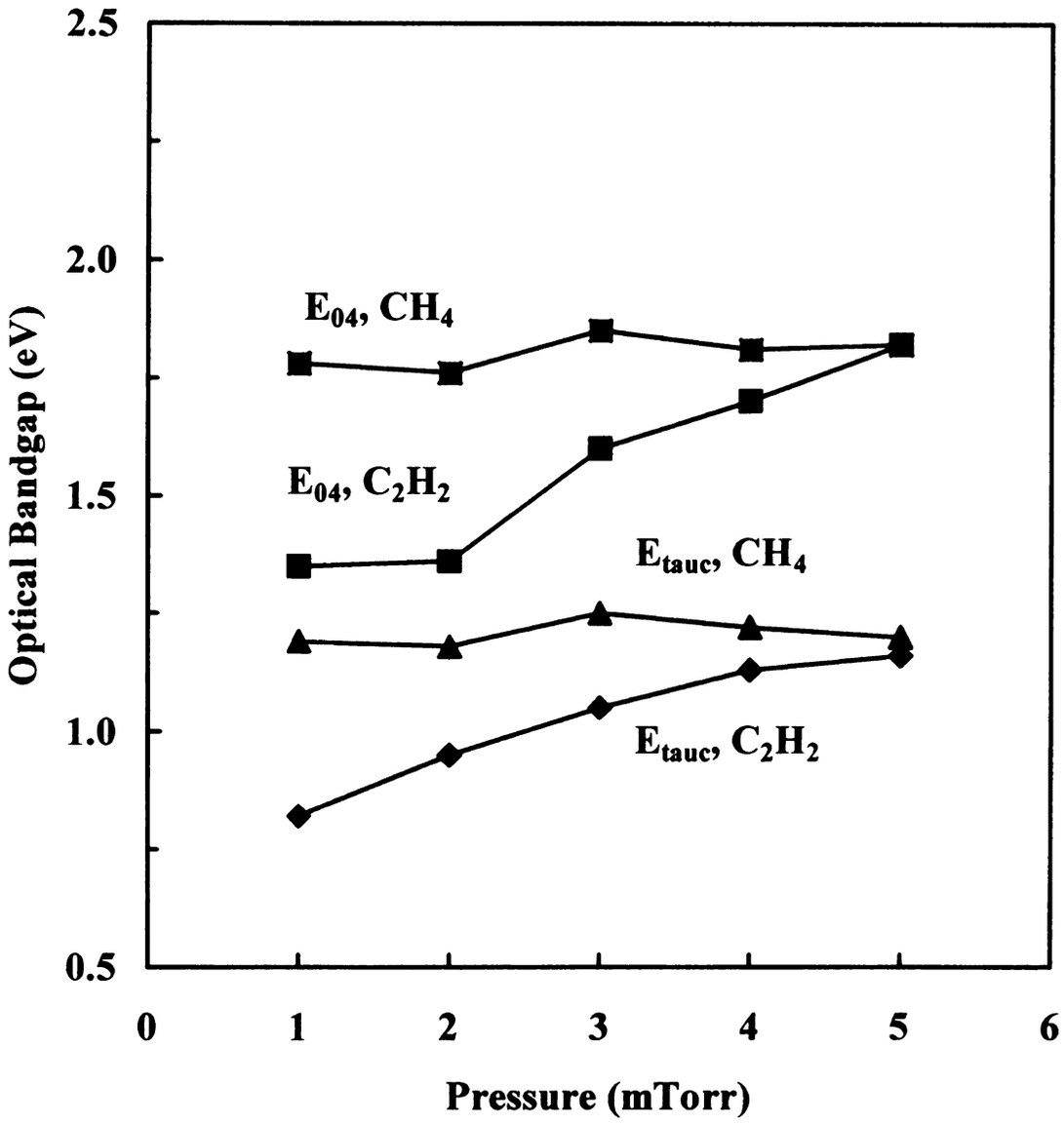

Fig. 5 - 19: Optical bandgap (E_{tauc} and E_{04}) of methane and acetylene deposited films versus deposition pressure.

acetylene based films. A possible additional reason is the change of the fraction of ion types coming from the variation of the partial pressure of gas types in the discharge as the discharge pressure increases. The ratio of the partial pressure of argon to the partial pressure of hydrogen is expected to decrease for argon-acetylene discharges as the discharge pressure increases. This occurs because the hydrogen partial pressure will be increased by the increased dissociation of acetylene gas at higher pressure. So the ratio of the partial pressure of argon gas to the partial pressure of hydrogen gas can be higher at low pressure than at high pressure in argon- acetylene discharges. That will result in a lower ratio of the argon ions to hydrogen ions, thus a lower ion bombardment effect in the deposition process at higher discharge pressures.

The methane-based films show minimal change for the pressure variation. In the argon-methane discharge the partial pressure of hydrogen gas is almost at the same level as the partial pressure of argon, as seen in Fig. 5-4, while in the argon-acetylene discharge the level of partial pressure of hydrogen is about 1/3 of the argon level, as seen in Fig. 5-6. Thus, the hydrogen will compete more with argon in ionization and dilute more the argon ion bombardment effect in the deposition process in the argon-methane discharge than in the argon-acetylene discharge. Hence, the argon ion bombardment effect is expected smaller in argon-methane discharges than in argon-acetylene discharges. Therefore, the decreased ion flux to neutral flux ratio produced by the increased discharge pressure only shows a slight effect on the film properties in the figures. And the probable change of ion type fractions by the variation of discharge pressure does not seem to change enough to show its large effect on the film properties in the argon-methane discharges

5.3.4 The Effect of Argon Flow Rate

The film properties and deposition rate versus argon flow ratio (i.e. the ratio of argon flow rate to acetylene flow rate) for both the methane-argon and acetylene-argon discharges are shown in Fig. 5-20 - Fig. 5-22. These films were deposited at 3 mTorr pressure and 200 W microwave input power with -50 V rf induced substrate bias in the methane-argon discharge and -20 V rf induced substrate bias in the acetylene-argon discharge. The two different rf induced substrate bias conditions were selected, so that both the methane-based and the acetylene-based films had similar densities and hydrogen content at a 3 mTorr deposition condition. The figures show that the deposition rate and optical bandgap have decreasing trends for argon-methane discharge, and the index of refraction has increasing trend for both methane-based films and acetylene-based films as the argon flow ratio increases. The trends are the same with those of the rf induced substrate bias effect case. Thus, the increased argon flow rate results in the increased ion bombardment effect in the deposition process as like the case of the increased magnitude of the rf induced substrate bias. This fact is very natural and expected because the increased argon flow will increase the argon partial pressure, thus argon ions resulting in the enhanced ion bombardment effect.

The data indicates that the addition of argon has no or only a small effect on the films deposited from the acetylene gas and a significant influence on the films deposited from methane. Specifically, both the optical bandgap and the deposition rate for the acetylene-argon films show no variation versus argon addition of 0 to 0.8 argon flow ratio. Increasing the argon flow ratio lowers the film's optical bandgap for methane-based

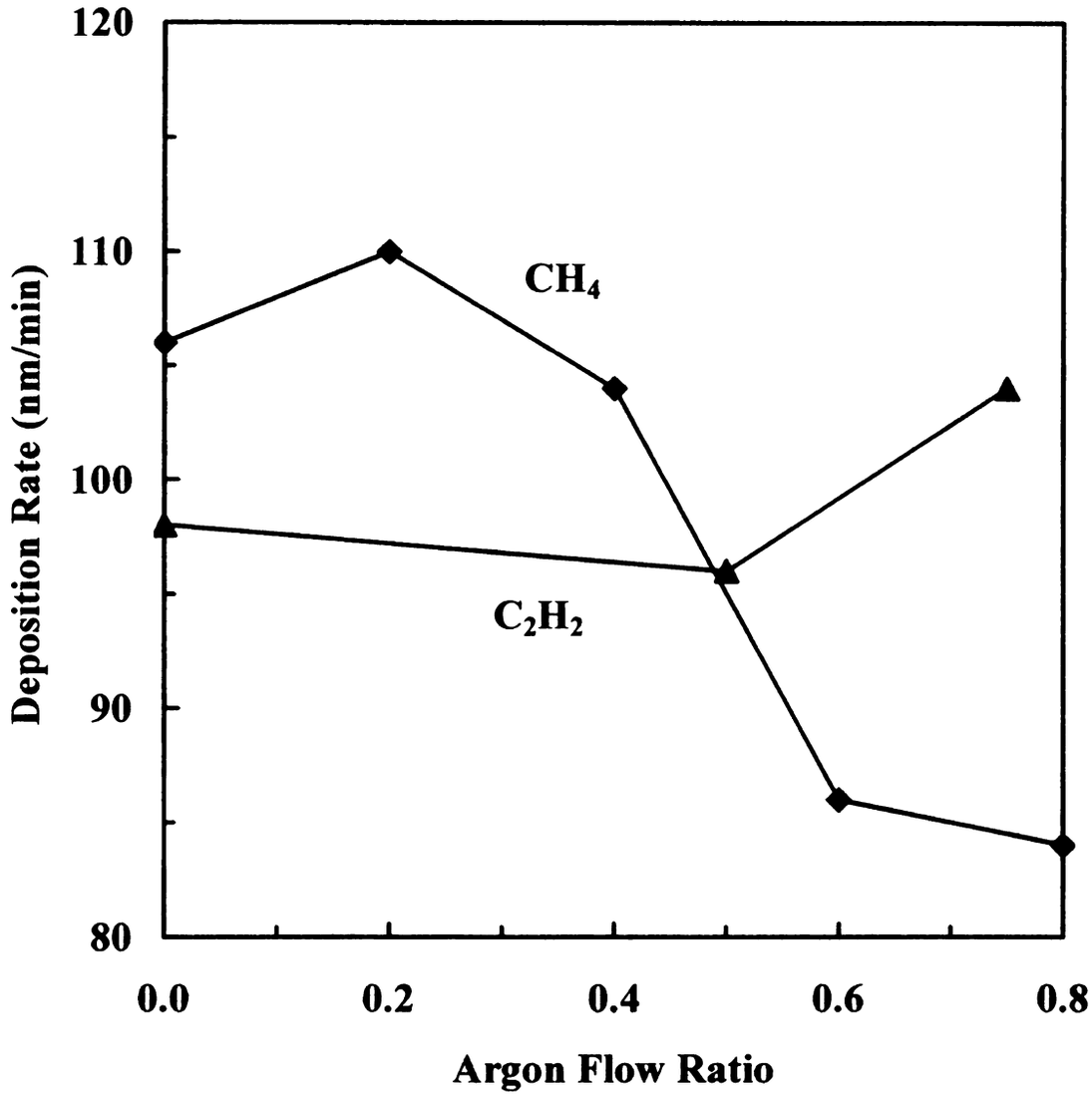

Fig. 5 - 20: Deposition rate of methane and acetylene deposited films versus argon flow ratio.

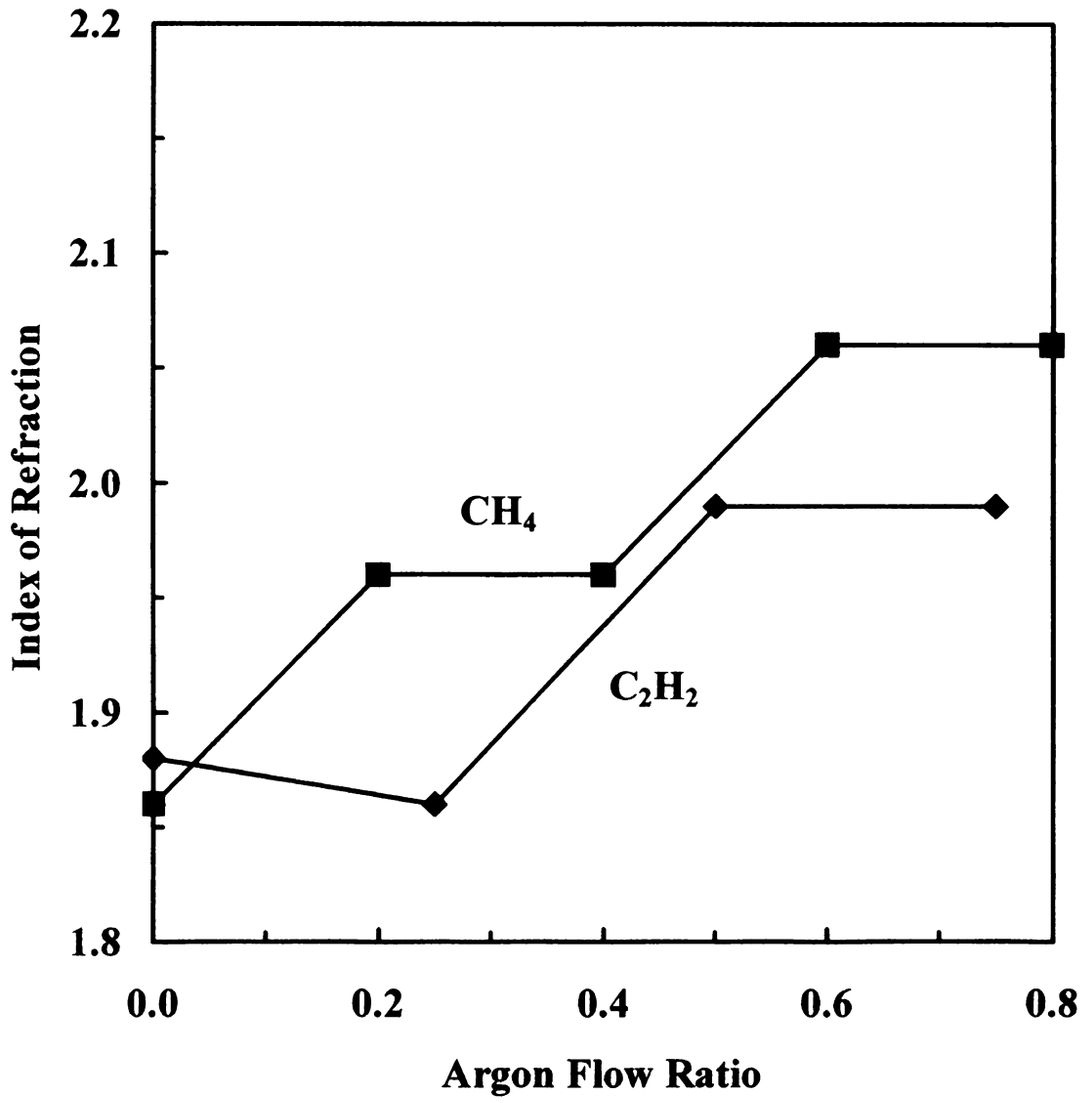

Fig. 5 - 21: Index of refraction of methane and acetylene deposited films versus argon flow ratio.

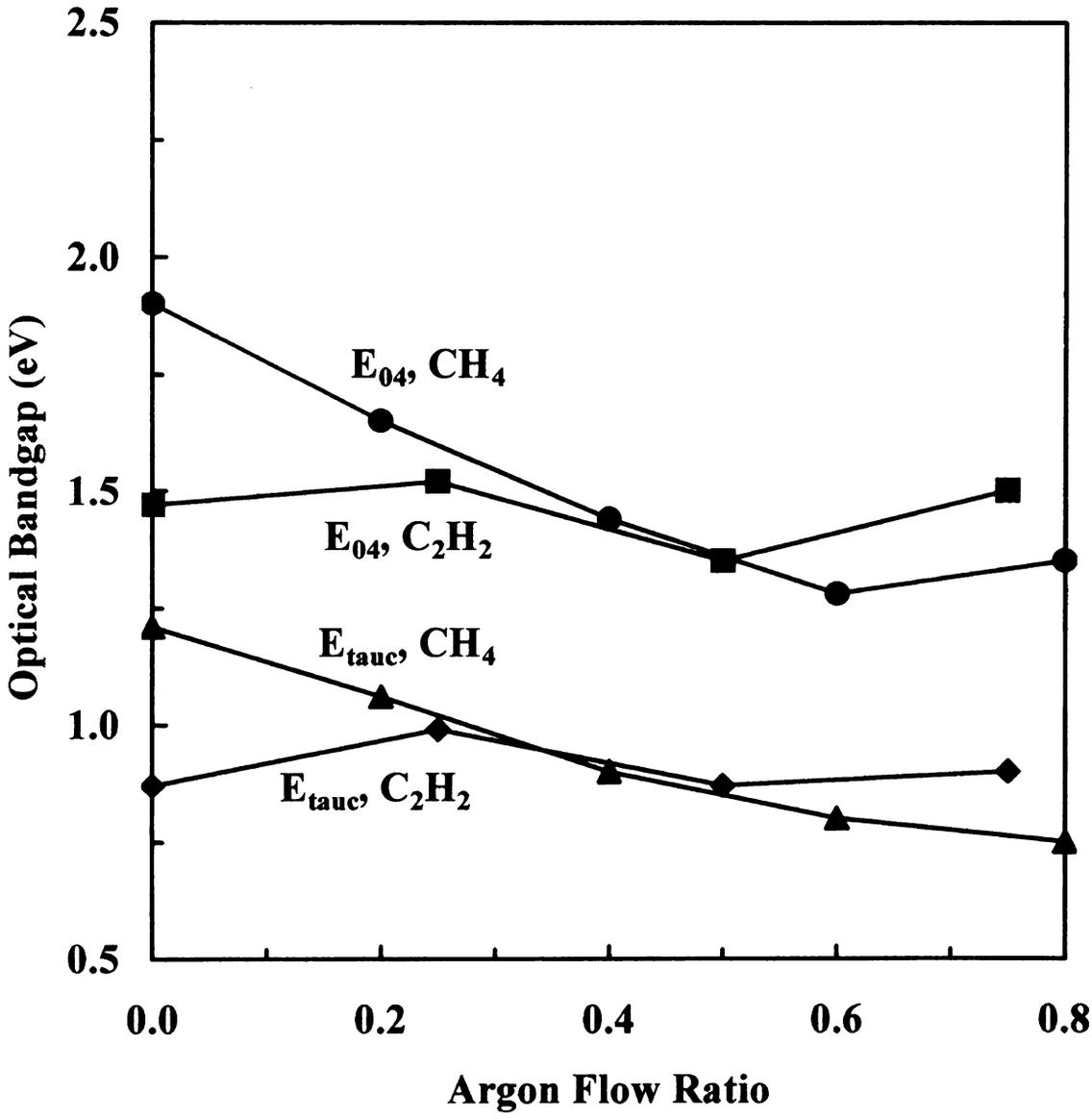

Fig. 5 - 22: Optical bandgap (E_{tauc} and E_{04}) of methane and acetylene deposited films versus argon flow ratio.

films but it does not effect the acetylene-based films as shown in Fig. 5-21. Similarly, the deposition rate and the refractive index change more versus argon flow ratio in methane based films as compared to acetylene based films as shown in Fig. 5-20 and Fig. 5-22. Thus, the methane-based films are more sensitive to the argon addition than the acetylene-based films. The partial pressure of hydrogen is higher in the argon-methane discharge than in the argon-acetylene discharge as seen in Fig. 5-4 and Fig. 5-6. So the addition of argon can more effectively replace the hydrogen gas by the added argon gas to some extent in the argon-methane discharges as compared to the argon-acetylene discharge. Thus, the argon ion bombardment effect can be more effectively enhanced by the addition of a certain amount of argon in the argon-methane discharge than in argon-acetylene discharge. For an another reason the momentum of argon ions is 4.5 times and 1.6 times bigger than hydrogen ions and methane ions, respectively (see Table 5-4 for the momentum). On the other hand, the partial pressure of hydrogen is lower in argon-acetylene discharges, thus the added argon will mainly compete in ionization with acetylene gas. But the momentum of argon ion is only 1.2 times bigger than acetylene ions. Thus, the ion bombardment effect of the increased argon ions is not very different from the acetylene ions in the argon-acetylene discharge, but is much bigger than the hydrogen ions and methane ions in the argon-methane discharges. Therefore, the methane-based films were more sensitive to the addition of argon than the acetylene-based films.

5.4 Summary

Hydrogenated amorphous carbon films were deposited at pressures in the millitorr range using discharges of argon-acetylene and argon-methane mixtures. The input microwave power was 250 W. The rf induced substrate bias, deposition pressure and argon flow rate were varied to investigate their effect on the film properties.

The film properties varied from higher deposition rate, lower refractive index, higher optical bandgap, lower density, higher hydrogen content films to lower deposition rate, higher refractive index, lower optical bandgap, higher density, lower hydrogen content films as the magnitude of rf induced substrate bias increased. The rf induced substrate bias provides the ion bombardment energy onto the surface of the growing film. The higher ion bombardment energy is expected to break the bonds of adsorbed hydrocarbon species and to expel hydrogen from the film structure resulting in the densification of the film structure more easily and more effectively. The films of less hydrogen content will have higher density and lower optical bandgap. The densification of films will reduce the deposition rate and increase the refractive index.

The two discharge types of argon-acetylene and argon-methane mixtures produced significantly different film properties. Films deposited from argon-acetylene discharges have a higher deposition rate, higher film density, lower hydrogen content, higher refractive index and lower optical bandgap than the film deposited from argon-methane discharges. Acetylene molecules have two times more carbon atoms and two times less hydrogen atoms in them than methane molecules, which explains the higher

deposition rate and lower hydrogen content of the acetylene-based films than the methane-based films. The higher density, higher refractive index and lower optical gap of the acetylene-based films are also explained by the lower hydrogen content of the films. The film properties are summarized in Table 5-5 from Fig. 5-10 to Fig. 5-14 for easy comparison of the effects of rf induced substrate bias and the two different discharges.

Table 5-5: Comparison of film properties from argon (50 %)-methane (50 %) and argon (50 %)-acetylene (50 %) discharges, and from two different rf induced substrate biases of 0 and -60 V.

Discharges	Argon-methane		Argon-acetylene	
RF induced substrate bias	0 (V)	-60 (V)	0 (V)	-60 (V)
Deposition rate (nm/min)	40	10	80	60
Density (g/cm^3)	0.9	2.2	1.6	2.4
Hydrogen content (%)	65	30	33	25
Refractive index	1.8	1.9	1.9	2.2
E_{04} (eV)	3.1	1.8	2.4	1.5
E_{tauc} (eV)	2.0	1.2	1.3	0.8

As the deposition pressure increased, the deposition rate and the optical bandgap increased and the refractive index decreased for both methane-based films and acetylene-based films. These facts suggest the films can be densificated more effectively at lower pressure and also suggest the ion bombardment effect decreases with the increasing discharge pressure and changes significantly for argon-acetylene discharge cases, and changes minimally for argon-methane discharge cases. The decreasing trend of ion bombardment effect with the increasing pressure is expected because the ion density does not increase as fast as neutral flux as the discharge pressure increases resulting in the

decrease of the ratio of ion flux to neutral flux onto the substrates. Thus, the ion bombardment effect decreased as the discharge pressure increases and this explains the pressure effect on the film properties. The acetylene-based films responded more sensitively to the variation of discharge pressure. This is explained with a significant fraction of the ions being heavier ions in argon-acetylene discharges.

As the argon flow ratio increased into the discharge chamber, the optical bandgap decreased and the refractive index increased. This fact suggests the films were densificated as the argon flow ratio increased and is an expected result because the argon ion bombardment will be enhanced with the increased argon flow ratio.

The effect of argon flow ratio was higher for the methane-based films than the acetylene-based films. Because the hydrogen species in the argon-methane discharge are at a higher level than in the argon-acetylene discharge at 50 % argon and 50 % hydrocarbon flow rates, the addition of more argon will replace hydrogen species with the argon more effectively in argon-methane discharges than in argon-acetylene discharges. Therefore, as the argon flow ratio increases, the argon to hydrogen species ratio in the argon-methane discharges will increases more quickly than in the argon-acetylene discharges enhancing the argon ion bombardment effect. Thus, the methane-based films have higher film property variation as the argon flow ratio changes.

Therefore, the properties of the films deposited at pressures in the millitorr range with the argon-hydrocarbon gas mixtures are strongly influenced by the argon ion bombardment energy and argon ion flux on the surface of growing films. The argon ion energy is determined by the rf induced substrate bias and the argon ion flux on the surface of growing films is dependent on the argon to hydrogen species ratio in the

discharge chamber. The species ratio is varied by the deposition pressure and the ratio of argon flow to hydrocarbon gas flow into the deposition chamber. The ion bombardment effect determined the hydrogen content and the variation of film properties in the film deposition at pressures in the millitorr range can be mainly explained with the consideration of the hydrogen content of the films.

The variation of the properties in the films deposited at pressures in the millitorr range can be mainly explained with the consideration of the hydrogen content of the films. In contrast, the variation of film properties in the film deposition at pressures in the submillitorr range is mainly attributed to the film composition of sp^3/sp^2 ratio as discussed in Chapter 4.

Chapter 6

6. Conclusions

Hydrogenated carbon films were deposited in an ECR-CVD system with a rf biased substrate using acetylene, acetylene-argon and methane-argon gases mixtures. The films were deposited at pressures in the submillitorr range (0.2-0.6 mTorr) for acetylene discharges and at pressures in the millitorr range (1-5 mTorr) for acetylene-argon and methane-argon discharges. The former clearly showed the effects of ion energy and ion flux to neutral flux ratio on the film properties in the process of deposition and the latter revealed that the two discharge types of argon-methane and argon-acetylene mixture produced significantly different film properties and the optical properties of the films can be controlled by the variation of deposition conditions. The study of discharge properties provides some information on the discharge deposition conditions such as ion energy, rate-limiting process of the deposition, ionization levels of the discharges and a rough estimation of ion types.

The films deposited at pressures in the submillitorr range have a peak (1.3 eV for E_{tauc} and 1.8 eV for E_{04}) in their optical bandgap at -200 V of rf induced substrate bias, when operated at 0.2 mTorr with acetylene feed gas. The result is consistent with other researcher's investigations and matches well with the subplantation model showing that an sp^3 peak occurs at ion energies of 90-100 eV per carbon atom in the deposition process. The variation of optical bandgap in films deposited at conditions near -200 V of rf induced substrate bias is rendered primarily by the carbon sp^3 to sp^2 ratio. The high

values of optical bandgaps of films deposited at lower magnitude of rf induced substrate biases (<100 V) are considered due to high hydrogen content of the films.

The low deposition temperature was critical for the films to have the peak value of optical bandgap at -200 V of rf induced substrate bias. In particular the optical bandgap of films deposited at higher temperature gave a lower value (1.19 eV for E_{tauc}) than the peak value (1.44 eV for E_{tauc}) at -200 V of rf induced substrate bias. The effects of pressure and microwave power on the film's properties were not clearly shown in this investigation within the deposition variable space.

The effect of substrate position was clear so that the peak of the optical bandgaps appeared at substrate position located closer to the plasma generation region where the ion flux to neutral flux ratio is larger. The result indicates that the ion flux to neutral flux ratio is also a critical factor to obtain films of a high optical bandgap with a high sp^3 ratio. Thus the deposition of the films at pressures in the submillitorr range clearly showed the effect of ion energy and ion flux to neutral flux ratio on the film properties. The flux ratio was roughly estimated to be about 10 % and the threshold ratio of ion flux to neutral flux for deposition of ta-C:H films is found to be in the range of 0.06-0.1. The occurrence of peak of the optical bandgap at -200 V of rf induced substrate bias conforms to the explanation of the subplantation model of deposition for ECR deposition and demonstrated agreement with the other ta-C:H film depositions in the literature. However, the ion flux to neutral flux ratio of this investigation (10 %) is estimated lower than the other values (more than 90 %) in literature.

The deposition at pressures in the submillitorr range, therefore, showed that ta-C:H films can be deposited with the microwave ECR deposition system of this

investigation and the deposition rate (90 nm/min) is higher than those of the plasma beam deposition (15 nm/min) and the filtered ion beam deposition.

For the films deposited at pressures in the the millitorr range the film properties varied from higher deposition rate, lower refractive index, higher optical bandgap, lower density, higher hydrogen content films deposited at low rf induced biases to lower deposition rate, higher refractive index, lower optical bandgap denser, lower hydrogen content films deposited at high ion energies. The two discharge types of argon-methane and argon-acetylene mixture produced significantly different film properties including higher density, lower hydrogen content, higher optical absorption, higher refractive indices and higher deposition rates for the acetylene-based films as compared to the methane-based films. Insight into the deposition mechanism for each of these discharge types was gained by studying the variation in film properties produced by variations in the deposition conditions. Two specific results are, first, that as the pressure is changed the methane/argon films do not change in properties, whereas, the acetylene-based films do change properties, and second when the argon flow ratio in acetylene and methane discharges is changed, the methane-based films show a large change in properties and the acetylene-based films do not change properties.

The properties of the films deposited at pressures in the millitorr range with the argon-hydrocarbon gas mixtures are strongly influenced by the argon ion bombardment energy and argon ion flux on the surface of growing films. The argon ion energy is determined by the rf induced substrate bias and the argon ion flux on the surface of growing films is dependent on the argon to hydrogen species ratio in the discharge chamber. The species ratio is varied by the deposition pressure and the ratio of argon

flow to hydrocarbon gas flow into the deposition chamber. The ion bombardment effect determined the hydrogen content and the variation of film properties in the film deposition at pressures in the millitorr range can be mainly explained with the consideration of the hydrogen content of the films.

The film property and deposition rate variations with discharge conditions together with data collected on the discharge itself using a partial pressure analyzer and a Langmuir probe provides a picture of the discharge deposition conditions. The conclusions reached for both the methane and acetylene discharges is that most of the carbon entering the discharge in the hydrocarbon gas flow is activated to be either an ion or a neutral radical which deposits on either the substrate or the chamber walls. The rate-limiting process for the deposition is the flow of carbon species into the plasma source. The deposition in the methane-argon discharge proceeds with the dominant species in the processing chamber being hydrogen and argon with the relative percentages of each changing based on the input flow rate of each gas. For films deposited from acetylene-argon discharges the acetylene is activated and it deposits on the walls, leaving argon as dominant species in the processing chamber.

Comparison of the results of depositions at submillitorr and millitorr range of deposition pressure yields that low pressure reduces the neutral flux to the surface. Further, the removal of argon and the application of a -200 V rf induced substrate bias in the submillitorr range of pressure provide the proper ion bombardment ion energy onto the layer of growing film for deposition of ta-C:H giving the peak value of optical bandgap at the –200 V rf induced substrate bias. The study of deposition at pressures in the millitorr range also showed the film properties could be varied to some extent by the

selection of deposition source gases and varying the other deposition conditions such as rf induced substrate bias, deposition pressure and argon flow ratio. The variation of film properties in the film deposition at pressures in the millitorr range can be mainly explained with the consideration of the hydrogen content of the films. But in contrast the variation of film properties in the film deposition at pressures in the submillitorr range is mainly attributed to the film composition of sp^3/sp^2 ratio.

In this investigation the direct measurement of film composition, i.e. percent sp^3, percent sp^2, percent argon and percent helium was not done. The film composition governs the film's mechanical, optical properties. The measurement techniques of ion types in the plasmas, their ratios in the plasma and the exact carbon ion flux to neutral flux ratio onto the substrate were not completed in this study. Therefore the unmeasured or undetermined film composition, the internal variables of plasma and film properties would be useful future investigations to fully understand the film deposition and film properties.

The film's electrical properties like dielectric constant, bandgap and resistance, mechanical properties like hardness, friction coefficient, stress, heat conduction coefficient and coefficient of thermal expansion, and etch properties would be interesting investigation areas for the optical, mechanical and electrical applications of the films. The applications could be optical filters, protective coatings, active electrical devices, and insulating layers in electronic packaging.

List of References

[1] P. Koidal, C. Wild, R. Locher, and R. E. Sah, *Amorphous Hydrogenated Carbon Films and Related Materials: Plasma Deposition and Film Properties.* in *Diamond and Diamond-like Films and Coatings*, R. E. Clausing, L. L. Horton, J. C. Angus, and P. Koidl, Eds. New YorK: Plenum Press, 1991.

[2] J. Robertson, "Deposition of Diamond -Like Carbon," *Phil. Trans. R. Soc. Lond. A*, vol. 342, pp. 277-286, 1993.

[3] M. Weiler, S. Sattel, T. Giessen, K. Jung, H. Ehrhardt, V. S. Veerasamy, and J. Robertson, "Preparation and Properties of Highly Tetrahedral Hydrogenated Amorphous Carbon," *Phys. Rev. B*, vol. 53, pp. 1594, 1996.

[4] G. F. Zhang, L. J. Guo, Z. T. Liu, X. K. Xiu, and X. Zheng, "Studies on Diamondlike Carbon Films for Antireflection Coatings of Infrared Optical Materials," *J. Appl. Phys.*, vol. 76, pp. 705, 1994.

[5] A. H. Lettington, *Applications of Diamond-Like (Hard Carbon) Films.* in *Diamond and Diamond-like Films and Coatings*, R. E. Clausing, L. L. Horton, J. C. Angus, and P. Koidl, Eds. New York: Plenum Press, 1991.

[6] M. Allon-Alaluf, L. Klibanov, A. Seidman, and N. Croitoru, "Metal Contacts and Electrical Processes in Amorphous Diamond-Like Carbon Films," *Diamond Relt. Mater.*, vol. 5, pp. 1275, 1996.

[7] M. Allon-Alaluf, L. Klibanov, and N. Croitoru, "Iodine Doping of Amorphous Diamond-like Carbon Films," *Diamond Relat. Mater.*, vol. 5, pp. 1497, 1996.

[8] L. Klibanov, M. Allon-Alaluf, N. Croitoru, and A. Seidman, "Study of Photoconductivity in Thin Amorphous Diamond-like Carbon (a: DLC) Films Prepared by Glow Discharge Technique," *Diamond Relat. Mater.*, vol. 5, pp. 1414, 1996.

[9] N. Konofaos and C. B. Thomas, "Characterization of Heterojunction Devices Constructed by Amorphous Diamondlike Films on Silicon," *J. Appl. Phys.*, vol. 81, pp. 6238, 1997.

[10] S. Egret, J. Robertson, W. I. Milne, and F. J. Clough, "Diamond-like Carbon Metal-Semiconductor-Metal Switches for Active Matrix Displays," *Diamond Relat. Mater.*, vol. 6, pp. 879, 1997.

[11] C. H. Lee and K. S. Lim, "Boron-Doped Amorphous Diamondlike Carbon as a New p-type Window Material in Amorphous Silicon p-i-n Solar Cells," *Appl. Phys. Lett*, vol. 72, pp. 106, 1998.

[12] Y. Catherine, *Preparation Techniques for Diamond-Like Carbon.* in *Diamond and Diamond-like Films and Coatings*, R. E. Clausing, L. L. Horton, J. C. Angus, and P. Koidl, Eds. New York: Plenum Press, 1991.

[13] A. Grill and V. Patel, "Effects of Bias and Inert Gas on Properties of Diamond-Like Carbon Deposited by d.c. PA CVD," *Diamond and Related Materials*, vol. 4, pp. 62, 1994.

[14] J. W. Zou, K.Reinchelt, K. Schimidt, and B. Dischler, "The Deposition and Study of Hard Carbon Films," *J.Appl. Phys.*, vol. 65, pp. 3914, 1989.

[15] M. Weiler, S. Sattel, K.Jung, H.Ehrhardt, V. S. Veerasamy, and J. Robertson, "Highly Tetrahedral, Diamond-like Amorphous Hydrogenated Carbon Prepared from a Plasma Beam Source," *Appl. Phys. Lett.*, vol. 64, pp. 2797, 1994.

[16] P. J. Fallon, V. S. Veerasamy, C. A. Davis, J. Robertson, G. Amaratunga, W. I. Milne, and J. Koskinen, "Properties of Filtered-Ion Beam Deposited Diamondlike Carbon as a Function of Ion Energy," *Phys. Rev. B*, vol. 48, pp. 4777, 1993.

[17] Y. Lifshitz, G. D. Lempert, S. Lotter, I. Avigal, C. U. Saguy, and R. Kalish, "The Influence of Substrate-Temperature during Ion-Beam Deposition on the Diamond-like or Graphitic Nature of Carbon-Films," *Diamond and Relat. Mater.*, vol. 2, pp. 285, 1993.

[18] Y. Lifshitz, G. D. Lempert, S. Lotter, I. Avigal, C. U. Saguy, R. Kalish, J.Kulik, D. Marton, and J. W. Rabalais, "The Effect of Ion Energy on the Diamond-like Graphitic (sp^3/sp^2) Nature of Carbon Films Deposited by Ion-Beam," *Diamond Relat. Mater.*, vol. 3, pp. 542, 1994.

[19] C. Ronning, E. Dreher, J.-U. Thiele, P. Oelhafen, and H. Hofsass, "Electronic and Atomic Structure of Undoped and Doped ta-C Films," *Diamond Relat. Mater.*, vol. 6, pp. 830, 1997.

[20] S. F. Yoon, H. Yang, A. Rusli, J. Ahn, and Q. Zhang, "The Effects of Self-Generated DC Bias on the Characteristics of Diamond-like Carbon Films Prepared using ECR-CVD," *Diamond Relat. Mater*, vol. 7, pp. 70, 1998.

[21] M. Zarrabian, N. Fourches-Coulon, G. Turban, M. Lancin, and C. Marhic, "Effect of Negative Bias Voltage on a-C:H Films Deposited in Electron Cyclotron Resonance Plasma," *Diamond Relat. Mater.*, vol. 6, pp. 542, 1997.

[22] S. C. Kuo, E. E. Kunhardt, and A. R. Srivatsa, "Deposition of Diamond-like Carbon Film Using Electron Cyclotron Resonance Plasma," *Appl. Phys. Lett.*, vol. 59, pp. 2532, 1991.

[23] T. Fujita and O. Matsumoto, "Deposition of Carbonaceous Films using ECR Plasma Apparatus Deposition of Colorless, Tranparent and Semiconducting Film from Methane Plasma," *J. Electrochem. Soc.*, vol. 136, pp. 2624, 1989.

[24] A. Zeinert, B. Racine, K. Zellama, M. Zarrabian, G. Turban, and A. Sadki, "Comparative Study of the Optical and Structural Properties of a-C:H Films Deposited by Conventional Diode and Microwave ECR Assisted RF Plasma," *Diamond Relat. Mater.*, vol. 7, pp. 486, 1998.

[25] P. W. Pastel and W. J. Varhue, "The Effect of Radio Frequency Substrate Biasing in the Deposition of Diamond-like Carbon Films in an Electron Cyclotron Resonance Discharge," *J.Vac.Sci.Technol. A*, vol. 9, pp. 1129, 1991.

[26] S. F. Yoon, H. Yang, Rusli, J. Ahn, Q. Zhang, and T. L. Poo, "Influence of Substrate Temperature and Microwave Power on the Properties of a-C:H Films Prepared using the ECR-CVD Method," *Diamond Relat. Mater.*, vol. 6, pp. 1683, 1997.

[27] S. F. Yoon, Rusli, J. Ahn, Q. Zhang, Y. S. Wu, and H. Yang, "DC Bias Effects in the Deposition of a-C:H Films using the Screen-grid Method in Electron Resonance Chemical Vapor Deposition," *Diamond and Relat. Mater.*, vol. 7, pp. 1213, 1998.

[28] F. S. Pool and Y. H. Shing, "Deposition of Diamondlike Films by Electron Cyclotron Resonance Microwave Plasma," *J. Appl. Phys.*, vol. 68, pp. 62, 1990.

[29] P. S. Andry, P. W. Pastel, and W. J. Varhue, "Comparison of Diamond-like Carbon Film Deposition by Electron Cyclotron Resonance with Benzene and Methane," *J. Mater. Res.*, vol. 11, pp. 221, 1996.

[30] K. Kuramoto, Y. Domoto, H. Hirano, S. Kiyama, and S. Tsuda, "High Quality Diamondlike Carbon Thin Film Fabricated by ECR Plasma CVD," *Appl. Surf. Sci.*, vol. 113/114, pp. 227, 1997.

[31] J. C. Angus and Y. Wang, *Diamond-like Hydrocarbon and Carbon Films.* in *Diamond and Diamond-like Films and Coatings*, R. E. Clausing, L. L. Horton, J. C. Angus, and P. Koidl, Eds. New York: Plenum Press, 1991.

[32] W. Jacob and W. Moller, "On the Structure of Thin Hydrocarbon Films," *Appl. Phys. Lett.*, vol. 63, pp. 1771, 1993.

[33] P. Reinke, W. Jacob, and W. Moller, "Influence of the Ion energy on the Growth and Structure of Thin Hydrocarbon Films," *J. Appl. Phys.*, vol. 74, pp. 1354, 1993.

[34] S. f. J. Robertson, "Electronic Structure of Diamond-like carbon," *Diamond Relat. Mater.*, vol. 6, pp. 212, 1997.

[35] J. Ristein, J. Shafer, and L. Ley, "Effective Correlation Energies for Defects in a-C:H from a Comparison of Photoelectron Yield and Electron Spin Resonance Experiments," *Diamond Relat. Mater.*, vol. 4, pp. 508, 1995.

[36] J. F. e. al., "Structure and Bonding of Hydrogen Plasma Generated Carbon Films: An Electron Loss Study," *Solid State Commun.*, vol. 47, pp. 687, 1983.

[37] J. Robertson, "Structural Models of a-C and a-C:H," *Diamond Relat. Mater.*, vol. 4, pp. 297, 1995.

[38] C. H. Lee, W. R. L. Lambrecht, B. Segall, P. C. Kelires, T. Frauenheim, and U. Stephan, "Electron Structure of Dense Amorphous Carbon," *Phys. Rev. B*, vol. 49, pp. 11448, 1994.

[39] D. A. Drabold, P. A. Fedders, and P.Strumm, "Theory of Diamondlike Amorphous Carbon," *Phys. Rev. B*, vol. 49, pp. 16415, 1994.

[40] J. Robertson, "The Deposition Mechanism of Diamond-like a-C and a-C:H," *Diamond Relat. Mater.*, vol. 3, pp. 361, 1994.

[41] J. Robertson, "Deposition Mechanism of a-C and a-C:H," *Non-Crystalline Solids*, vol. 164-166, pp. 1115, 1993.

[42] J. Robertson, "Deposition Mechanism for Promoting sp^3 Bonding in Diamond-like Carbon," *Diamond Relat. Mater.*, vol. 2, pp. 984, 1993.

[43] J. C. Angus, P. Koidl, and S. Domitz, "Carbon Thin Films," in *Plasma Deposited Thin Films*, J. Mort and J. Jansen, Eds. Boca Raton: CRC Press, 1986.

[44] W. Moller, "Hydrogen Trapping and Transport in Carbon," *J. Nucl. Mater.*, vol. 162, pp. 138, 1989.

[45] J. F. Ziegler, J. P. Biersack, and U. Littmark, *Stopping and Range of Ions in Solids*. New York: Pergamon, 1985.

[46] F. Seitz and J. S. Koehier, *Solid State Physics*, vol. Vol. 2. New York: Academic Press, 1956.

[47] I. Koponen, M. Hakovirta, and R. Lappalainen, "Modeling the Ion Energy Dependence of the sp^3/sp^2 Bonding Ratio in amorphous Diamondlike Films

Produced with a Mass-Separated Ion beams," *J. App. Phys.*, vol. 78, pp. 5837, 1995.

[48] J. Asmussen, T. A. Grotjohn, and D. K. Reinhard, *Lecture note on EE989, Lecture 13, p20*, 1999.

[49] R. Kleber, M. Weiler, A. Kruger, S. Sattel, G. Kunz, K. Jung, and H. Ehrhardt, "Influence of Ion Energy and Flux Composition on the Properties of Plasma-Deposited Amorphous Carbon and Amorphous Hydrogenated Carbon Films," *Diamond Relat. Mater.*, vol. 2, pp. 246, 1993.

[50] J. Asmussen, "Electron Cyclotron Resonance Microwave Discharges for Etching and Thin Film Deposition," in *Handbook of Plasma Processing Technology*, S. M. Rossnagel, J. J. Cuomo, and W. D. Westwood, Eds. New Jersey: Noyes Publications, 1990.

[51] M. A. Lieberman and A. J. Lichtenberg, *Principles of Plasma Discharges and Materials Processing*. New York: John Wiley & Sons, Inc., 1994.

[52] B. K. Kim and T. A. Grotjohn, "Hydrogenated Amorphous Carbon Films Deposited in an ECR-CVD Discharge Reactor using Acetylene," *Diamond Relat. Mater.*, pp. (accepted for publication).

[53] B. K. Kim and T. A. Grotjohn, "Investigation of an ECR Plasma Source used for the Deposition of Diamond-like Carbon films," presented at The 23rd IEEE International Conference on Plasma Science, Boston, MA, 1996.

[54] B. K. Kim and T. A. Grotjohn, "Investigation of the Optical Properties of Diamond-like Carbon Films," *MRS Proceedings*, vol. 498, pp. 109-114, 1997.

[55] B. K. Kim and T. A. Grotjohn, "Characterization of the Optical and Electrical Properties of Amorphous Carbon Films," presented at Material Research Society Fall Meeting, Boston, MA, 1997.

[56] B. K. Kim, "Plasma Discharge Properties of Methane-Argon and Acetylene-Argon ECR-CVD Discharges," presented at International Conference of Plasma Science, Raleigh, NC, 1998.

[57] B. K. Kim and T. A. Grotjohn, "Amorphous Carbon Films Grown from Methane-Argon and Acetylene-Argon ECR-CVD Discharges," presented at The 10th European Conference on Diamond-like Materials, Carbon Nonotubes, Nitrides and silicon Carbide, Prague, Czech Republic, 1999.

[58] B. K. Kim and T. A. Grotjohn, "Investigation of the Plasma Properties and Fluxes in a Hydrogenated Amorphous Carbon Deposition Process," presented at 46th International Symposium of the American Vacuum Society, Seattle, Washington, 1999.

[59] B. K. Kim and T. A. Grotjohn, "Comparison of a-C:H Films Deposited from Methane-Argon and Acetylene-Argon Mixtures by Electron Cyclotron Resonance-Chemical Vapor Deposition Discharges," *Diamond Relat. Mater.*, 2000.

[60] J. Hopwood, D. K. Reinhard, and J. Asmussen, "Experimental Conditions for Uniform Anisotropic Etching of Silicon with a Microwave Electron Cyclotron Resonance Plasma System," *J. Vac. Sci. Technol. B.*, vol. 6, pp. 1896, 1988.

[61] J. Hopwood, D. K. Reinhard, and J. Asmussen, "Charged Particle Densities and Energy Distributions in a Multipolar Electron Cyclotron Resonant Plasma Etching Sources," *J. Vac. Sci. Technol. A*, vol. 8, pp. 3103, 1990.

[62] L. Ley, "Photoemission and Optical Properties," in *The Physics of Hydrogenated Amorphous Silicon II*, J. D. Joannopoulos and G. Lucovsky, Eds. Berlin: Springer-Verlag, 1984.

[63] N. Mutsukura, S.-i. Inoue, and Y. Machi, "Deposition Mechanism of Hydrogenated Hard-carbon Films in a CH4 rf Discharge Plasma," *J.Appl. Phys.*, vol. 72, pp. 43, 1992.

[64] S. Liu, S. Gangopadhyay, G. Sreenivas, S. S. Ang, and H. A. Naseem, "Infrared Studies of Hydrogenated Amorphous Carbon (a-C:H) and Its Alloys (a-C:H,N,F)," *Phys. Rev. B*, vol. 55, pp. 13020, 1997.

[65] K. Mui, D. K. Basa, F. W. Smith, and R. Corderman, "Optical Constants of Series of Amorphous Hydrogenated Silicon-Carbon Alloy films: Dependence of Optical Response on Film Microstructure and Evidence for Homogeneous Chemical Ordering," *Phys. Rev. B*, vol. 35, pp. 8089, 1987.

[66] B. Dischler, A. Bubenzer, and P. Koidl, "Hard Coatings with Low Optical Absorption," *Appl. Phys. Lett.*, vol. 42, pp. 636, 1983.

[67] A. Grill and B. S. Meyerson, "Development and Status of Diamondlike Carbon," in *Synthetic Diamond: Emerging CVD Science and Technology*, K. Spear and J. P. Dismkes, Eds. new York: John Wiley & Sons Inc., 1994.

[68] S. Kaplan, F. Jansen, and M. Machonkin, "Characterization of Amorphous Carbon-Hydrogen Films by Solid-State Neuclear Magnetic-Resonance," *Appl. Phys. Lett.*, vol. 47, pp. 750, 1985.

[69] J. Schwan, S. Ulrich, K. Jung, H. Ehrhardt, R. Samlenski, and R. Brenn, "Deposition of ta-C:H Films by r.f. Plasma Discharges," *Diamond Relat. Mater.*, vol. 4, pp. 304, 1995.

[70] J. A. Hopwood, "Macroscopic Properties of a Multipolar Electron Cyclotron resonance Microwave-Cavity Plasma Source for Anisotropic Silicon Etching," in *ph.D. Dissertation*: Michigan State University, 1990.

[71] L. H. Chou, "Hydrogenated Amorphous Carbon Films Prepared by Plasma-Enhanced Chemical-Vapor Deposition," *J. Appl. Phys.*, vol. 72, pp. 2027, 1992.

[72] A. Gehan, J. Amaratunga, S. Ravi, and P. Silva, "Influence of dc Bias Voltage on the Refractive Index and Stress of Carbon-Diamond Films Deposited from a CH4/Ar rf Plasma," *J. Appl. Phys.*, vol. 70, pp. 5374, 1991.

[73] D. L. Pappas and J. Hopewood, "Deposition of Diamond-like Carbon using a Planar Radio-Frequency Induction Plasma," *J. Vac. Sci. Technol.*, vol. A, 12, pp. 1576, 1994.

[74] N. Mutsukura and K. Miyatani, "Deposition of Diamond-like Carbon Film in CH4-He r.f. Plasma," *Diamond Relat. Mater.*, vol. 4, pp. 342, 1995.

[75] N. Mutsukura and K. Yoshida, "Deposition of DLC Films in CH4/Ar and CH4/Xe r.f. Plasma," *Diamond Relat. Mater*, vol. 5, pp. 919, 1996.

[76] N. Mutsukura and K. Yoshida, "Deposition of DLC Films in CH4/Ne and CH4/Kr r.f. Plasmas," *Diamond Relat. Mater.*, vol. 6, pp. 547, 1997.

[77] J. Hopwood and J. Asmussen, "Neutral Gas Temperatures in a Multipolar Electron-Cyclotron Resonance Plasma," *Appl. Phys. Lett.*, vol. 58, pp. 2473, 1991.

[78] P. Koidl, C. Wild, R. Rocher, and R. E. Sah, "Amorphous, Hydrogenated Carbon Films and Related Materials: Plasma Deposition and Film Properties," in *Diamond and Diamond-like Films and Coatings*, R. E. Clausing, L. L. Horton, J. C. Angus, and P. Koidl, Eds. New York and London: Plenum Press, 1991.